Compact RF planar filters-improvement of the out-of-band rejection and tunabiliity

Mirna Akra

UNIVERSITÉ DE GRENOBLE

THÈSE

Pour obtenir le grade de

DOCTEUR DE L'UNIVERSITÉ DE GRENOBLE
et **DE l' L'UNIVERSITÉ LIBANAISE**

Spécialité : **Optique et Radio fréquence**

Arrêté ministériel : 7 août 2006

Présentée par

« Mirna AKRA »

Thèse dirigée par **« Philippe FERRARI », «Akil JRAD»** et co-encadrée par **« Emmanuel PISTONO »**

préparée au sein du **Laboratoire IMEP-LAHC**
dans **l'École Doctorale Électronique, Électrotechnique, Automatique et Traitement de Signal** et **LaSTRe** dans **l'École Doctorale des Sciences et technologie**

Étude de filtres RF planaires miniatures. Amélioration de la réjection hors-bande et accordabilité

Thèse soutenue publiquement le **« 18 Mars 2014 »**,
devant le jury composé de :

M. Fransisco MEDINA
Professeur, Université de Seville (Espagne), Examinateur
M. Cédric QUENDO
Professeur, Université de Bretagne Occidentale, Brest, Rapporteur
M. Gaëtan PRIGENT
Maitre de conférences HDR, ENSEEIHT Toulouse, Rapporteur
M. Soubhi ABOU CHAHINE
Professeur, Université Arabe de Beirut (Liban), Rapporteur
M. Philippe FERRARI
Professeur, Université Joseph Fourrier, Grenoble, Directeur de thèse
M. Akil JRAD
Professeur, Université Libanaise, Tripoli (Liban), Co-Directeur de thèse
M. Emmanuel PISTONO
Maitre de conférences, Université Joseph Fourrier, Grenoble, co-encadrant de thèse

A ma mère

A mon père

A mon mari

En modeste témoignage de gratitude pour le soutien et la sympathie qu'ils n'ont cessé de m'exprimer.

A mes frères

A mes Sœurs

A toute ma famille

A tous mes amis

Remerciements

Le travail de synthèse que nécessite la rédaction d'une thèse est difficile, mais à présent que je me retrouve face à mes remerciements, je me sens toute aussi impuissante. Par où commencer ? Un ordre chronologique ? Très bien… cela va m'amener à un début original, mais ce n'est pas grave, je me lance ! Pour m'avoir permis de mener ce projet à bien et de vivre de tels moments, je tenais donc à Remercier:

La région Rhône-Alpes et L'AUF (Agence Universitaire de la Francophonie) qui ont permis le financement de mon séjour en France.

Mon directeur de thèse à l'Université libanaise, Monsieur Akil JRAD de m'avoir accordé cette confiance de démarrer une thèse avec l'université de Grenoble avec qui il a des connaissances…c'est là ou l'histoire a commencé…

Mon directeur de thèse à l'Université de Grenoble, Monsieur Philippe FERRARI, de m'avoir accueilli au sein du laboratoire IMEP-LAHC, de l'intérêt qu'il a porté à ce travail ainsi que de la confiance qu'il m'a accordé tout au long de celui-ci. Sa disponibilité et sa forte compétence scientifique ont été essentielles à l'accomplissement de mes travaux de recherche. Qu'il trouve ici l'expression de ma profonde et respectueuse gratitude.

Monsieur Emmanuel PISTONO, Co-directeur de thèse, pour m'avoir fait profiter de son savoir et de ses connaissances, sa disponibilité, sa sympathie, son écoute et ces encouragements….

Monsieur le Professeur Fransisco MEDINA, pour m'avoir fait l'honneur de présider le jury de cette thèse. Je tiens à lui exprimer mes sentiments respectueux.

Monsieur Cédric QUENDO pour l'intérêt qu'il a porté à ce mémoire en acceptant d'en être l'un de ces rapporteurs.

Monsieur Gaetan PRIGENT pour avoir accepté la charge d'être rapporteur de ma thèse.

Monsieur Soubhi ABOU CHAHINE pour avoir accepté d'examiner le travail de thèse et de faire partie de ce jury. Je tiens à lui exprimer mes remerciements les plus sincères.

Toute ma gratitude à toutes les personnes ayant relu, corrigé et commenté mon manuscrit et ayant ainsi participé à son amélioration.

C'est aussi un plaisir pour moi d'associer en une même pensée tous les membres du laboratoire. Un grand merci à Monsieur Nicolas CORRAO, responsable de la plateforme hyperfréquence pour sa disponibilité, sa patience, et son aide au cours des différentes mesures RF. Ainsi qu'à Antoine GACHON pour ses contributions au bon fonctionnement de la plateforme HOC (Hyperfréquences, Optomicroondes et CEM). Je tiens à remercier tous les personnels administratifs et techniques du laboratoire : Brigitte, Dalhila, valérie, Annaick, Isabelle, Joelle, Chahla, Serge et Luc. Je tiens à exprimer ma reconnaissance à Hamza pour tous les échanges scientifique que j'ai eus avec lui lors de ma première année de thèse. Je n'oublie pas à remercier tous les doctorants qui sont succédés au bureau 353. Un spécial merci à une collègue, une amie et une sœur avec laquelle j'ai passé mes trois années de thèse Fatima Barrami à qui je souhaite la réussite et tout le bonheur. Je pense également à tous les doctorants que j'ai partagés avec mes déjeuners.

Je poursuivrai ces remerciements avec tous mes professeurs de l'Université Libanaise et mes amis au liban.

Il y a aussi mes amies que j'ai passés avec eux tant de temps. Je pense à Iman, Selma, Rim, Lineda, Sarah…Vous êtes des vraies sœurs. Le temps passé avec vous m'a apporté beaucoup de bien être et de bonheur.

Un Merci du fond du cœur à mes parents, mes sœurs, mes frères et à ma grande famille au Liban…Les mots ne suffisent pas pour exprimer l'amour, l'affection et l'attachement que je porte pour vous.

Enfin, je remercie mon amour, mon mari qui est à côté de moi depuis deux ans. Merci (Habibi) waoul pour le bonheur que t'as apporté à ma vie…

Title

Étude de filtres RF planaires miniatures. Amélioration de la réjection hors-bande et accordabilité.

Abstract

The purpose of this work was to develop RF bandpass filters in PCB technology, with three main objectives. The first objective was to develop synthesis formulas to simplify the design procedure of the filter. The second was to achieve wide out-of-band rejection without modifying the in-band filtering characteristics. The third objective was to control the center frequency of the filter by using varactor diode.

The bandpass filter topology treated in this thesis is based on Stub-Loaded Resonators (SLR). The main features of this filter topology were treated. Equivalent circuits based on *J*-inverters and susceptance parameters were derived. Based on these equivalent circuits, synthesis formulas were developed. Simulations were presented to validate the synthesis theory. For a proof-of-concept, third order stripline bandpass filters were designed and fabricated based on this synthesis. Analysis technique using odd- and even- mode was achieved on the SLR. Thus resonance odd- and even-mode conditions were derived. These conditions aim to easily control the first spurious frequency. Moreover, to go further in improving the out-of-band rejection a new technique, called "U corner structure", was developed and design rules were derived. Based on these design rules an extended out-of-band rejection was achieved without any modification in the passband and by maintaining the compactness of the filter. A first spurious frequency was localized at up to nine times the working frequency in the case of the Parallel-coupled Stub-Loaded resonator (PC-SLR) filter. Also, by applying this technique into the classical parallel-coupled filter the first and second spurious frequencies were rejected. To address the issue of tunable filters, the SLRs were correctly loaded by variable capacitors (varactor diode). The center frequency of the PC-SLR filter was easily controlled by maintaining a large out-of-band rejection.

Key words: Planar bandpass filter, stripline technology, microstrip technology, classical parallel-coupled line filters, *J*-inverter, odd- and even-modes, U corner, miniaturization, out-of-band rejection, tunable filter.

Introduction

Communications in the field of radio frequency (RF), which covers a frequency range from several hundred MHz to a few GHz, have grown rapidly in recent years, stimulated in particular by the world-wide growth in digital mobile communication in the late 80s. In the last few years, great innovation has araised in the mobile features, from a device which only receives and makes calls to a device supporting many services due to the emergence of Wifi, GPS, and Bluetooth standards. These services require wide range of data rates and bandwidth over several frequency bands in the RF spectrum, leading to the point of data saturation. Besides, in many fields, from space, defense, security, to medical applications, RF systems are required. Thus efforts are carried out in order to improve compactness and to minimize the costs and power consumption of components and systems. Among these components, filters are the ones of the most concerned. They permit the transmission of wanted signal and prevent or attenuate the unwanted ones. Thus, it is essential to develop and provide filters based on miniature resonators, with simple design theory and wide out-of-band rejection by pushing parasitic harmonics to as higher frequency as possible. In addition, the issue of multiple standards can be addressed by the achievement of tunability feature. Thus, various tunable resonator configurations have recently attracted the interest of researchers.

The purpose of the thesis work was focused on the development of planar filters in PCB technology, with three main objectives appropriate to the context described above:

- The development of design rules to simplify the optimization procedure (chapter 2),
- The design and the exploration of new methods and techniques to improve the out-of-band rejection, without the need of a hard work of

modeling, to support a high performance when interference is present (chapter 3),

- The development of tunable filters to address the issue of multiple standards (chapter 4).

Thus, my thesis work is based on developing a bandpass filter topology. This topology is based on Stub-Loaded Resonators. These resonators reduce the footprint of conventional parallel-coupled bandpass filters. Also, they are efficient in improving the filter response namely the out-of-band rejection. Moreover, they prove an ability to be easily tuned in terms of center frequency.

The **first chapter** describes the main features of filters with a particular interest on bandpass filters. It introduces basic characteristics of planar technologies, which are useful to design passive planar filters. It highlights too compact filter topologies, the main techniques for miniaturization and for spurious suppressions.

In the **second chapter**, the principle of the Stub-Loaded Resonator (SLR) is given. Design equations of parallel-coupled bandpass filter based on these resonators are derived. The miniaturization rules are also listed. This resonator exhibits an interesting characteristic in term of compactness. These theoretical results are verified through simulated and measured data.

In the **third chapter**, in order to highlight the great interest of the SLR, a detailed even- and odd-mode study is described. The goal of this study is to show the flexibility of this resonator topology in the harmonic suppression. It is capable of controlling the first spurious frequency. By carefully choosing the SLR electrical parameters, significant improvement in the out-of-band rejection can be obtained and thus frequency symmetry response can be easily achieved compared to the classical parallel-coupled topology. Moreover, a multispurious suppression can be achieved by incorporating an innovative feeding network called “U corner”. The

out-of-band can be highly extended to more than nine times the working frequency while maintaining reasonable filter dimension.

The **last chapter** describes and analyses the capacitively loaded SLR. By using varactor diode as a variable capacitance, the center frequency of the SLR can be tuned by keeping the first spurious frequency unaltered.

Chapter I. Filter Basics

I.1. Introduction

Filters are indispensable devices in the field of telecommunication. Filters are used for the rejection of unwanted signal frequencies, permitting the transmission of wanted ones, and for separating frequencies or in summing signals having different frequencies in duplexers or multiplexers [1].

With the development of multi-service wireless communication systems, filters must satisfy a number of specific criteria, namely compactness since most mobile platforms have a limited space for required filters, sharp and wide out-of-band rejection by generating transmission zeros or attenuation poles, and tunability.

This chapter introduces the main features of filters; a particular attention is dedicated to bandpass filters where basic concepts and theories that form the foundation for design of bandpass filters are presented. This is followed by a description of different filter technologies. Finally, the main techniques for miniaturization and to obtain wide out-of-band rejection of microstrip bandpass filters are briefly discussed. Tunable filter configurations will be detailed in Chapter IV.

I.2. Principle and synthesis of bandpass filter

I.2.1. Signal filtering

Filters are often used in electronic systems to emphasize signals in certain frequency ranges and reject signals in other frequency ranges [1]. Filters can be separated in five categories: low-pass, high-pass, band-pass, band-stop, and all-pass or phase shift filter.

A ***low-pass filter*** allows signal frequencies below the low-cut off frequency (this is the frequency that define the limits of the filter range, it is the desirable cut-off frequency of the filter) to pass and attenuates frequencies above the cut-off frequency. It is commonly used to reduce environmental noise and provide a smoother signal. The opposite of the low-pass filter is the ***high-pass filter***, which attenuates signals below cutoff frequency; this filter can be used as blocking DC from circuitry sensitive to non-zero voltage or RF devices. It can also be used in conjunction with a low-pass filter, to obtain a ***band-pass filter*** that allows signals in a specific band of frequencies to pass, while signals at all other frequencies are attenuated. The ***band-stop filter*** is the opposite of the band-pass filter. The ***all-pass*** or ***phase-shift filter*** has no effect on the amplitude of the signal in the whole frequency range; its function is to change the phase of the signal without affecting its amplitude. In this thesis, only bandpass filter will be considered.

Since filters are defined by their frequency domain effects on signals, the most useful analytical and graphical descriptions of filters also fall into the frequency domain. Thus, curves of gain vs frequency and phase vs frequency are commonly used to illustrate filter characteristics, and the most widely used mathematical tools are based on the frequency domain.

To understand the bandpass filter theory, it is necessary to briefly study transfer functions.

I.2.2. Transfer function

Microwave filter synthesis began with the ***image impedance parameter method*** and was useful for low frequency filters [2]. A more modern procedure for designing filters which allows a high degree of control over the passband and stopband amplitude and phase characteristics is the ***insertion loss method*** [2]. Filters can be classified into four categories distinguished from each other by terms of locations of

transmission zeros and poles of their transfer functions. Namely, ***Butterworth, Chebyshev***, ***Elliptic*** and ***Bessel*** filter. The ***Butterworth*** filter has no ripple in the passband and because of this it is called a maximally flat filter. The ***Chebyshev*** filter has a deeper attenuation beyond the cut-off frequency than the same order Butterworth filter, at the expense of ripple in its passband. The ***Elliptic function response*** allows obtaining transmission zeros close to the passband in order to increase the rejection slope; thus this filter has a steeper attenuation beyond the cut-off frequency than the Chebyshev filter, such filter is complex in practical realization. The linear phase response concerns the ***Bessel filter*** whose transfer function is derived from a Bessel polynomial and ***Gaussian filter,*** whose transfer function is derived from a Gaussian function, have a poor selectivity.

In this thesis, only bandpass filter based on Chebyshev prototype filter are considered.

Chebyshev bandpass filter

The Chebychev filtering function can be synthesized by a low pass network composed of capacitive and inductive elements, whose elements values are normalized to make the source resistance or conductance equal to one (as seen in Figure I-1).

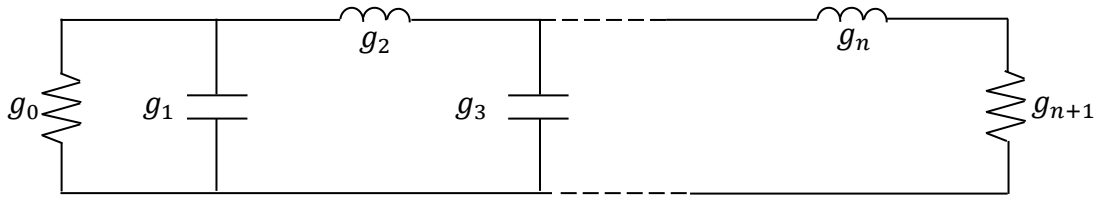

Figure I-1. Low pass prototype filter.

Knowing the elements values of the lowpass prototype filter shown in Figure I-1, the next step is to look for the corresponding bandpass filter design, which can be

obtained directly from the prototype by a lowpass to bandpass transformation (Figure I-2) [1].

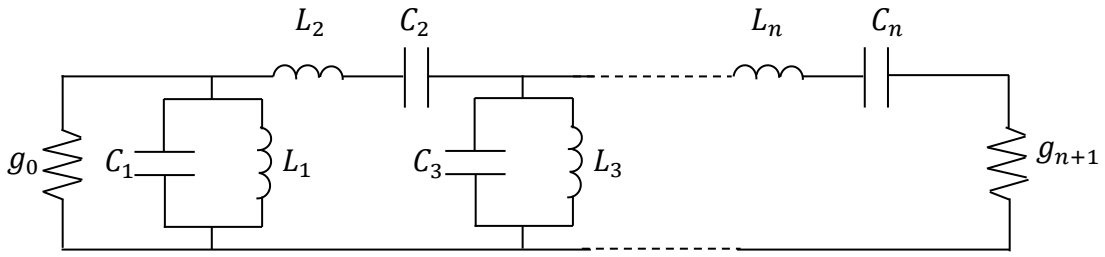

Figure I-2. Practical bandpass filter based on the lowpass to bandpass transformation.

I.2.3. J and K inverters

The filter structure in Figure I-2 consists of series resonators alternating with shunt resonators, an arrangement which is difficult to achieve in practical microwave structure when implementing filter with a particular type of transmission line. In microwave filter it is much more practical to use a structure which approximates the circuit containing only resonators of the same type based on "***impedance*** and ***admittance inverters***" as shown in Figure I-3.

A load impedance (or admittance) connected at one end is seen as an impedance (or admittance) that has been inverted with respect to the characteristic impedance (or admittance) squared at the input [1], [2]. Thus, a series *LC* resonator (or shunt *LC* resonator) with an inverter on each side looks like a shunt *LC* resonator (a series *LC* resonator) from its external terminals.

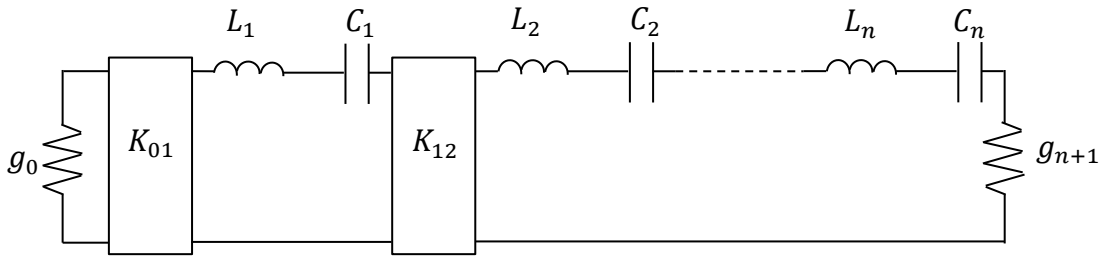

Figure I-3. Passband filter based onimpedance inverter.

Impedances inverter of characteristic impedance k and admittance inverters of characterictic admittance Jcan be constructed by using a quarter-wave transformer of electrical length of ($\pm 90°$). These inverters are defined as two port passive circuits by

$$\begin{bmatrix} 0 & \pm j \cdot k \\ \pm \frac{j}{k} & 0 \end{bmatrix} \tag{I-1}$$

$$\begin{bmatrix} 0 & \pm j \cdot \frac{1}{J} \\ \pm j \cdot J & 0 \end{bmatrix} \tag{I-2}$$

I.3. Planar Filter

Modern systems require high performed filters with very low losses, small size, sharp cut-off, and high rejection at the stopband. Thus, different resonators and techniques have been introduced for RF and microwave filters to achieve different filters with these performances using planar transmission lines.

Planar transmission lines are composed of a solid dielectric substrate having one or two layers of metallization, with the signal and ground currents flowing on separate conductors.

Planar transmission lines used in microwave frequencies can be broadly divided into two categories: those that can support a TEM (or Quasi-TEM) mode of propagation, and those that cannot. For TEM (or Quasi-TEM) modes the determination of characteristic impedance and phase velocity of single and coupled lines reduces to finding the capacitances associated with the structure.

I.3.1. Technologies

The most widely used transmission lines are microstrip line, coplanar waveguide (CPW), and stripline.

a) Microstrip line

Microstrip line (Figure I-4) is a transmission line which consists of a conducting strip separated from a ground plane by a dielectric layer. The dielectric constant varies between 2 to 10 times that of free space, with the penalty that the existence of two different dielectric constants (below and above the strip) introduces a variability of propagation velocity with frequency that causes some complications in microstrip analysis and design [6], [14]. Thus a concept of effective dielectric constant was introduced, which is expected to be greater than the dielectric constant of air and less than that of the dielectric substrate. In addition, the substrate discontinuity causes its dominant mode to be hybrid (Quasi TEM). Figure I-4 shows the general structure of a microstrip line. The main advantages of microstrip line are that it is a suitable technique for MICs (Microwave Integrated Circuit), and the radiation that it provides can be used for antenna design. The main disadvantage of this type of transmission lines is that via holes are necessary in the case of shunt connection, inducing a complex modelling of these vias. The characteristic impedance of the microstrip line is depending on the width of the guided wave line, substrate thickness, and the effective dielectric constant of the substrate [3].

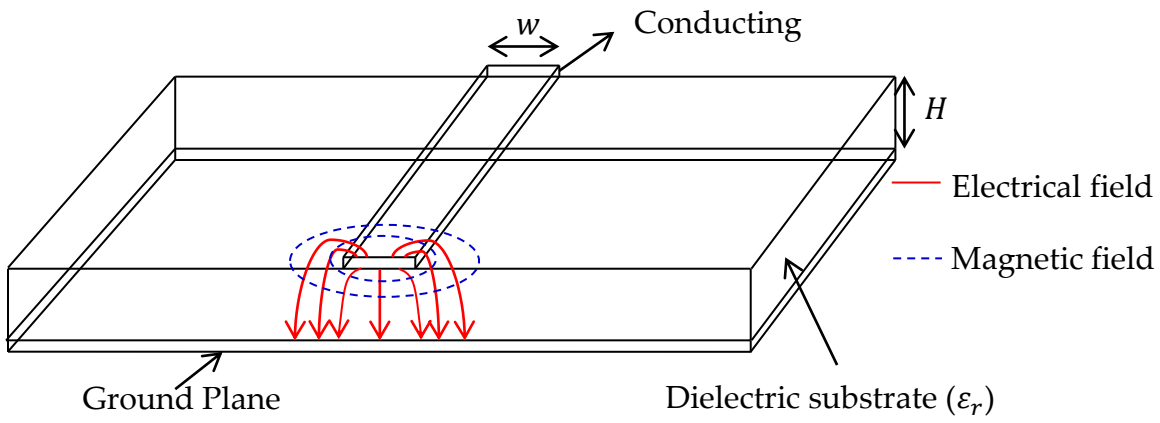

Figure I-4. Structure of a microstrip line [3].

b) Coplanar waveguide

Coplanar waveguide (CPW) is basically a single strip located between two ground planes on the same side of the substrate, see Figure I-5. This type of transmission line can be easily integrated with the MIC's. Furthermore shunt connections can be easily realized without the need of via holes. In addition it is less sensitive to the substrate thickness that in the case of microstrip. Both ground planes must be at the same potential to avoid the asymmetric propagation mode.

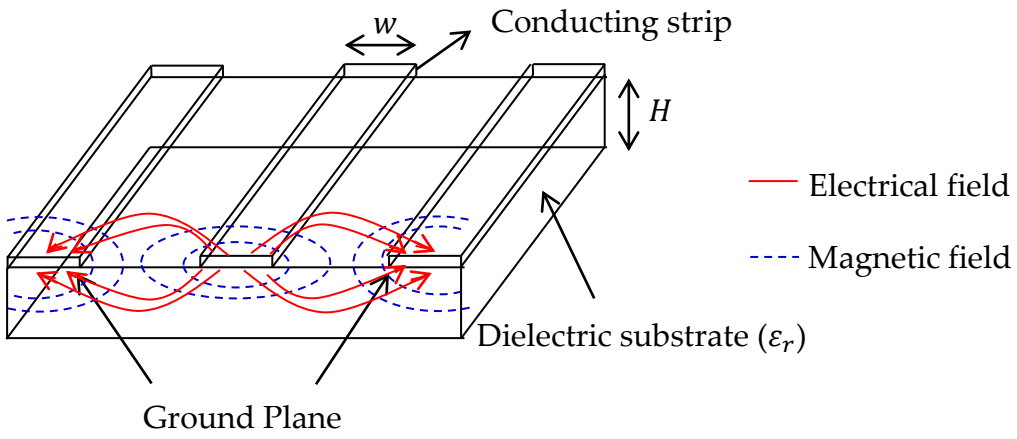

Figure I-5. Structure of coplanar waveguide transmission line.

c) Stripline

Stripline is essentially a flat metal transmission line between two ground planes, with the ground planes separated by a dielectric substrate material. The metal transmission line is embedded in a homogeneous and isotropic dielectric, thus the phase velocity and the characteristic impedance remain constant with frequency. The width of the transmission line, the thickness of the substrate, and the relative dielectric constant of the substrate material determine the characteristic impedance of the transmission line. Difficulties with stripline include ground planes that must be shorted together, requiring electrical via connections between the two metal ground planes. Stripline second ground plane also results in a narrower transmission line widths, for a given substrate thickness and characteristic impedance, than for microstrip.

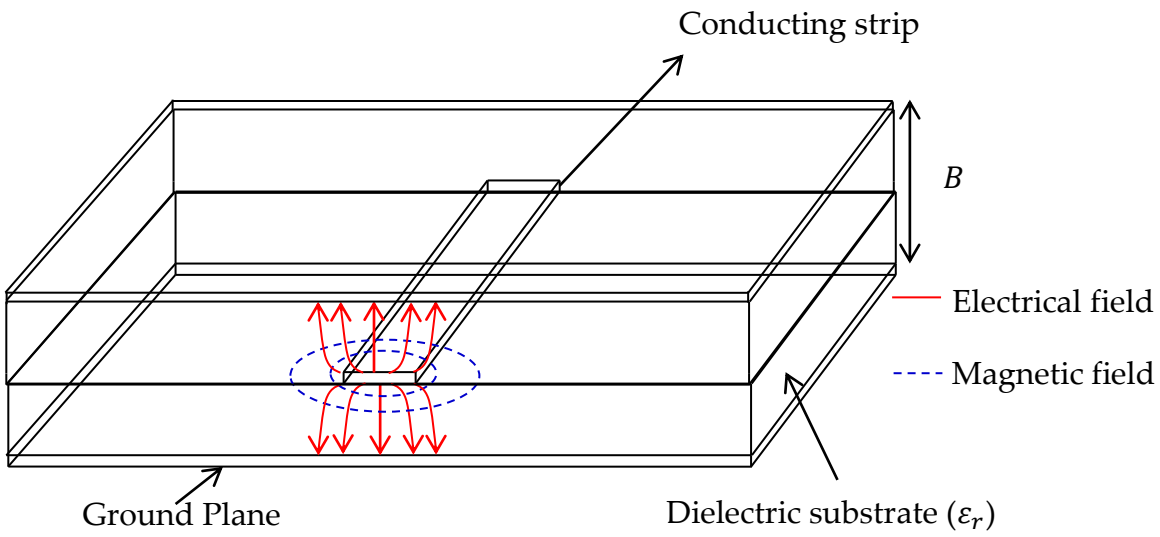

Figure I-6. Structure of a stripline technology.

d) Conclusion

As previously mentioned, transmission lines in stripline technology are embedded in a homogeneous medium. Thus, the phase velocity for coupled transmission lines of both even- and odd- modes are the same, on the contrary for a

microstrip coupled lines. Thus, the stripline technology is more convenient to validate synthesis formulas for a new filter topology. Hence, the stripline will be considered herein to validate the Parallel-Coupled Stub-Loaded-Resonator (PC-SLR) bandpass filter (as will detailed in Chapter II). However, the design procedure of a stripline topology is more difficult and expensive to fabricate than microstrip. Consequently, microstrip and CPW topologies remain more used than stripline one.

I.3.2. Topologies

Different planar resonators have been introduced for RF and microwave bandpass filters to achieve filters with high performance (low losses, small size, sharp cut-off, and high out-of-band rejection). The main used resonators are described below.

a) Half wavelength resonator

It basically consists of transmission line section having a length of half wavelength at the corresponding center frequency. Early filters based on these resonators are ***end-coupled*** and ***parallel-coupled bandpass filters*** [4] (as illustrated in Figure I-7). Their design equations have been well documented [1]-[6]. The parallel arrangement (Figure I-7(b)) gives compact size (the length of the filter is reduced approximately by half), compared to the end-coupled bandpass. Also it gives relatively large coupling for a given spacing between resonators, thus this filter structure is particularly more convenient for constructing wider bandwidth than the end-coupled filter.

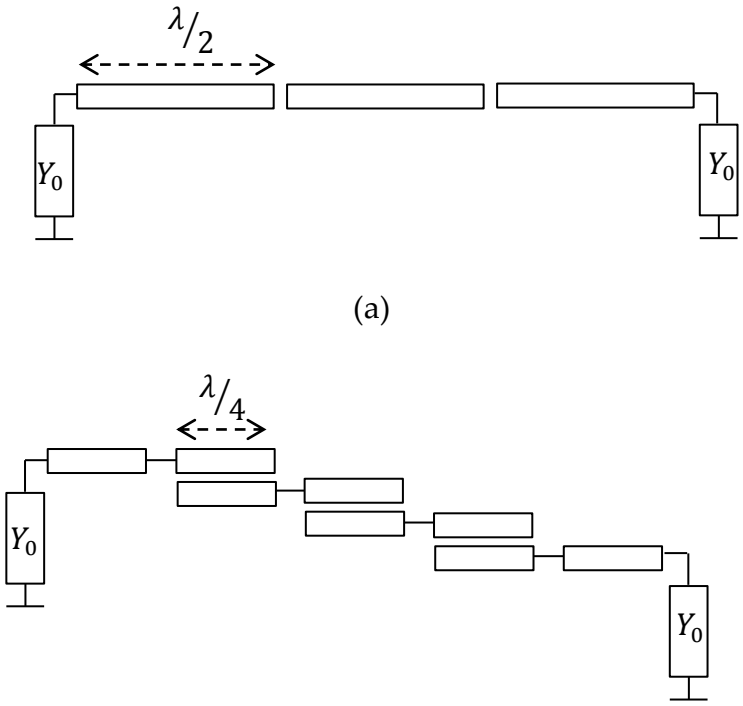

Figure I-7. Schematic circuit of (a) the end-coupled , and (b) the parallel-coupled bandpass filters.

The ***Hairpin bandpass filters*** also known as U-shape [7],[8] and open-loop [9]-[10] bandpass filters are also based on half wavelength resonators. They are obtained by folding the resonators of the parallel-coupled filter, thus the same design equations can be used. Open-loop resonators have great advantages in reducing filter size. They have different coupling nature depending on the coupling sides [3] which can be used to obtain transmission zeros in the out-of-band rejection. If the two arms of each hairpin resonator are closely spaced, they function as a pair of coupled line themselves, which can have an effect on the coupling as well.

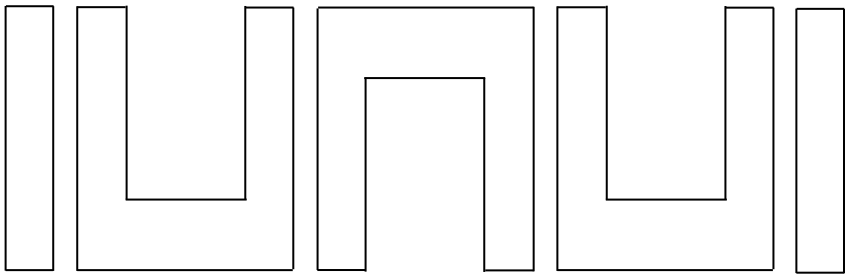

Figure I-8.Hairpin bandpass filter.

When designing in microstrip, these half wavelength resonator filters suffer from the spurious response at twice the passband working frequency. This causes response asymmetry in the upper stopband and could greatly limit its applications.

b) Quarter wavelength resonator

Interdigital filters (Figure I-9) consists of parallel-coupled quarter-wavelength resonators which are short-circuited at one end and open-circuited at the other end. Interdigital microstrip filters have the first spurious frequency at three times the working frequency, thus they present a large out-of-band rejection as compared to the parallel-coupled and end-coupled microstrip bandpass filters. Coupling between interdigital lines is strong thus gap between resonators can be large, making interdigital filters simpler to fabricate for wide bandwidth applications, with small filter dimension [11].

Theory and design procedure for interdigital bandpass filters depends on the configuration of the feeding ports. Thus the design equations for filters with coupled-line Input/Output (I/O) (Figure I-9 (a)) can be found in [12]. Based on [13], design equations for the type of interdigital bandpass filter with tapped-line I/O (Figure I-9 (b)) are presented.

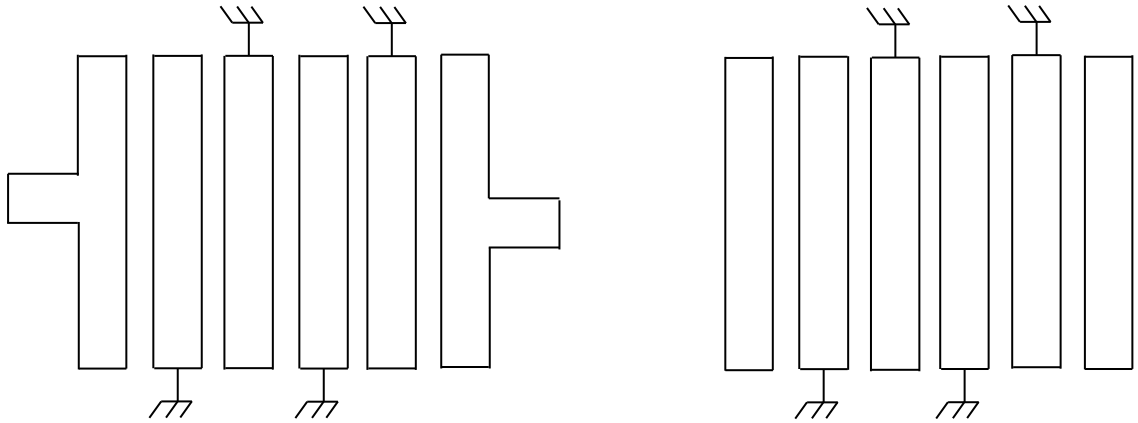

(a) (b)

Figure I-9. Layout of interdigital bandpass filter using (a) coupled-line and (b) tapped-line, Input/Output.

Combline bandpass filters consist of array of parallel resonators which are short-circuited at one end with a loading capacitor at the other end [3]. These filters are very compact since the length of the resonators is shorter than $\lambda/4$, due to the loading capacitor.. The first spurious of a combline filter is located at more than three times the working frequency.

I.4. Miniaturization techniques in planar technology

Filters based on parallel-coupled microstrip line structure have been widely used in the RF front end of microwave and wireless communication systems for decades. One of the most common filter topologies is based on half wavelength resonators with quarter wavelength coupled line sections (as seen in Figure I-7 (b)). Good repetition and easy design are attractive features of this filter topology. However, since the conventional bandpass filters are relatively bulky, large efforts were invested in the miniaturization of these types of filters.

Many methods for the miniaturization of planar filters have been proposed and they are summarized in four categories. The first is based on the use of high dielectric

constant substrate. The second proposed a lumped element approach. The third is based on the use of meandered transmission lines. Finally, the fourth category deals with the use of slow-wave transmission lines.

I.4.1. High dielectric constant substrate

Dielectric constant, is an index representing the degree to which substrate can store electric charge. The higher the value is, the more electric charge can be stored. Thus, the dielectric constant of the substrate can determine the size of a circuit. Indeed, this technique produces a reduction of the wave propagation velocity on the transmission line and the consequent reduction of the wavelength for a given frequency (I-3). Thus the slow-wave effect can be evaluated.

$$v_p = \frac{c}{\sqrt{\varepsilon_{reff}}} = \frac{2\cdot\pi}{\beta}\cdot f \qquad \text{(I-3)}$$

where β is the propagation constant, f is the working frequency, c is the velocity of light in vacuum and ε_{reff} is the relative effective permittivity.

This technique has proved its effectiveness in miniaturization of bandpass filters as demonstrated for example in [15]-[18]. In [15] seven-pole stripline end-coupled bandpass filters were fabricated using a high dielectric constant substrate. This substrate is composed of Zirconium-tin-titanium oxid [$(Z_nS_n)TiO_4$] (dielectric constant$\varepsilon_r = 38$, dielectric loss tangent $tan\delta = 10^{-4}$). These bandpass filters were designed with a 140-MHz bandwidth at 3 dB, and center frequencies of 6.04 GHz and 8.28 GHz with an insertion loss of 6.6 dB. In [16], two miniaturized hairpin 5% bandwidth bandpass filters were fabricated on two very high dielectric constant substrates: the first one being composed of barium and strontium titanates (dielectric constant$\varepsilon_r = 80$, dielectric loss tangent$tan\delta = 10^{-4}$, substrate thickness $h = 2$ mm) and the second one composed of niobium-niodinum titanate (dielectric constant $\varepsilon_r = 90$, substrate thickness $h = 1$ mm). A high reduction gain was obtained. Nevertheless, difficulties were highlighted about the realization of 50-Ω

transmission-line characteristic impedance on these substrates due to the high dielectric constant value. Indeed, the characteristic impedance Z_c of a transmission line (in microstrip, stripline, or CPW technology…) is inversely proportional to the relative permittivity. Thus, a high dielectric constant substrate leads to low line widths. This is the main drawback of using this technique.

I.4.2. Lumped element approach

Using lumped elements (fabricated entirely using printed circuit or thin film technologies) is another approach to filter miniaturization [3]. This technique allows high out-of-band rejection. Lumped inductors can be designed as spiral or meander transmission lines and capacitors consist of interdigital or MIM (Metal-Insulator-Metal) structures [3]. These elements have the advantage of small size, and low cost. However, it is very difficult to realize a truly lumped element and thus parasitic effects must be considered inducing spurious appearing in the out-out-band. For example, the shunt parasitic capacitance to the ground may affect the performance of the inductor.

I.4.3. Meandered transmission lines

The distributed approach considering meandered transmission lines can be used [19]-[20]. For example, in [19], a dual-mode microstrip bandpass filter was fabricated based on a meander loop resonator. This dual-mode meander loop achieves more than 50% size reduction against ring, square patch and disk resonators. In [20], a CPW bandpass filter was miniaturized to half of its initial size using this technique. However, this technique needs an important work to model parasitic couplings.

I.4.4. Slow-wave transmission lines

From transmission line theory, the propagation constant and phase velocity of a lossless transmission line are given respectively by $\beta = \omega \cdot \sqrt{LC}$ and $v_p = \frac{1}{\sqrt{LC}}$, where L

and C are the inductance and capacitance per unit length along the transmission line. Thus, slow-wave propagation can be accomplished by effectively increasing the L and C values. One way to do this consists in introducing periodic variations along the direction of propagation. Slow-wave resonators are generally realized by loading basic transmission lines by inductances and/or capacitances. These elements affect the transmission line parameter and thus reduce the phase velocity of the periodically loaded transmission line. In microstrip, these elements can be added to the conducting strip (series inductance or parallel capacitance) [21]-[25] or by drilling holes in the substrate or by etching patterns in microstrip ground plane. These patterned structures are sometimes referred to as defected ground structures or slotted ground structure [26], [27].

I.5. Out-of-band rejection techniques

As previously mentioned the parallel-coupled bandpass filter topology is commonly used due to its ease of synthesis method, and low cost. This type of filters can be implemented by using a variety of technologies. Stripline, coplanar waveguide (CPW) and microstrip are typical examples. In the original paper by S. B. Cohn [4] the filter is implemented in stripline technology. In stripline technology as previously mentioned, the dielectric medium between conductors is homogeneous. In this case, the propagating even and odd modes of the coupled transmission lines have identical phase velocity. Spurious frequencies appear at odd harmonics ($3 \cdot f_0, 5 \cdot f_0$ …).

However, when designed in microstrip technology, this filter presents spurious frequencies at multiples of the working frequency ($2 \cdot f_0, 3 \cdot f_0, 4 \cdot f_0, \ldots$). These spurious peaks appear in the out-of-band rejection at even harmonics ($2 \cdot f_0, 4 \cdot f_0, \ldots$) due to the inequality of even- and odd- mode phase velocities [28]. This leads to a poor out-of-band rejection.

Consequently, different techniques have been proposed to improve the out-of-band rejection of this filter topology. However, the first spurious at $2 \cdot f_0$ is the most concerned since it degrades the passband symmetry and blocks the capacity to extend the out-of-band rejection. In order to eliminate this even harmonic, many techniques are useful. Much effort has been made to equalize the phase velocities of even and odd modes by differentiating their traveling routes [29]-[32]. For example, the structures in [29], and [30] use capacitors to extend the traveling path of the odd mode. In [28], an over-coupled resonator is proposed to extend phase length for the odd mode to compensate difference in the phase velocities. In [31] the sinusoidal modulation of the coupled-lines strip widths and in [32] the corrugated coupled microstrip lines are used to extend odd-mode path. However, most of these approaches need an important work of modeling. Design techniques use the stepped impedance resonators (SIRs) [33], where the first spurious frequency can be rejected to higher frequencies by a convenient choice of the impedance ratio parameter.

Recently, multispurious suppression has been an important research topic. The over-coupled stage in [34] is an extension of [28]. Varying the coupling length of coupled-lines can tune zeros at spurious harmonics. Measured data present a first spurious at $5 \cdot f_0$ for out-of-band rejection better than 30 dB in the out-of-band. The wiggly-line in [35] is a significant extension of [31] and allows obtaining a rejection bandwidth up to five times the operating frequency. In [36], stages of $\lambda/4$, $\lambda/6$ and $\lambda/8$ are tuned to cancel the spurious at $2 \cdot f_0, 3 \cdot f_0$ and $4 \cdot f_0$, respectively. In [37], SIRs are used to mutltispurious suppression. Bandpass filters with stopband up to $4.4 \cdot f_0, 6.5 \cdot f_0$ and $8.3 \cdot f_0$ are presented.

I.6. Conclusion

In this thesis, the distributed compact filter topology based on parallel-coupled stub-loaded resonators (PC-SLRs) is introduced. One of the main features of the

Stub-Loaded Resonators (SLRs) is the capability of reducing resonator surface area. Thanks to a careful study of the spurious frequencies, a large rejection bandwidth extending to three times the working frequency can be achieved. The high rejection bandwidth has been further improved thanks to an efficient optimization of the feed lines by using a **"U-corner"** topology. Without modifying the in-band filtering characteristics, the rejection bandwidth can be enlarged to more than **nine times the working frequency**. This out-of-band improvement is achieved without deterioration of the filter surface area by only adjusting the U-corner structure. A detailed design methodology is described. Another key advantage is the tunability. Both theory and experiments prove the easy control of the center-frequency tuning range by the convenient choice of the SLR parameters.

Refernces

[1] G.-L. Matthaei, L.-Young, and E.-M.-. T. Jones, Microwave Filters, Impedance-Matching Networks, and Coupling Structures.: Artech House, 1980.

[2] D.-M. Pozar, Microwave Engineering, 3rd edition, New York: Wiley, 2005.

[3] J.-S. Hong, and M.-J. Lancaster, Microstrip filters for RF/Microwave applications, New York: Wiley, 2001.

[4] S.-B. Cohn, "Parallel-coupled transmission-line-resonator filters," IRE Transactions on Microwave Theory and Thechniques, vol. 6, no. 2, pp. 223-231, April 1958.

[5] D. Ahn, C.-S. Kim, M.-H. Chung, D.-H. Lee, D.-W. Lew, H.-J. Hong, "The design of parallel-coupled line filter with arbitrary image impedance", in IEEE MTT-S Int. Symp. Dig., Baltimore, USA, June 7-12, 1998.

[6] D. Kajfez, and S. Govind, "Effect of Difference in Odd- and even- mode Wavlengths on a Parallel-Coupled Bandpass Filter," IEE Electronics Letters , vol. 11, no. 5, pp. 117-118, Mar. 1975.

[7] E. G. Cristal, and S. Frankel, "Hairpin-line and hybrid-line/half wavelength parallel-coupled line filters", IEEE Trans. Microwave Theory and Thech., vol. 20, no. 11, pp. 719-728, Nov. 1972.

[8] G.-L. Matthaei, N.-O. Fenzi, R.-J. Forse, and S.-M. Rohfing, "Hairpin-comb filters for HTS and other narrow-band applications", IEEE Trans. Microwave Theory and Thech., vol. 45, no. 8, pp. 1226-1231, Aug. 1997.

[9] J.-S. Hong and M.-J. lancaster, "Cannonical microstrip filter using square open-loop resonators", IEE Electronics Letters , vol. 31, no. 23, pp. 2020-2022, Nov. 1995.

[10] J.-S. Hong, and M.-J. Lancaster, "Couplings of microstrip square open-loop resonator for cross coupling planar filters", IEEE Trans. Microwave Theory and Thech., vol. 44, no. 12, pp. 2099-2109, Dec. 1996.

[11] R. Levy, R.-V. Snyder, and G. Matthaei,"Design of microwave filters", IEEE Trans. Microwave Theory and Thech., vol. 50, no.3 , pp. 783-793, Mar.2002.

[12] G.-L. Matthaei, "Interdigital bandpass filters", IEEE Trans. Microwave Theory and Thech., vol. 10, no.6 , pp. 479-492, Nov.1962.

[13] S. Gaspi, and J. Adelman, "Design of combline and interdigital filters with tapped-line input", IEEE Trans. Microwave Theory and Thech., vol. 36, no. 4, pp. 759-763, Apr. 1998.

[14] H.-M. Lee, and Chih-Ming Tsai, "Improved coupled-microstrip filter design using effective even- mode and odd- mode characteristic impedances", IEEE Trans. Microwave Theory and Thech., vol. 53, no. 9, pp. 2812-2818, Sept. 2005.

[15] F.-J. Winter, J.-J. Taub, and M. Marcelli, "high dielectric constant stripline bandpass filters", in IEEE MTT-S Int. Symp. Dig., Boston, USA, July 10-14, 1991.

[16] P. Pramanik, "Compact 900-MHz hairpin-line filters using high dilectric constant microstrip line", in IEEE MTT-S Int. Symp. Dig., Atlanta, USA, June 14-18, 1993.

[17] C.-H. Hsu, H.-T. Soong, C.-L. Huang, and M.-T. Kao, "Microstrip rectangular ring bandpass filter design using high permittivity substrate", in 17th Asia Pacific Microwave Conference, Suzhou, China, Dec. 4-7, 2005.

[18] A.-J. Kennerley, I.-C. hunter, "Miniature microwave filters using high permittivity ceramics", in IEEE MTT-S Int. Symp. Dig., Vancouver, Canada, Feb. 20-22, 1995.

[19] J. S. Hong and M. Lancaster, "Microstrip bandpass filter using degenerate modes of a novel meander loop resonator," IEEE Microwave and guided wave letters, vol. 5, no. 11, pp. 371-372, Nov. 1995.

[20] S.S. Liao, H.K. Chen, Y.C. Chang, and K.T. Li, "Novel reduced-rize coplanar-waveguide bandpass filter using the new folded open stub structure", IEEE Microwave and Wireless Components Lett., vol. 12, no. 12, pp. 476-478, Dec. 2002.

[21] B.S. Kim, J.W. Lee, and M.S. Song, "An implementation of harmonic suppression microstrip filters with periodic grooves", IEEE Microwave and Wireless Components Lett., vol. 14, no. 9, pp. 413-415, Sept. 2004.

[22] Lei Zhu, "Guided-wave characteristics of periodic coplanar waveguides with inductive loading-unit-length transmission parameters", IEEE Trans. Microwave Theory and Tech., vol. 51, no. 10, pp. 2133-2138, Oct. 2003.

[23] J. Marimuthu and M. Esa, "Experimental performance of harmonic suppressed bandpass filter," in Asia Pasific conference on applied electromagnetics, pp. 1-5, Melaka, Malaysia, Dec. 2007.

[24] A. Manchec, C. Quendo, J.F. Favennec, E. Rius, and C. Person, "synthesis of capacitive-coupled dual-behavior resonator (CCDBR) filters," IEEE Trans. Microwave Theory Tech., vol. 54, no. 6, pp. 2346-2355, June2006.

[25] T.T. Boon, J.Y. Jong, T.C. Siou, M.S. Leong, and B.L. Ooi, "A miniaturized dual-mode ring bandpass filter with a new perturbation," IEEE Trans. Microwave Theory Tech., vol. 53, no. 1, pp. 343-348, Jan. 2005.

[26] A. Griol, A. Mira, A. Martinez, J. Marti, and J. Corral, "Microstrip multistage Coupled Ring Bandpass Filters Using Photonic Bandgap Structures for Harmonic Suppression," IEE Electronics Letters, vol. 39, no. 1, pp. 68–70, Jan. 2003.

[27] A. Abdel-Rahman, A. Ali, S. Amari, and A. Omar, "compact bandpass filters using defected ground structure (DGS) coupled resonators", in IEEE MTT-S Int. Symp. Dig., Long Beach, CA, June 12-17, 2005.

[28] J.-T. Kuo, S.-P. Chen, and M. Jiang, "Parallel-Coupled Microstrip Filters With Over-Coupled End Stages for Suppresion of Spurious Responses", IEEE Microwave wireless Components Lett., vol. 13, no. 10, pp.440-442, Oct. 2003.

[29] S.-L. March, "Phase velocity compensation in parallel-coupled microstrip", in IEEE MTT-S Int. Symp. Dig.,Dallas, USA, June 15-17, 1982.

[30] I.-J. Bahl, "Capacitively compensated high performance parallel coupled microstrip filters," in IEEE MTT-S Int. Symp. Dig., Long Beach, USA, June 13-15, 1989.

[31] T. Lopetegi, M.-A. G. Laso, J. Hermandez, M. Bacaicoa, D. Benito, M.-J. Garde, M. Sorolla, and M. Guglielmi, "New Microstrip "Wiggly-Line" Filters with Spurious Passband Suppression", IEEE Trans. Microwave Theory and Tech., vol. 49, no. 9, pp. 1593-1598, Sept. 2001.

[32] J.-T. Kuo, and M.-H. Wu, "Corrugated parallel-coupled line bandpass filters with multispurious suppression", IET Microwave Antennas Propag., vol. 1, no. 1, pp. 718-722, June 2007.

[33] M. Makimoto, and S. Yamashita, "Bandpass filters using parallel coupled stripline stepped impedance resonators", IEEE Trans. Microwave Theory and Tech., vol. 28, no. 12, pp. 1413-1417, Dec. 1980.

[34] M. Jiang, M.-H.Wu, and J.-T.Kuo, "Parallel-Coupled Microstrip Filters With Over-Coupled Stages for Multispurious Suppression", in IEEE MTT-S Int. Symp. Dig. , Long Beach, CA, June 12-17, 2005.

[35] T. Lopetegi, M.-A.G. Laso, F. Falcone, F. Martin, J. Bonache, L. Garcia, M. Perez-Cuevas Sorolla, and M. Guglielmi, "Microstrip "wiggly-line" bandpass filters with multispurious rejection", IEEE Microwave wireless Components Lett., vol. 14, no. 11, pp.531-433,Nov. 2004.

[36] M. Jiang, M.-H. Wu, and J.-T. Kuo, "Parallel-coupled microstrip filters with over-coupled stages for multispurious suppression", in IEEE MTT-S Int. Symp. Dig. , Long Beach, CA, June 12-17, 2005.

[37] J.-T. Kuo, and E. Shih, "Microstrip Stepped Impedance Resonator Bandpass Filter With an Extended Optimal Rejection Bandwidth",IEEE Trans. Microwave Theory and Tech., vol. 51, no. 5, pp. 1554-1559, April 2003.

Chapter II. Compact Stub-Loaded Parallel-Coupled Bandpass Filter: Synthesis and Miniaturization Rules

II.1. Introduction

Recently, with the rapid growth of wireless communication systems, the miniaturization and performance improvement of wireless communication components have become increasingly necessary to enhance system performance and to reduce fabrication cost. In particular, the miniaturization of planar transmission line filters inspired a great deal of interest due to their advantage as a planar circuit due to their simplicity in fabrication, as well as their low cost.

In order to obtain compact RF and microwave filters based on planar technologies, several miniaturization approaches exist. Miniaturized of planar filter can be achieved by using high dielectric constant substrates [1]-[4], this technique yields acceptable miniaturization ratios however, only low characteristic impedances and large gaps can be achieved. Thus meeting drastic templates could become very difficult. Another miniaturization approach can be obtained by using slow wave transmission lines to reduce the phase velocity and then the guided wavelength [5], [6]. Also, the distributed approach considering meandered and folded transmission lines can be used [7]-[9], but at the expense of an important work to model parasitic couplings.

In this chapter, a distributed but compact filter topology is presented, based on parallel-coupled open-ended transmission lines loaded by short-circuited stubs. A background theory of such resonators is presented, describes the principle of the Stub-Loaded Resonator (SLR), with a careful comparison between measurement and simulation results for the determination of the resonant frequency. This is followed

by a discussion on the miniaturization rules of the (SLR) describing how to improve the compactness of the filter. A comparison between the electrical length of the SLR and that of classical half open-ended and quarter-wavelength resonators is then carried out. Next, the complete synthesis method of such bandpass filter, built in an inhomogeneous medium, with arbitrary coupled line lengths, is developed. This chapter also deals with the problems of parallel-coupled lines' filters, when they are built in inhomogeneous medium (such as microstrip) due to the difference of mode velocities.

II.2. Parallel-Coupled Stub-Loaded Resonator bandpass filter structure

Cascading parallel-coupled line sections give rise to bandpass filter structure. The conventional *n* stage parallel-coupled bandpass filter based on half-wavelength resonators, has been widely used in many microwave and millimeter wave systems. This type of filter is popular since it has a planar structure, good repeatability, and a simple synthesis procedure [10]-[12]. The required physical size of conventional microstrip bandpass filters is a limitation to circuit miniaturization. The PC-SLR (Parallel-Coupled Stub-Loaded Resonator) bandpass filter, subject of our study, is proposed to solve this disadvantage. Advantages of this filter are its compactness (more than 50 % size reduction can be achieved as compared to the conventional bandpass filter), and a large upper out-of-band rejection [13], [14].

The basic configuration of an *n*-stage PC-SLR bandpass filter is based on open-ended transmission lines loaded from their middle by a short-circuited stub as shown in Figure II-1. The SLR is effective in realizing compact bandpass filter. This resonator behaves like short-circuited quarter wavelength resonator, allowing a reduction of the longitudinal filter dimension since the coupled lines are smaller than

quarter wavelength. The resonance characteristics of the PC-SLR bandpass filter structure have been studied both theoretically and experimentally.

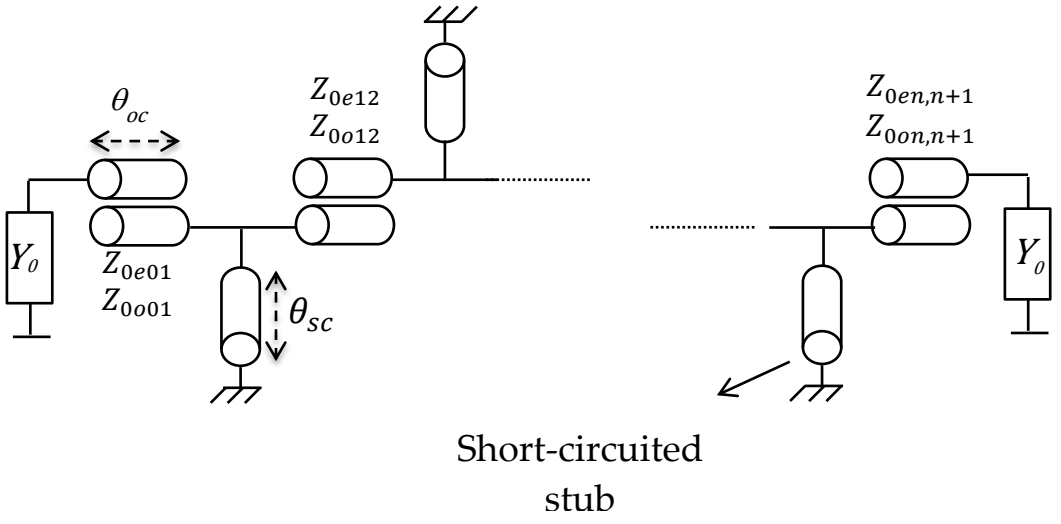

Figure II-1. Parallel-Coupled Stub-Loaded Resonator Bandpass filter.

II.3. Theoretical study of the stub-loaded resonator

The theoretical study of the SLR, based on computing its input admittance Y_{in}, allows a detailed study of its fundamental resonance frequency and determines the miniaturization rules of this resonator structure.

II.3.1. Topology of the SLR

Figure II-2 presents the topology of the proposed SLR resonator. It consists of an open-ended elementary transmission line of electrical length $2 \cdot \theta_{oc}$ ("*oc*" for open-circuit), and characteristic impedance Z_{oc} , loaded at its center by a short-circuited stub of electrical length θ_{sc} ("*sc*" for open circuit) and characteristic impedance Z_{sc}.

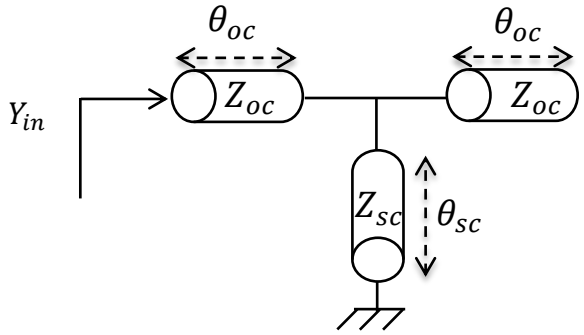

Figure II-2. Schematic view of an elementary SLR.

II.3.2. Fundamental resonance frequency of the SLR

This section discusses the condition of fundamental resonance frequency of the symmetrical SLR. Let us define f_0 as the fundamental resonance frequency of the SLR. The expression of this resonance frequency is derived from the input admittance Y_{in}. Simplifications on the expression of f_0 are proposed in order to propose a simple expression for the study of the stub-loaded resonators. These simplifications are then validated theoretically by simulations and measurements.

a) Fundamental resonance condition

The resonator structure to be considered here is shown in Figure II-3 (a). The input admittance Y_{in} of the SLR resonator from the open-ended transmission line can be calculated by considering *ABCD* matrix operations. We consider ideal lossless transmission lines as a first approximation.

The *ABCD* matrix of each transmission line (stub and open-ended transmission line) is given in (II.1):

$$\begin{bmatrix} A & B \\ C & D \end{bmatrix} = \begin{bmatrix} cos(\theta_{oc,sc}) & jZ_{oc,sc}\, sin(\theta_{oc,sc}) \\ j\frac{sin(\theta_{oc,sc})}{Z_{oc,sc}} & cos(\theta_{oc,sc}) \end{bmatrix} \quad \text{(II.1)}$$

By considering the short-circuited condition of the stub ($V = 0$) and the open-ended condition of the elementary open-ended transmission line ($I = 0$) (Figure II-3 (a)), their input admittances Y_{in_sc} and Y_{in_oc} are hence given by:

$$Y_{in\_sc} = \frac{1}{j \cdot Z_{sc} \cdot tan(\theta_{sc})} \tag{II.2}$$

$$Y_{in\_oc} = \frac{j \cdot tan(\theta_{oc})}{Z_{oc}} \tag{II.3}$$

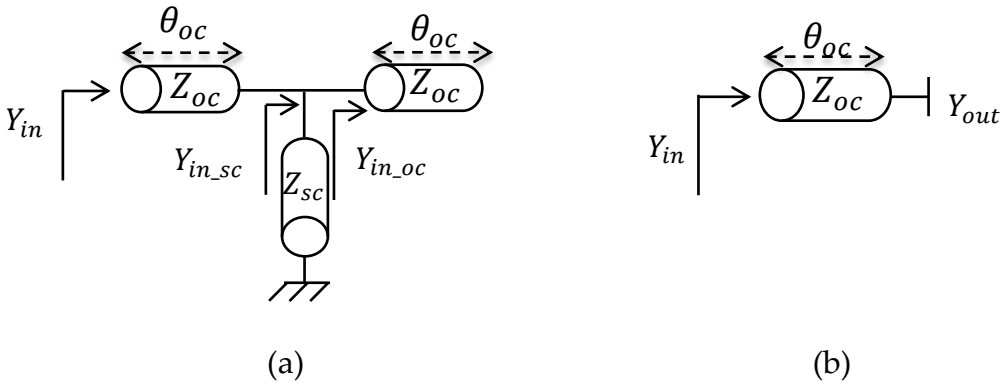

(a) (b)

Figure II-3. (a), (b) Equivalent circuits for derivation of the input admittance Y_{in}.

The output admittance Y_{out} in Figure II-3 (b) can be expressed from (II.2) and (II.3) by:

$$Y_{out} = j \cdot (Y_{oc} \cdot tan(\theta_{oc}) - Y_{sc} \cdot cot(\theta_{sc})) \tag{II.4}$$

where Y_{oc} and Y_{sc} are the characteristic admittance of the open-ended transmission line and the short-circuited stub, respectively.

Using the expression of Y_{out} and based on the equivalent circuit in Figure II-3 (b), the input admittance is then expressed by:

$$Y_{in} = j \cdot Y_{oc} \cdot \frac{2 \cdot \tan(\theta_{oc}) \cdot \tan(\theta_{sc}) - R_Z}{\tan(\theta_{oc})(R_Z - \tan(\theta_{oc}) \cdot \tan(\theta_{sc})) + \tan(\theta_{sc})} \tag{II.5}$$

where $R_Z = \frac{Z_{oc}}{Z_{sc}}$ is defined as the characteristic impedance ratio.

The resonance condition can be easily obtained for $Y_{in} = 0$ and it can be expressed as:

$$R_Z = 2 \cdot \tan(\theta_{oc}) \cdot \tan(\theta_{sc}) \quad \text{(II.6)}$$

From this condition it is obvious that the resonance condition of SLR is determined by electrical transmission lengths (θ_{oc},θ_{sc}) and impedance ratio, while in the case of a classical half wavelength open-ended resonator, the resonance condition is only determined by the electrical length of the transmission line. This gives to the PC-SLR filter an extra degree of freedom as compared to a classical parallel-coupled bandpass filter.

b) Stub-loaded resonator behavior, based on an approximated expression of the fundamental resonance frequency

This section aims to derive a simple equation in order to study the behavior of a single SLR. In order to simplify the resonance condition in (II.6), considering small electrical lengths since we are interested in miniature transmission lines (where non-quarter wavelength are used) and by using "Taylor series" approximation the fundamental resonance frequency can be derived from (II.6) and can be estimated as

$$f_0 = \frac{1}{2.\pi}\sqrt{\frac{R_Z}{2.K_{sc}.K_{oc}}} \quad \text{(II.7)}$$

where K_{sc} and K_{oc} are the phase delays of short and open-ended transmission lines, respectively. They are expressed as:

$$K_i = \sqrt{\varepsilon_{reff\_i}}.\frac{l_i}{c}\text{, with } i\text{=}sc \text{ or } oc \quad \text{(II.8)}$$

where ε_{reff_sc}, ε_{reff_oc} and l_{sc}, l_{oc} are the relative effective permittivities and physical lengths of the short-circuited stub and the open-ended elementary transmission line, respectively.

From (II.7), it is obvious that f_0 is inversely proportional to the short-circuited stub length l_{sc} and the open-ended transmission line length l_{oc}. As for SIRs [15], the particularity of this SLR is the dependence R_Z ratio on f_0. The smaller the R_Z ratio,

the smaller the resonant frequency is. Hence, by considering a small characteristic impedance ratio a compact filter is achieved.

c) Validation: simulated third order PC-SLR bandpass filter

In order to verify the resonance condition given by equation (II.7), an unloaded resonator was designed with Agilent ADS™ on a RT5880 substrate (relative permittivity ε_r = 2.2; dielectric loss tangent $tg\ \delta$ = 0.0009; dielectric thickness h = 787 μm; copper thickness t = 17 μm).

For this resonator, the characteristic impedances Z_{sc} and Z_{oc} equal 118.6 Ω and 50.7 Ω, respectively, leading to a characteristic impedance R_Z ratio of 0.4. The microstrip widths are 0.4 mm and 2.3 mm, leading to effective relative permittivities ε_{reff_sc} = 1.7 and ε_{reff_oc} = 1.9, respectively. The physical lengths were fixed to 19.8 mm and 10.9 mm, to obtain a resonance frequency equal to 1 GHz. Inductance of 0.53 nH and series resistance of 0.1 Ω were added to the ADS via hole model in the simulated SLR circuit. These values of inductance and series resistance correspond to values carefully estimated by comparison of several circuits incorporating via holes in order to well-take the via parasitic into account.

Figure II-4 shows the photograph of the unloaded SLR. In order to measure the resonance frequency, the resonator was slightly coupled to near and far end feeding transmission lines. Let us notice that the physical length of the open-ended transmission line (2. l_{oc}) equals 21.8 mm, corresponding to 0.1 λ_{oc} (where λ_{oc} is the guided wavelength of the open-ended transmission line), leading to a resonator length more than four times smaller than a typical half-wavelength resonator.

Figure II-5 shows the comparison between the measured and simulated parameters of the slightly coupled SLR. Measurement results show a resonant frequency lower by 5 MHz from the simulation prediction (0.5 %), thus providing the validity of the approximated frequency expression.

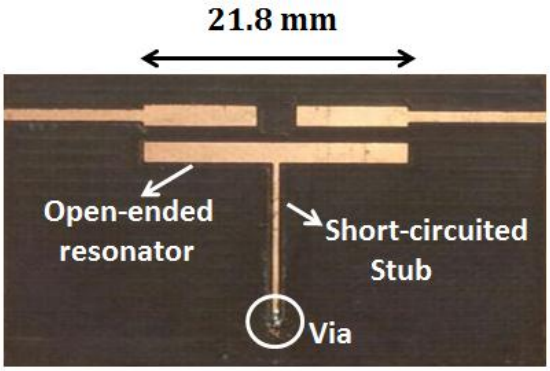

Figure II-4. Photograph of the slightly coupled SLR.

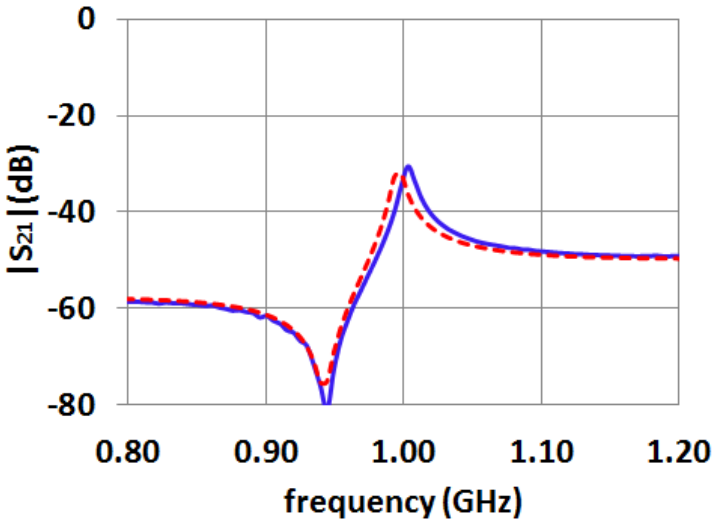

Figure II-5. Measured (blue solid line) and simulated (red dashed line) transmission parameter for a slightly coupled SLR.

II.3.3. Miniaturization rules of the SLR

This section defines the miniaturization rules for the SLR, based on the fundamental resonance condition presented in the previous section. First, the miniaturization of the open-ended resonators was considered, i.e. the longitudinal dimension. Next the total SLR electrical length was considered.

a) Optimum longitudinal dimension

The relationship between θ_{oc} and θ_{sc} is derived from (II.6) as:

$$\theta_{oc} = \operatorname{atan}\left(\frac{R_Z}{2.\tan(\theta_{sc})}\right) \qquad \text{(II.9)}$$

Figure II-6 shows the electrical length $2.\theta_{oc}$ versus the electrical length θ_{sc} at the resonant frequency f_0, for different R_Z values varying from 0.2 to 6.

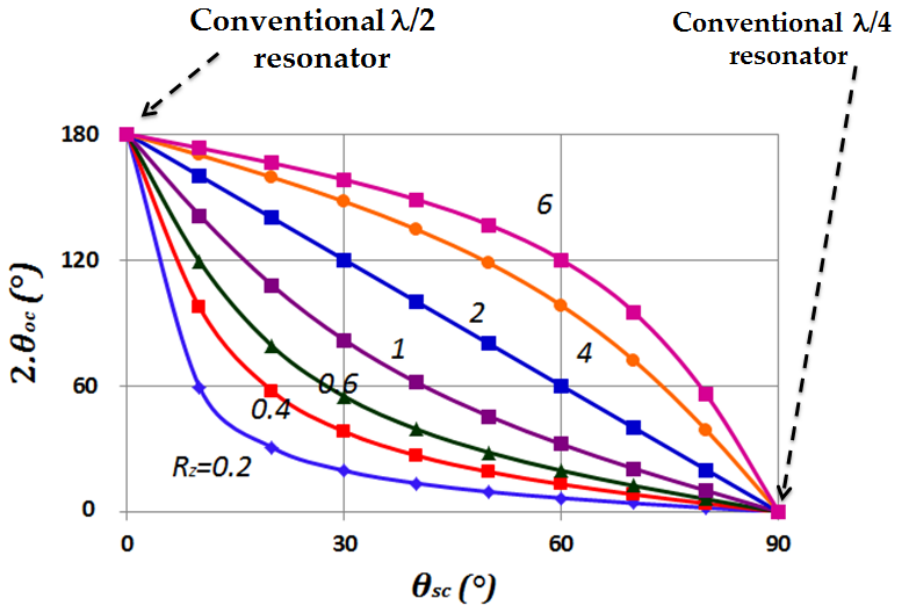

Figure II-6. The electrical length of the open-ended transmission line $2.\theta_{oc}$ versus the electrical length of the short circuited stub θ_{sc} at f_0.

It is obvious from Figure II-6 that to obtain small longitudinal electrical lengths of the SLR, given by $2\theta_{oc}$, and thus of the filter, it is necessary to consider a long short-circuited stub (a folded stub could be realized to obtain compact transversal filter dimensions). However, in this case, it is evident that small relative bandwidths will be achieved since small coupling sections θ_{oc} are considered. The smaller R_Z, the smaller θ_{oc} and θ_{sc}, at the resonance frequency f_0. For example, a compact longitudinal SLR of 60° open-ended electrical length transmission line corresponding to one-third of a classical half-wavelength resonator, can be obtained by considering each of the following cases: ($R_Z = 0.2, \theta_{sc} = 9.8°$), ($R_Z = 0.4, \theta_{sc} = 19.1°$), ($R_Z = 4, \theta_{sc} = 73.1°$) ….

b) Optimum total SLR electrical length

The overall length of the SLR can be defined as:

$$\theta_T = \theta_{sc} + 2\theta_{oc}$$

$$\theta_T = \theta_{sc} + 2\,\mathrm{atan}\left(\frac{R_Z}{2\tan(\theta_{sc})}\right) \qquad \text{(II.10)}$$

Figure II-7 presents the plot of the total electrical length of the SLR (θ_T) versus the electrical length of the short circuited stub electrical length θ_{sc}, for different R_Z values.

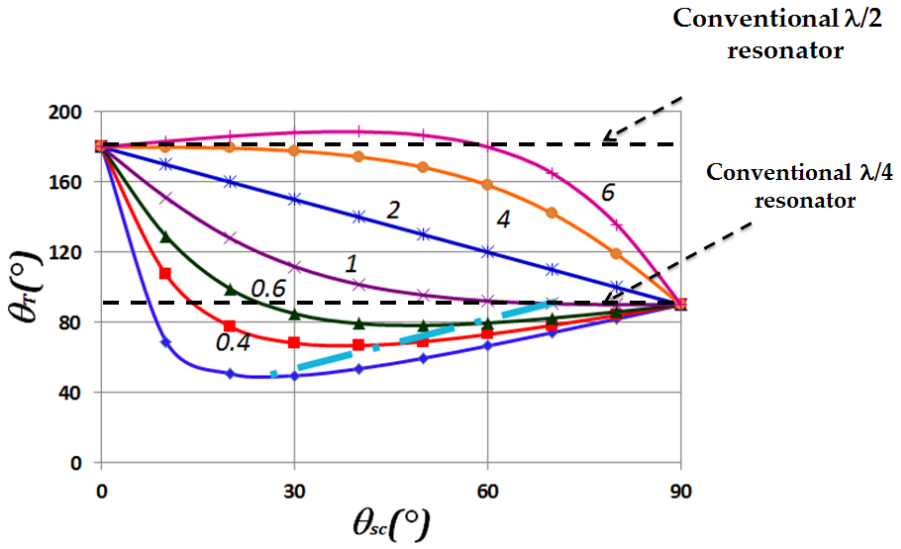

Figure II-7. Total electrical length of the stub-loaded resonator (θ_T) versus θ_{sc} at f_0 compared to the electrical length of conventional half and quarter wavelength resonators.

We notice that θ_T reaches its minimum values for $R_Z \leq 1$ and maximum value for $R_Z > 1$. Thus, a great reduction can be achieved by considering small characteristic impedance ratios. Let us notice that decreasing the characteristic impedance ratio leads to a small width of the short-circuited stub. At IMEP-LAHC the smallest width size that can be made in our technology is around 0.25 mm. The dashed cyan straight line traced at Figure II-7 gives the minimum electrical lengths of the SLR. $R_Z = 0.2$ leads to a minimum 49° total electrical length, which is approximately the half of a classical quarter-wavelength resonator.

c) Optimization of the PC-SLR topology

Based on the above analysis a compact filter in term of longitudinal dimension can be achieved by choosing a long short-circuited stub. From Figure II-6, the

proposed PC-SLR bandpass filter can be 50 % smaller as compared to the classical parallel-coupled bandpass filter.

If the total electrical length is considered, the choice of a good compromise between θ_{sc} and θ_{oc}can lead to a total electrical length twice shorter as compared to a conventional quarter-wavelength resonator, as shown in Figure II-7, for $R_z = 0.2$ and $\theta_{sc} \approx 25°$.

In this work, we were interested in achieving high PC-SLR surface miniaturization. Thus, our PC-SLR filters were designed using small R_Z and θ_T values, with the constraint of achievable short-circuited stub width and realizable gap size of the parallel-coupled sections, depending on the employed substrate and the targeted relative bandwidth.

II.4. Synthesis method of the PC-SLR bandpass filter in a homogeneous technology

This section describes a synthesis method for the parallel-coupled filters based on stub-loaded resonators. By considering *J*-inverters, synthesis formulas are derivated for TEM transmission lines (such as stripline). For these TEM transmission lines, odd and even characteristic impedances and electrical lengths of each coupled-line section can be well determined analytically. Simulations are presented to validate the theory for three relative bandwidths 4, 6 and 8 %. For a proof-of-concept a third order stripline bandpass filter was designed with passband ripple of 0.01 dB and relative bandwidth of 4.5 %. Theory, simulations and measurements are in good agreement and thus validate the theory.

II.4.1. Design procedure

a) Parallel Coupled Section

As previously described the electrical length of the open-ended resonator θ_{oc} is not limited to π/2 for SLR. This is the main difference compared to conventional coupled-line filters. It justifies the development of a new synthesis procedure. Paralell-coupled lines of electrical length θ_{oc}, applied to a homogeneous technology, and their equivalent circuit using *J*-inverter as described in [16]-[18] are recalled in Figure II-8. The electrical parameters of this circuit are expressed by even- and odd-mode impedances (Z_{0e}, Z_{0o}), and electrical coupling θ_{oc}.

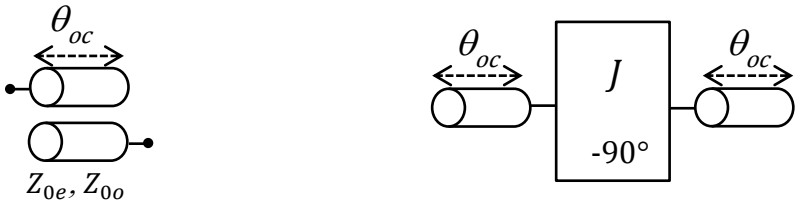

(a) (b)

Figure II-8. (a) Parallel-Coupled line and (b) Equivalent circuit using J-inverter.

The *ABCD* matrix of this parallel-coupled line $[ABCD]_{cc}$ ('cc' for coupled-line circuit) (Figure II-8 (a)) derived from the $[Z]$ matrix is given by [16]:

$$[ABCD]_{cc} = \begin{bmatrix} \frac{Z_{0e}+Z_{0o}}{Z_{0e}-Z_{0o}} cos(\theta_{oc}) & j\frac{(Z_{0e}-Z_{0o})^2-(Z_{0e}+Z_{0o})^2.cos^2(\theta_{oc})}{2(Z_{0e}-Z_{0o}).sin(\theta_{oc})} \\ j.\frac{2.sin(\theta_{oc})}{Z_{0e}-Z_{0o}} & \frac{Z_{0e}+Z_{0o}}{Z_{0e}-Z_{0o}}.cos(\theta_{oc}) \end{bmatrix} \quad \text{(II.11)}$$

In the case of homogeneous technology, the electrical even- and odd- mode electrical lengths are equal since the phase velocities for both modes are equal. From studies in [17]-[18], the coupled circuit in Figure II-8 (a) should behave in the same way as an equivalent circuit consisting of two single transmission lines of electrical length θ_{oc} and characteristic impedance Z_{oc} with an admittance inverter (Figure II-8). The *ABCD* parameters of the admittance inverter are obtained by considering it as a

quarter-wavelength transmission line of characteristic impedance $\frac{1}{J}$. Let us notice, that for a fixed narrowband filter, the inverter may be regarded as a frequency-independent element [11]. Using the *ABCD* matrices of each elements in Figure II-8 (b), the cascaded *ABCD* matrix of the equivalent circuit, [*ABCD*]ec ('ec' for equivalent parallel-coupled circuit) is given by:

$$[ABCD]_{ec} = \begin{bmatrix} \left(J.Z_{oc} + \frac{1}{J.Z_{oc}}\right).\sin(\theta_{oc}).\cos(\theta_{oc}) & j.\left(J.Z_{oc}^2.sin^2(\theta_{oc}) - \frac{1}{J}.\cos^2(\theta_{oc})\right) \\ j.\left(\frac{1}{J.Z_{oc}^2}.sin^2(\theta_{oc}) - J.cos^2(\theta_{oc})\right) & \left(J.Z_{oc} + \frac{1}{J.Z_{oc}}\right).\sin(\theta_{oc}).\cos(\theta_{oc}) \end{bmatrix} \quad \text{(II.12)}$$

Equating the $[ABCD]_{cc}$ and $[ABCD]_{ec}$ matrices of (II.11) and (II.12), we obtain:

$$\frac{Z_{0e}+Z_{0o}}{Z_{0e}-Z_{0o}}cos(\theta_{oc}) = \left(J.Z_{oc} + \frac{1}{J.Z_{oc}}\right).sin(\theta_{oc}).cos(\theta_{oc}) \quad \text{(II.13)}$$

$$\frac{(Z_{0e}-Z_{0o})^2-(Z_{0e}+Z_{0o})^2.\cos^2(\theta_{oc})}{2(Z_{0e}-Z_{0o}).\sin(\theta_{oc})} = (J.Z_{oc}^2.sin^2(\theta_{oc}) - \frac{1}{J}.\cos^2(\theta_{oc})) \quad \text{(II.14)}$$

$$\frac{2.\sin(\theta_{oc})}{Z_{0e}-Z_{0o}} = \frac{1}{J.Z_{oc}^2}.sin^2(\theta_{oc}) - J.cos^2(\theta_{oc}) \quad \text{(II.15)}$$

The odd- and even- mode characteristic impedances, derived from the above equations are given by [17]-[18]:

$$Z_{0e} = Z_{oc}\frac{1+Z_{oc}.J.cosec(\theta_{oc})+(Z_{oc}.J)^2}{1-(Z_{oc}.J)^2cot^2(\theta_{oc})} \quad \text{(II.16)}$$

$$Z_{0o} = Z_{oc}\frac{1-Z_{oc}.J.cosec(\theta_{oc})+(Z_{oc}.J)^2}{1-(Z_{oc}.J)^2cot^2(\theta_{oc})} \quad \text{(II.17)}$$

b) Equivalent circuits and slope parameters

This section presents equivalent circuits for the PC-SLR filter to develop further the design procedure. We consider an n^{th} order PC-SLR filter as shown in Figure II-1. The equivalent *J*-inverter circuit is shown in Figure II-9 (a). Figure II-9 (b) and (c) show the equivalent circuit of the first section expressed by the admittance Y_A of the input port and the admittance Y_B looking to the J_{01} inverter. Figure II-9 (d) represents the PC-SLR equivalent circuit based on susceptances B_i and B_b.

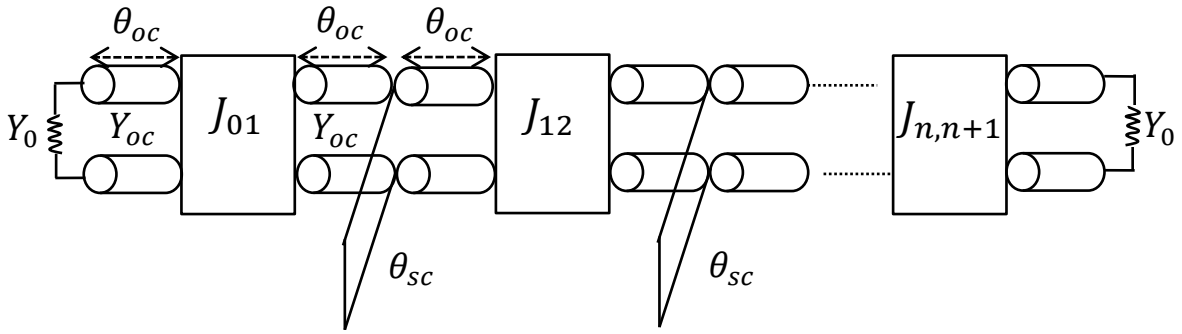

(a)

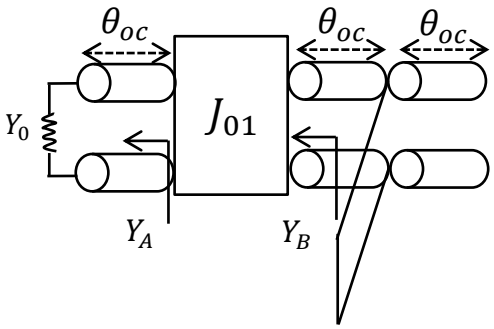

(b)

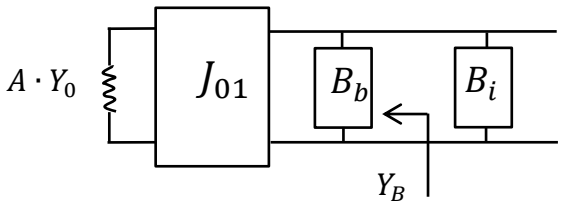

(c)

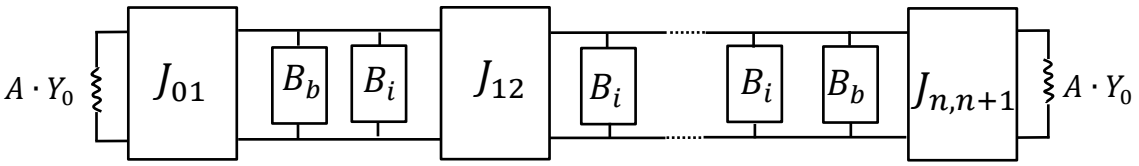

(d)

Figure II-9. (a) Equivalent J-inverter circuit of the PC-SLR filter. (b), (c) Equivalent circuits of the first section. (d) Equivalent circuit based on susceptance parameters for derivation of J-inverter equations.

The admittance Y_A shown in Figure II-9 (b), based on a *ABCD* matrix analysis can be expressed as:

$$Y_A = \frac{j \cdot Y_{oc} \cdot tan(\theta_{oc}) + Y_0}{1 + j \cdot tan(\theta_{oc}) \cdot \frac{Y_0}{Y_{oc}}} \tag{II.18}$$

The admittance Y_B is given by:

$$Y_B = \frac{J_{01}^2}{Y_A}$$

Using (II.18), it can be derived:

$$Y_B = \frac{J_{01}^2}{Y_0 \frac{1+\left(\frac{Y_{oc}}{Y_0}\right)^2 . tan^2(\theta_{oc})}{1+tan^2(\theta_{oc})}} + j \frac{J_{01}^2}{Y_{oc}} \cdot \frac{1-\left(\frac{Y_{oc}}{Y_0}\right)^2}{1+\left(\frac{Y_{oc}}{Y_0}\right)^2 \cdot tan^2(\theta_{oc})} \cdot tan(\theta_{oc}) \tag{II.19}$$

The susceptance B_b in Figure II-9 (c) can be expressed from (II.19) by:

$$B_b = \frac{J_{01}^2}{Y_{oc}} \cdot \frac{1-\left(\frac{Y_{oc}}{Y_0}\right)^2}{1+\left(\frac{Y_{oc}}{Y_0}\right)^2 \cdot tan^2(\theta_{oc})} \cdot tan(\theta_{oc}) \tag{II.20}$$

Let us define *A* as:

$$A = Y_0 \frac{1+\left(\frac{Y_{oc}}{Y_0}\right)^2 . tan^2(\theta_{oc})}{1+tan^2(\theta_{oc})} \tag{II.21}$$

The parameter B_i shown in Figure II-9 (c) expresses the susceptance parameter of the resonator drawn in Figure II-10.

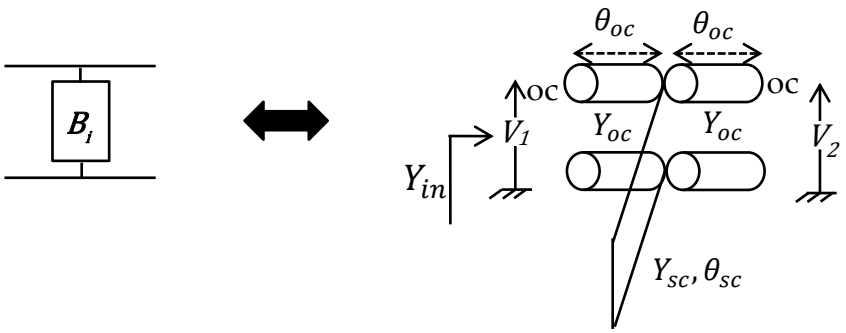

Figure II-10. Equivalent circuit for derivation of the susceptance parameter equation B_i.

B_i can be obtained from the input admittance Y_{in} (II.5) as:

$$B_i = Imag(Y_{in})$$

$$B_i = Y_{oc} \cdot \frac{2 \cdot tan(\theta_{oc}) \cdot \tan(\theta_{sc}) - R_Z}{tan(\theta_{sc}) + tan(\theta_{oc}) \cdot (R_Z - tan(\theta_{sc}) \cdot tan(\theta_{oc}))} \quad \text{(II.22)}$$

The slope parameters of B_i and B_b can be expressed as (II.23) and (II.24), respectively:

$$b_i = \frac{\omega_0}{2} \frac{dB_i}{d\omega}\Big|_{\omega=\omega_0} \quad \text{(II.23)}$$

$$b_i = Y_{oc} \cdot \frac{\left(16 \cdot \theta_{oc}\left(1 - cos^2(\theta_{sc})\right) + 8 \cdot R_Z \cdot \cos^2(\theta_{oc}) \left(\theta_{sc} + \theta_{oc} \cdot R_Z \cdot cos^2(\theta_{sc})\right) - 4 \cdot \theta_{oc} \cdot R_Z \cdot \sin(2 \cdot \theta_{sc}) \cdot \sin(2 \cdot \theta_{oc})\right)}{16 \cdot cos^2(\theta_{sc}) \cdot cos^4(\theta_{oc})(cos(2 \cdot \theta_{oc}) \cdot tan(\theta_{sc}) \cdot sec^2(\theta_{oc}) + R_Z \cdot tan(\theta_{oc}))^2}$$

$$b_b = \frac{\omega_0}{2} \frac{dB_b}{d\omega} = \frac{J_{01}^2 . \theta_{oc}}{2 Y_{oc} \cos(\theta_{oc})^2} \frac{\left(Y_0^2 - Y_{oc}^2 \tan(\theta_{oc})^2\right)}{\left(Y_0^2 + Y_{oc}^2 \tan(\theta_{oc})^2\right)} (Y_0^2 - Y_{oc}^2) \quad \text{(II.24)}$$

c) Filter design

According to the targeted center frequency (f_0), relative bandwidth (w) and ripple, the filter order and element values (g_i) can be determined after specifying the filter response (Chebyshev , Butterwoth, …).

The synthesis starts by choosing R_Z and θ_{oc} for the elementary SLR. Next, the value of θ_{sc} can be calculated from (II.6). The admittance inverter parameters $J_{j,j+1}$ can be calculated based on Figure II-9 (d) as follows:

$$J_{01} = J_{nn+1} = \sqrt{\frac{Y_0 . A . w . (b_i + b_b)}{g_0 g_1}} \quad \text{(II.25)}$$

By using (II.24), J_{01} can be written as follows:

$$J_{01} = \sqrt{\frac{Y_0 . A . b_i}{g_0 \cdot g_1 - Y_0 \cdot A \cdot \frac{W \cdot \theta_{oc} (Y_0^2 - Y_{0c}^2)(Y_0^2 - Y_{0c}^2 \cdot tan^2(\theta_{oc}))}{2 Y_{oc} \cdot . cos(\theta_{oc})^2 \cdot (Y_0^2 + Y_{0c}^2 \cdot tan^2(\theta_{oc}))^2}}} \quad \text{(II.26)}$$

$$J_{12} = J_{nn-1} = w \cdot \sqrt{\frac{(b_i + b_b) . b_i}{g_1 g_2}} \quad \text{(II.27)}$$

$$J_{jj+1} = w.\frac{b_i}{\sqrt{g_j g_{j+1}}} \qquad (j = 2 \ldots n\text{-}2) \qquad \text{(II.28)}$$

Once the J parameters are determined, the odd- and even-mode characteristic impedances of each coupled line can be computed using the formulas of the non-quarter-wavelength coupled lines (II.16) and (II.17). Using the values obtained for the electrical parameters, the physical parameters of the coupled lines can be calculated for a homogeneous medium (stripline). Note that the image impedance Z_{oc} of the open-ended resonator was set to 50 Ω.

II.4.2. Validation of the theory

a) Simulation responses

The design equations were validated through simulations where ideal transmission lines are considered. Third order PC-SLR filters were designed with passband ripple of 0.01, a center frequency of 879 GHz and with relative bandwith values of 2 % (designed with“case 1”), 4 % (“case 2”) and 8 % (“case 3”). Let notice that the bandwidth (w) mentioned in this section, for simulation result, is not 3-dB bandwidth, but the bandwidth related to the frequency range between the lowest and the highest frequencies, when the insertion loss is equal to the targeted ripple. This bandwidth is measured when ideal transmission lines are considered. Thus in the case of the 0.01 dB ripple chebychev PC-SLR bandpass filter, the bandwidth is the frequency range between the lowest and highest frequencies where the insertion loss is 0.01 dB. As previously mentioned, it is convenient to consider a small R_Z value (<1) in order to achieve compact PC-SLR size filters. Hence the filters were designed for characteristic impedance ratios R_Z = 0.2, 0.4, and 0.6. The following cases are considered:

- $R_Z = 0.2, \theta_{oc} = 12.3°$,
- $R_Z = 0.4, \theta_{oc} = 16.7°$,
- $R_Z = 0.6,\ \theta_{oc} = 19.8°$,

These electrical lengths were chosen in order to obtain a wide out-of-band rejection (as will be seen in Chapter III).

Case1: $w = 2$ %

Table II-1 gives the odd- and even- mode characteristic impedances (computed based on the above analysis) of the PC-SLR bandpass filters for a 2 % relative bandwidth, for R_Z = 0.2, 0.4, 0.6.

Table II-1. Electrical parameters of the third order PC-SLR filters for a 2 % relative bandwidth, for several R_Z values.

R_Z	θ_{oc} (°)	$Z_{0e01}(\Omega)$	$Z_{0o01}(\Omega)$	Z_{0e12} (Ω)	$Z_{0o12}(\Omega)$
0.2	12.3	112.84	32.37	52.89	47.44
0.4	16.7	98.14	33.79	53.03	47.3
0.6	19.8	92.85	34.47	53.23	47.16

Figure II-11 shows the simulation responses of the PC-SLR filters in a narrow band for $R_Z = 0.2, \theta_{oc} = 12.3°$ (red dotted line), $R_Z = 0.4, \theta_{oc} = 16.7°$ (blue dashed line), and $R_Z = 0.6, \theta_{oc} = 19.8°$ (dotted mallow line). It proves that the passband reponses coincide well with the specifications given for a 0.01 dB with a relative bandwidth of 2 %.

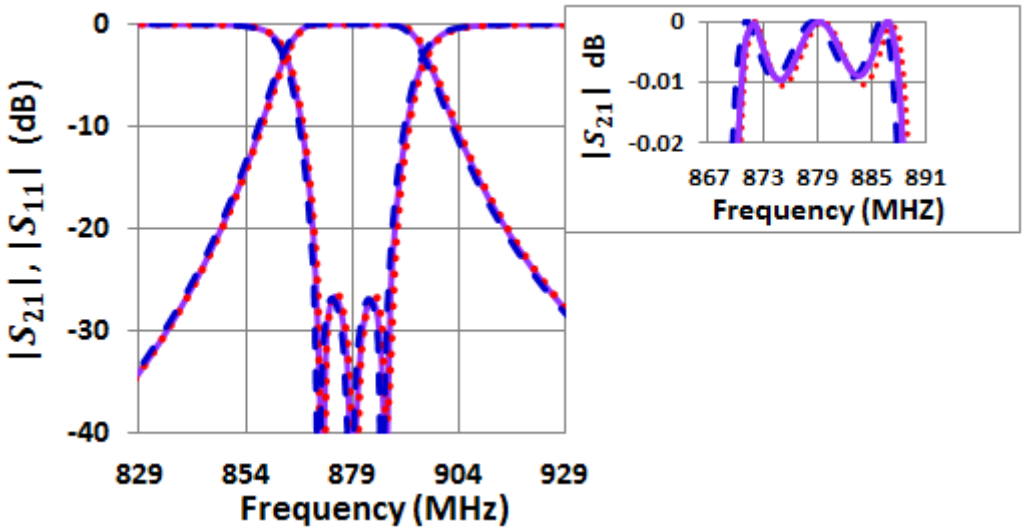

Figure II-11. Comparison of S-parameters simulation of the PC-SLR filters for $R_Z = 0.2, \theta_{oc} = 12.3°$(red dotted line), $R_Z = 0.4, \theta_{oc} = 16.7°$(blue dashed line), and $R_Z = 0.6, \theta_{oc} = 19.8°$ (dotted mallow line), for a 2 % relative bandwidth.

Case2: $w = 4$ %

Here again, the odd- and even- mode characteristic impedances are computed for R_Z = 0.2, 0.4, 0.6, but with a 4 % relative bandwidth (Table II-2).

Table II-2. Electrical parameters of the third order PC-SLR filters for a 4 % relative bandwidth, for several R_Z values.

R_Z	θ_{oc} (°)	$Z_{0e01}(\Omega)$	$Z_{0o01}(\Omega)$	Z_{0e12} (Ω)	$Z_{0o12}(\Omega)$
0.2	12.3	229.68	29.38	56.07	45.13
0.4	16.7	159.59	30.76	56.49	44.87
0.6	19.8	140.65	31.55	56.93	44.71

Figure II-12 shows the simulation responses of the PC-SLR filters in a narrow band for $R_Z = 0.2, \theta_{oc} = 12.3°$ (red dotted line), $R_Z = 0.4, \theta_{oc} = 16.7°$ (blue dashed line), and $R_Z = 0.6, \theta_{oc} = 19.8°$ (dotted mallow line). Also the passband responses coincide with the specifications given for a 0.01 dB with a relative bandwidth of 4 %. Hence the design method is validated.

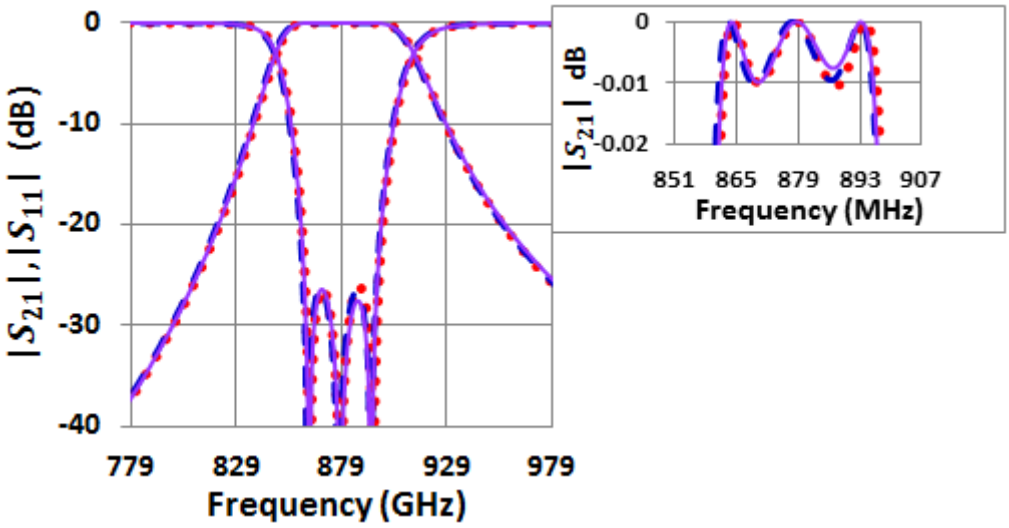

Figure II-12. Comparison of S-parameters simulation of the PC-SLR filters for $R_Z = 0.2, \theta_{oc} = 12.3°$(red dotted line), $R_Z = 0.4, \theta_{oc} = 16.7°$(blue dashed line), and $R_Z = 0.6, \theta_{oc} = 19.8°$ (dotted mallow line), for a 4 % relative bandwidth.

Case3: $w = 8$ %

Indeed, the more the fractional bandwidth the greater the required electrical length needed to achieve a stronger coupling. Thus for a 8 % relative bandwidth the two

cases ($R_Z = 0.2, \theta_{oc} = 12.3°$) and ($R_Z = 0.4, \theta_{oc} = 16.7°$) cannot be treated. Table II-3 gives the odd- and even- mode characteristic impedances.

Table II-3. Electrical parameters of the third order PC-SLR filters for a 8 % relative bandwidth.

R_Z	θ_{oc} (°)	$Z_{0e01}(\Omega)$	$Z_{0o01}(\Omega)$	Z_{0e12} (Ω)	$Z_{0o12}(\Omega)$
0.6	19.8	465.27	36.79	65.89	40.43

For 8 % relative bandwidth the passband response didn't coincide well with the specifications given for a 0.01 dB as shown in Figure II-13.

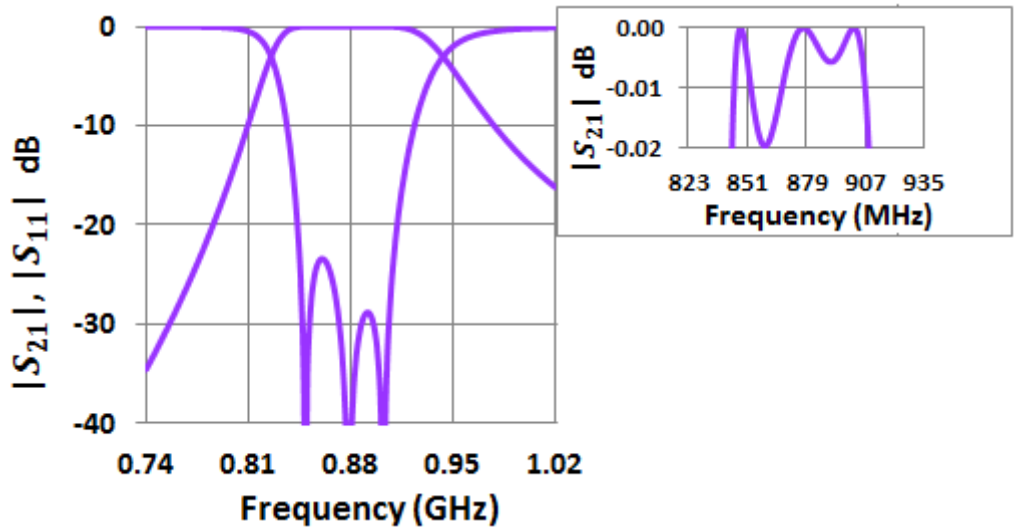

Figure II-13. S parameters of the PC-SLR filter $R_Z = 0.6, \theta_{oc} = 19.8°$ for a 8 % relative bandwidth.

Since the slop parameters are derivate near the center frequency, thus the desired response deteriorates when the designed bandwidth becomes larger as shown in Figure II-13.

b) Proof-of-concept filter design

For a proof-of-concept a third order PC-SLR bandpass filter was designed, with passband ripple of 0.01 dB, a relative bandwidth of 4 %, and a center frequency f_0 of 879 MHz, in a stripline technology. The open-ended transmission line electrical length was set to 29°. This value of θ_{oc} was chosen in order to obtain achievable gap

size, with a minimum gap of around 110 µm in the technology used. The maximum achievable value was chosen for characteristic impedance of the stub, i.e. $Z_{sc} = 171\ \Omega$, in order to get the minimum R_Z value, leading to good compactness along with a maximum rejection band width [14]. The odd- and even- impedances were then calculated based on the above analysis.

The filter was designed with Agilent ADS™ and fabricated on a RT5880 substrate (dielectric constant $\varepsilon_r = 2.2$, dielectric loss tangent $tan\delta = 0.9.10^{-3}$, substrate thickness $B = 2 \cdot h = 6.35$ mm, copper thickness $t = 17$ µm). Using the values obtained for the electrical parameters, the physical parameters were calculated with the use of ADS LineCalc (Table II-4).

Table II-4. Parameters of the PC-SLR Filter.

		Parameters	Values
Electrical parameters of The PC-SLR	**Parallel-coupled Lines for input/output resonators**	Z_{0e01}	96 Ω
		Z_{0o01}	34 Ω
		θ_{oc}	29°
	Internal parallel-coupled lines	Z_{0e12}	55.6 Ω
		Z_{0o12}	45.5 Ω
		θ_{oc}	29°
Electrical parameters of The PC-SLR	**Parallel-coupled Lines for input/output resonators**	w_{01}	3 mm
		S_{01}	110 µm
		L_{01}	17.5 mm
	Internal parallel-coupled lines	w_{12}	5.1 mm
		S_{12}	1820 um
		L_{12}	17 um

Figure II-14 gives the photograph of the realized filter. Its total size is 78.7 mm × 26.9 mm (0.23 λ_0 × 0.079 λ_0) for a surface of 0.018 ${\lambda_0}^2$.

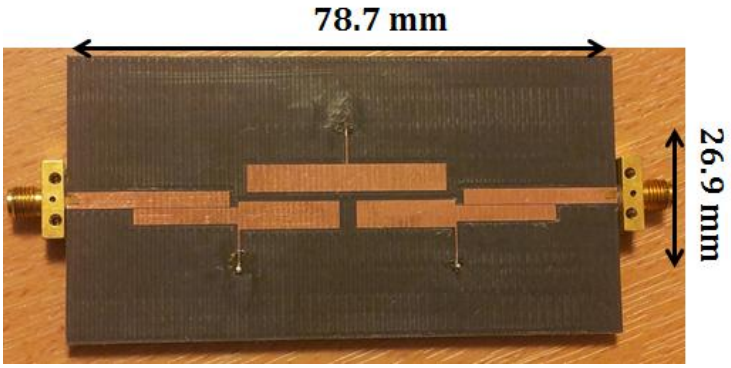

Figure II-14. Photograph of the 3rdorder PC-SLR bandpass filter in stripline technology.

Figure II-15 *Figure* II-15 shows the simulation and measurement responses of the PC-SLR filter, in a narrow band (Figure II-15 (a)) and wide band (Figure II-15 (b)), respectively.

The mallow dashed response represents the simulated *S* parameters of the PC-SLR filter with ideal transmission lines characterized. The blue solid and red dotted curves show the simulation and measurement results in stripline technology, respectively. Figure II-15 (a) shows that the measured insertion loss is approximately 2.4 dB, and the measured return loss is greater than 14 dB in the passband operating around the center frequency $f_0 = 879$ MHz. The first spurious frequency is located at ~3f_0 (Figure II-15 (b)).

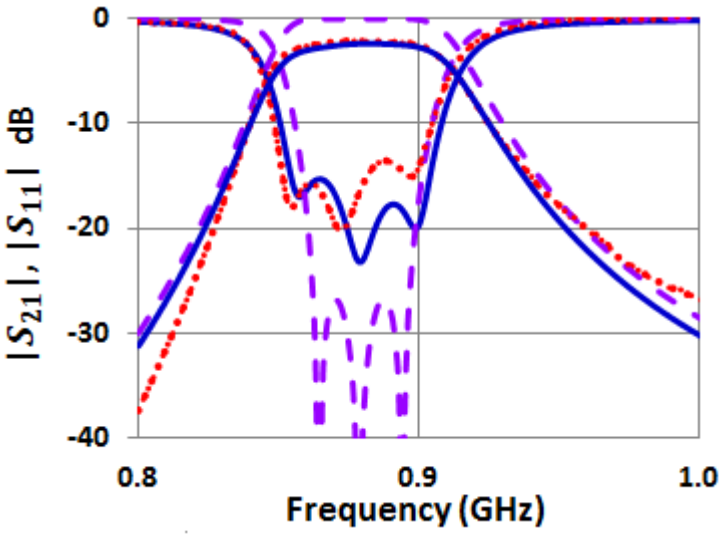

(a)

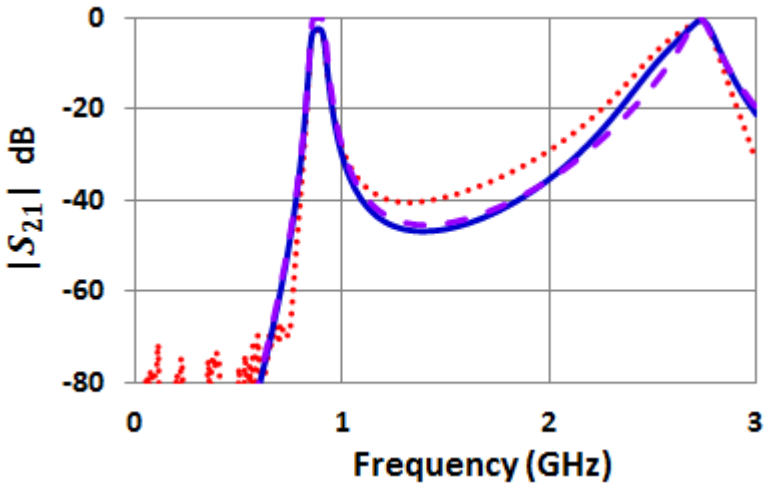

(b)

Figure II-15. S parameters of the PC-SLR bandpass filter: Simulation with ideal transmission lines (mallow dashed line) and with stripline technology (Blue solid line). Measurement (red dotted line) (a) Narrow band, (b) Large band.

Simulation and measurement responses in stripline technology are in good agreement, hence validating the design method. It is also important to note that the proposed bandpass filter achieves 36 % surface minimization in comparison with the conventional parallel-coupled bandpass filter with same specifications.

c) Conclusion

A complete synthesis procedure was introduced for the compact PC-SLR bandpass filter. Based on the filter equivalent circuits, slope parameters and admittance inverters expressions were derived. A third order PC-SLR filter was designed and fabricated in a stripline technology. Simulation and measurement results were in good agreement validated the synthesis method.

II.5. Synthesis method of bandpass filters in an inhomogeneous medium

II.5.1. Microstrip versus Stripline

A choice between microstrip and stripline involves considering a number of tradeoffs. Stripline technology, for example, requires more material layers, processing time and expense than for microstrip circuits operating at the same frequencies. Because of the second ground plane, the width of any given impedance line in stripline will be narrower than for a conductor with the same impedance in microstrip. While the inherently thinner strips support greater circuit densities, they also require tighter fabrication tolerances. For a single-ended (unbalanced) transmission line in microstrip, dielectric losses (defined by a substrate dissipation factor) will be less than for stripline, since some of the electrical field lines in microstrip are in air where the dissipation factor is negligible, with a penalty, that the existence of two different dielectric constants (below and above the strip) makes the circuit difficult to analyze in closed form. Finally, it is also not simple to use hybrid technology, by reporting surface mounted components, with stripline. This is probably the main reason why microstrip has becoming more and more attractive along the years, even if the inhomogeneity makes the designs sometimes more complicated.

II.5.2. Microstrip Filter design problems

The synthesis procedures of the classical parallel-coupled bandpass filters in [10]-[12] and PC-SLR filter described in the previous section are given for the case of TEM transmission lines (such as stripline) where odd- and even- characteristic impedances and phase velocities of each coupled-line section are well determined and equal. This

is not the case with microstrip technology where the mode velocities are different, leading to non-exact synthesis formulas.

In order to reduce the effect of difference between even- and odd- modes phase velocities an equivalent relative permittivity of quarter-wavelength coupled microstrip lines was introduced in [19]. A minor correction of electrical lengths was proposed to improve bandwidth ripple and return loss in the passband [19]. However, this correction is not effective for filter design using non-quarter wavelength (such as PC-SLR bandpass filter) [20]. In [20], a new concept of effective parameters was proposed for filters using non quarter-wavelength coupled sections. The coupled-lines microstrip filter was converted to its stripline equivalent with new effective parameters and then compared to the original filter design. But this method cannot be adopted for miniaturized non-quarter wavelength largely deviated from $\frac{\pi}{2}$. For this reason, when PC-SLR bandpass filters are built in microstrip technology, optimization with a circuit simulator is still necessary.

II.6. Chapter conclusion

A compact Parallel-coupled bandpass filter was described in this chapter. Fundamental characteristics of the PC-SLR were presented, such as resonance condition, fundamental resonance frequency, and equivalent circuits. Miniaturization rules were discussed to illustrate the fact that the SLR can be shortened by applying a small characteristic impedance ratio R_Z.

Design procedure was introduced. Slope parameters were derived from the proposed bandpass filter equivalent circuits. Using these slope parameters, equations for admittance inverters were carried out. For a proof-of-concept, a third order PC-SLR filter was designed and fabricated. The proposed design procedure and equations were validated through simulations and measurements comparison.

In addition, the problem of parallel-coupled lines built in an inhomogeneous medium (such as microstrip), leading to different mode velocities, was discussed, concluding that it is necessary to use circuit optimization for the design of PC-SLR filters in inhomogeneous medium.

References

[1] F. Winter, J. Taub, and M. Marcelli, "High-dielectric constant stripline band-pass filters," in IEEE MTT-S Int. Symp. Dig., Boston,USA, July 10-14, 1991.

[2] A.-J. Kennerley, and I.-C. Hunter, "Miniature microwave filters using high permittivity ceramics," in IEEE MTT-S Int. Symp. Dig., Vancouver, Canada, Feb. 20-22,1995.

[3] C.-H. Hsu, H.-T. Soong, and C.-L. Huang, "Microstrip rectangular ring bandpass filter design using high permittivity substrate," in the 17th Asia-Pacific Microw. Conf. Dig., Proc. Suzhou, China, Dec. 4-7, 2005.

[4] C. Johansson, and M. Robertsson, "Microstrip stepped impedance filters with variable dielectric or variable width," IEE Electronics Letters , vol. 41, no. 13, pp. 745-746, June 2005.

[5] J.-S. Hong, and M.-J. Lancaster, "Theory and experiment of novel microstrip slow-wave open-loop resonator filters ," IEEE Trans. Microwave Theory Tech. , vol. 45, no. 12, pp. 2358-2365, Dec. 1997.

[6] A. Gorur, C. Karpuz, and M. Alkan, "Characteristics of periodically loaded CPW structures," IEEE Microwave and Guided Wave Letters, vol. 8, no. 8, pp. 1051-8207, Aug. 1998.

[7] J.-S. Hong, and M. Lancaster , "Microstrip bandpass filter using generated modes of a novel meander loop resonator," IEEE Microwave and Guided Wave Letters, vol. 5, no. 11, pp. 371-372, Nov. 1995.

[8] K.-W. Eccleston, "Shunt-loaded fractal meandered microstrip," in IEEE MTT-S Int. Symp. Dig. , Changdu, Chine, Dec. 14-15, 2008.

[9] Y.-C. Chang, C.-H. Kao, M.-H. Weng, and R.-Y. Yang, "Design of the compact dual-bandpass filter with high isolation for GPS/WLAN applications," IEE Microwave and Wireless Components Lett. , vol. 9, no. 12, pp. 780-782, Dec. 2009.

[10] S.-B. Cohn, "Parallel-coupled transmission-line-resonator filters," IRE Transactions on Microwave Theory and Thechniques , vol. 6, no. 2, pp. 223-231, April 1958.

[11] D.-M. Pozar, Microwave Engineering, 3rd ed. New York: Wiley, 2005.

[12] G.-L. Matthaei, L.-Young, and E.-M.-. T. Jones, Microwave Filters, Impedance-Matching Networks, and Coupling Structures.: Artech House, 1980.

[13] M. Garcia, E. Pistono, H. Maouche, and P. Ferrari, "compact filters based on Stub-Loaded Parallel-Coupled Resonators", in the 40th European Microwave Conf. Dig., Paris, France, Sept. 28-30, 2010.

[14] M. Akra, H. Issa, E. Pistono, A. Jrad, N. Carrao, and P. Ferrari, "Parallel-coupled stub-loaded resonator filters with wide spurious suppression," in the 42th European Microwave Conf. Dig., Amsterdam, Niederland, Oct. 29-Nov. 1, 2012.

[15] M. Makimoto , Microwave Resonators and Filters for Wireless Communication.: Springer, 2000.

[16] G.-I. Zysman, and A.-K. Johnson, "Coupled transmission line networks in an inhomogeneous dielectric medium," IEEE Trans. Microwave Theory Thech., vol. 17, no. 10, pp. 753-759, Oct. 1969.

[17] M. Makimoto, and S. Yamashita, "Bandpass filters using parallel coupled stripline stepped impedance resonators", IEEE Trans. Microwave Theory Tech. , vol. 28, no. 12, pp. 1413-1417, Dec. 1980.

[18] M. Matsuo, H. Yabuki, and M. Makimoto, "The design of a half-wavelength resonator BPF with attenuation poles at desired frequencies," in IEEE MTT-S Int. Symp. Dig., Boston, USA, June 11-16, 2000.

[19] D. Kajfez, and S. Govind, "Effect of difference in odd- and even- mode wavlengths on a parallel-coupled bandpass filter," IEE Electronics Letters , vol. 11, no. 5, pp. 117-118, Mar. 1975.

[20] H.-M. Lee, and Chih-Ming Tsai, “Improved coupled-microstrip filter design using effective even- mode and odd- mode characteristic impedances”, IEEE Trans. Microwave Theory Thech., vol. 53, no. 9, pp. 2812-2818, Sept. 2005.

Chapter III. Parallel-Coupled Microstrip Bandpass Filters with Wide Spurious Response Suppression

III.1. Introduction

In modern microwave communication systems, for which several filters are needed to cover several frequency bands, miniaturization and wide out-of-band rejection are most of the time required for bandpass filters to both reduce the fabrication costs and enhance the system performance.

As previously mentioned, classical parallel-coupled microstrip bandpass filter is very popular and widely used since it has several advantages, including a low fabrication cost, and an easy design and integration. Nevertheless this type of filter suffers from a fundamental limitation, namely, the presence of spurious response at the harmonics of passband center frequency f_0 [1]. A lot of structures allow improving the bandwidth rejection but many of them need an important work of modeling.

For example, in [1]-[2], the over-coupled approach was considered to suppress spurious frequencies by tuning transmission zeros. In a similar way, in [3], a multispurious suppression was achieved by means of coupling control in both open-ended and interdigital parallel-coupled filters. In [4]-[5], periodic non-uniform coupled microstrip lines were incorporated on the traditionally designed parallel-coupled line microstrip filters in order to suppress spurious passbands. In [6], by combining the ideas of corrugated stages, over-coupled stages and tapped input/output, a parallel-coupled filter showing a wide out-of-band rejection was achieved. Defected ground structures can also be considered to obtain a wide out-of-band rejection [7]-[8]. Another solution consists to use stepped impedance

resonators (SIRs) to improve the out-of-band rejection and to make compact filters by properly choosing the segments characteristic impedance and the length ratios of the resonators [9]-[13]. By properly tapping the input/output resonators, the selectivity and the out-of-band rejection of the filter can be further improved [10]. In [11]-[13] non-uniform resonators were introduced to enhance the suppression of spurious responses. The filter in [13] exhibits the higher rejection level in the upper out-of-band rejection. The rejection level is better than 25 dB. The first spurious is located at approximately eight times the working frequency with a sacrifice in the return and insertion losses.

In this chapter, the distributed compact filter topology based on parallel-coupled stub-loaded resonator (PC-SLR) described in the previous chapter is considered. As discussed in the chapter II, one of the main features of this resonator structure is the capability of reducing resonator surface area. Another feature of this resonator is discussed in this chapter; spurious frequencies can be easily controlled during the design steps by choosing the convenient open-ended electrical length value and the characteristic impedance ratio. This chapter presents a complete resonant mode analyses. It also investigates the optimal electrical lengths allowing pushing the first spurious frequency to as high frequency as possible. Next, to go further in improving the upper out-of-band rejection, a specific feeding network called "U corner" is used. Without modifying the in-band filtering characteristics, the out-of-band rejection can be enlarged. This out-of-band improvement is achieved without deterioration of the filter surface area by only adjusting the *U-corner structure*. A detailed design methodology is described.

In a similar way, a multispurious suppression was achieved by incorporating this feeding network on the classical parallel-coupled bandpass filter to validate the design concept.

III.2. Resonance modes of the Stub-Loaded Resonator

Figure III-1 shows the structure for typical SLR. Since this resonator is symmetrical in structure, along AB Plane, it is convenient to analyze it by using even- and odd analysis technique.

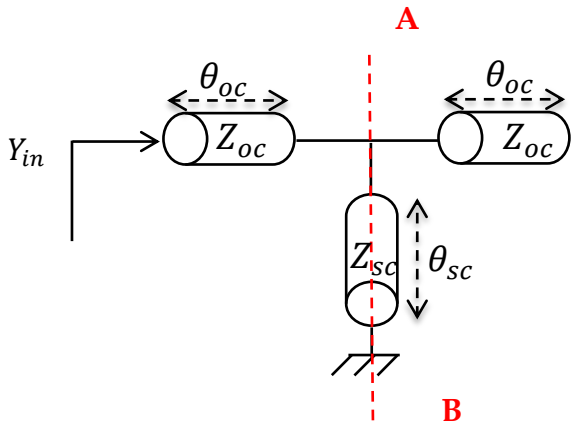

Figure III-1. Schematic view of an elementary SLR.

III.2.1. Odd-mode resonance frequencies

When odd mode excitation is applied to the two open ends of the SLR shown in Figure III-1, there is a null voltage along the AB plane. Thus the midpoint is short-circuited and the stub can be ignored. This leads to the odd-mode equivalent circuit shown in Figure III-2.

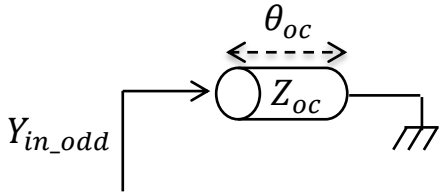

Figure III-2. Odd mode equivalent circuit.

The odd mode input admittance Y_{in_odd} is then given by:

$$Y_{in\_odd} = \frac{1}{j \cdot Z_{oc} \cdot tan(\theta_{oc})} \quad \text{(III.1)}$$

The resonance condition can be obtained by considering the open-ended condition ($I = 0$):

$$Y_{in\_odd} = 0 \quad \text{(III.2)}$$

From (III.1) and (III.2) the resonance condition can be expressed as:

$$C \cdot \pi - 2 \cdot k_{odd\_i} \cdot \theta_{oc} = 0 \quad \text{(III.3)}$$

where C is a positive odd number ($C = 1,3,5, \dots$) and $k_{odd\_i} = \frac{f_{spi\_odd}}{f_0}$ is the i^{th} normalized odd mode resonant frequency with respect to the fundamental resonant frequency f_0.

It is obvious from (III.3) that the odd-mode spurious frequencies can be simply tuned by changing the open-ended transmission line electrical length θ_{oc}.

Figure III-3 shows the normalized spurious frequency k_{odd_i} versus the electrical length θ_{oc} of the open-ended transmission line. Note that the first spurious frequency ($k_{odd\_1} \cdot f_0$) is obtained for $C = 1$.

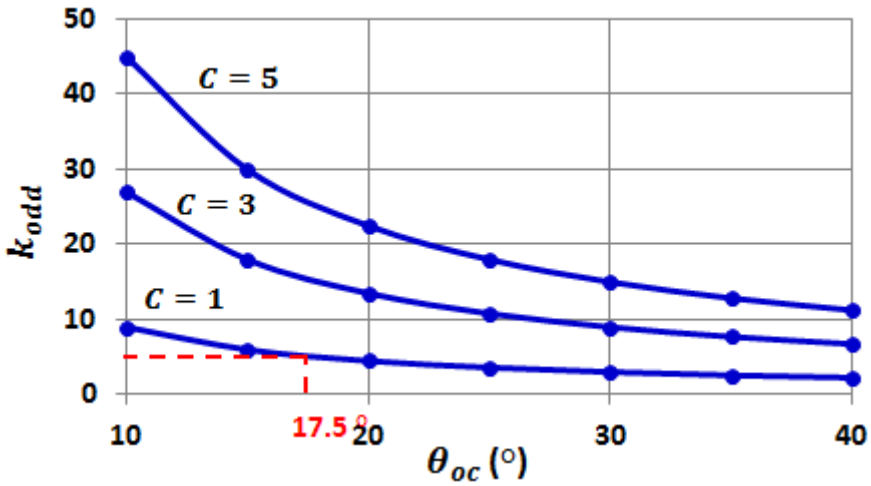

Figure III-3. Normalized odd-mode resonant frequencies for a given open-ended electrical length θ_{oc}.

As shown in Figure III-3, the smallerθ_{oc} the higher the normalized first spurious frequency k_{odd_1} is. Thus, to achieve both high PC-SLR longitudinal miniaturization and wide odd-mode out-of-band rejection, it is necessary to choose small θ_{oc} values. However, to obtain realizable gap size in classical PCB technology (i.e. > 100µm) of the parallel-coupled sections the smallest θ_{oc} that can be token for the PC-SLR filter topology is around 17.5°. Thus, the largest odd-mode out-of-band rejection cannot extend to almost $5 \cdot f_0$, as shown in Figure III-3. In that condition, second and third-order odd-mode resonance frequencies, will be located at $15.4 \cdot f_0$ and $25.7 \cdot f_0$, respectively.

III.2.2. Even-mode resonance frequencies

For even-mode excitation, there is a current flowing through the center of the open-ended transmission line. Thus, we can symmetrically bisect the SLR to obtain the equivalent circuit given in Figure III-4.

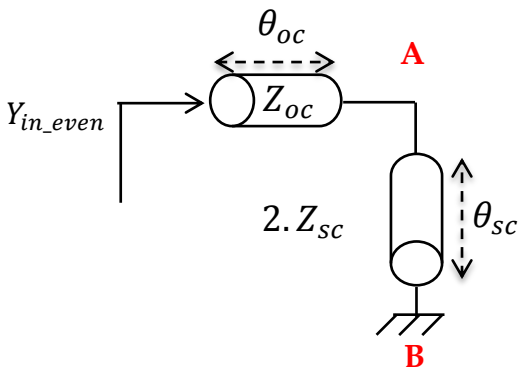

Figure III-4. Even mode equivalent circuit.

By considering the short-circuited condition of the stub ($V = 0$), the input admittance Y_A is given by:

$$Y_A = \frac{1}{j \cdot (2 \cdot Z_{sc}) \cdot tan(\theta_{sc})} \quad \text{(III.4)}$$

The even-mode admittance Y_{in_even} can be expressed from (III.4) as:

$$Y_{in\_even} = \frac{1-\frac{2}{R_Z}\cdot tan(\theta_{sc})\cdot tan(\theta_{oc})}{j\cdot Z_{sc}\cdot(2\cdot tan(\theta_{sc})+R_Z\cdot tan(\theta_{oc}))} \quad \text{(III.5)}$$

Like for the odd mode, the resonance condition can be obtained by considering the open-ended condition ($I = 0$):

$$Y_{in\_even} = 0 \quad \text{(III.6)}$$

Then the even-mode resonance condition can be easily obtained from (III.5) and (III.6):

$$tan\left(k_{even\_i}\cdot\theta_{oc}\right)\cdot tan\left(k_{even\_i}\cdot\theta_{sc}\right) - tan(\theta_{oc})\cdot tan(\theta_{sc}) = 0 \quad \text{(III.7)}$$

where $k_{even\_i} = \frac{f_{spi\_even}}{f_0}$ is the i^{th} normalized even-mode resonant frequency with respect to the fundamental resonant frequency f_0.

The spurious resonance frequencies can be tuned by changing the R_Z ratios and the electrical length of the open-ended transmission line. Based on (III.7), Figure III-5 (a), (b), and (c) gives the normalized first ($k_{even\_1} = \frac{f_{sp1\_even}}{f_0}$), second ($k_{even\_2} = \frac{f_{sp2\_even}}{f_0}$), and third ($k_{even\_3} = \frac{f_{sp3\_even}}{f_0}$) even-mode normalized spurious frequencies, respectively, versus the electrical length θ_{oc}, for several R_Z ratios.

Based on the analysis carried out in chapter II, it is convenient to consider small R_Z ratios (<1) in order to achieve compact size filters. Hence the curves in Figure III-5 are plotted for R_Z = 0.2, 0.4, 0.6, 0.8 and 1. We notice that each k_{even_i} has i maximum values. Hence it is quite easy to obtain a wide out-of-band rejection.

As shown in Figure III-5, the widest band between the first even-mode spurious resonant frequency and the fundamental one can be obtained by considering each of the following cases:

- $R_Z = 0.2, \theta_{oc} = 17.5°, k_{even\_1} = 9.2,$
- $R_Z = 0.4, \theta_{oc} = 22.5°, k_{even\_1} = 6.3,$
- $R_Z = 0.6,\ \theta_{oc} = 27.5°, k_{even\_1} = 5.2,$
- $R_Z = 0.8, \theta_{oc} = 32.5,\ k_{even\_1} = 4.6,$
- $R_Z = 1, \theta_{oc} = 35°,\ k_{even\_1} = 4.1.$

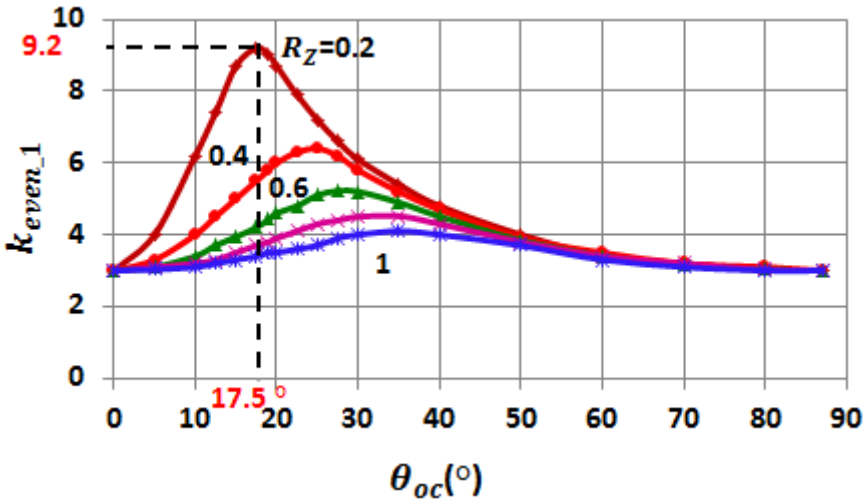

(a)

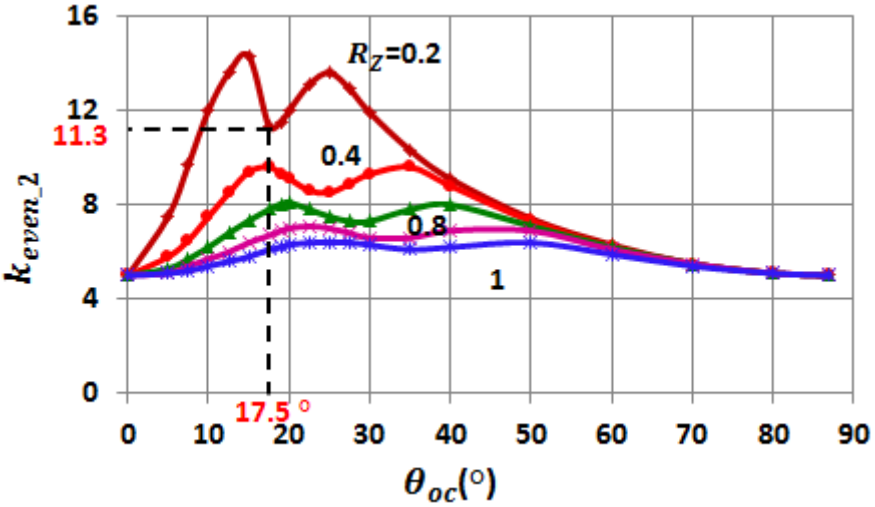

(b)

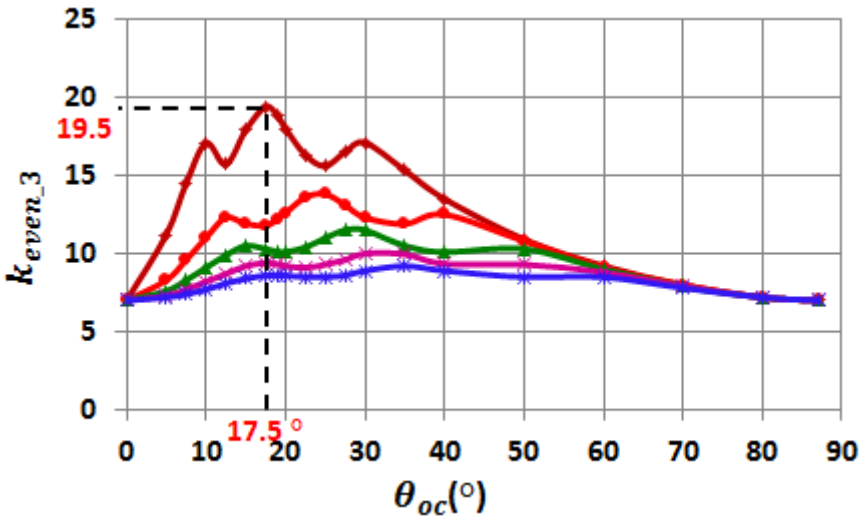

(c)

Figure III-5. Normalized even mode spurious frequencies versus the elementary open-ended electrical length θ_{oc} for several R_Z values.

From Figure III-5, one can observe that the largest value of k_{even_i} is obtained when using the smallest value of R_Z. This means that a small value of the characteristic impedance ratio leads to wide even-mode spurious resonances rejection. Hence by considering a small characteristic impedance ratio (relative to a high short-circuited stub characteristic impedance), a compact structure and a wide rejected band are achieved.

Then, the optimal R_Z and θ_{oc} values for obtaining a maximal $\frac{f_{sp1\_even}}{f_0}$ are 0.2 and 17.5°, respectively. For these selected values the highest order even-mode resonance frequencies are located at $9.2 \cdot f_0$, $11.3 \cdot f_0$ and $19.5 \cdot f_0$. But the optimal parameters for obtaining maximal rejection should be selected based on a simultaneous analyzed of k_{even_i} and k_{odd_i}.

III.2.3. Optimization of the resonator topology for improving the out-of-band rejection

Figure III-6 gives the odd and even higher order resonant frequencies in the same plots.

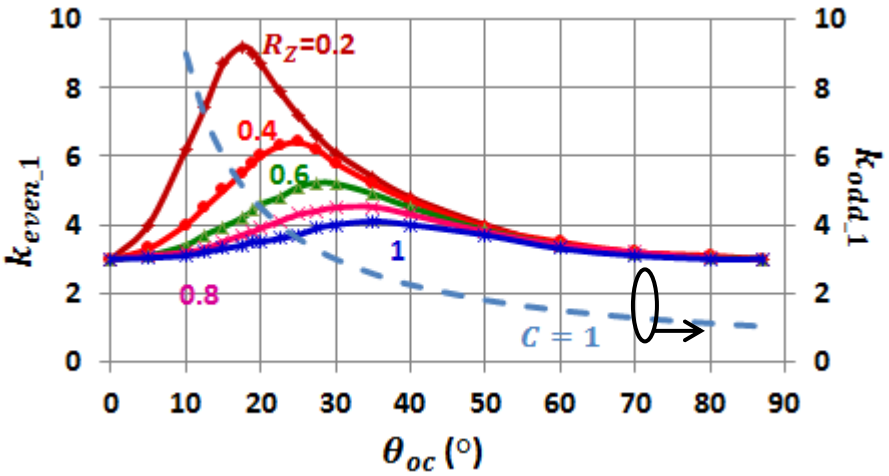

(a)

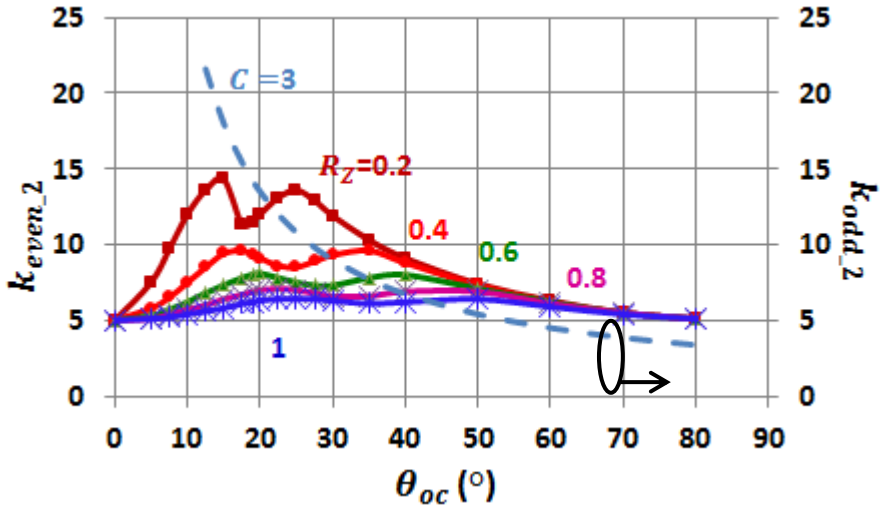

(b)

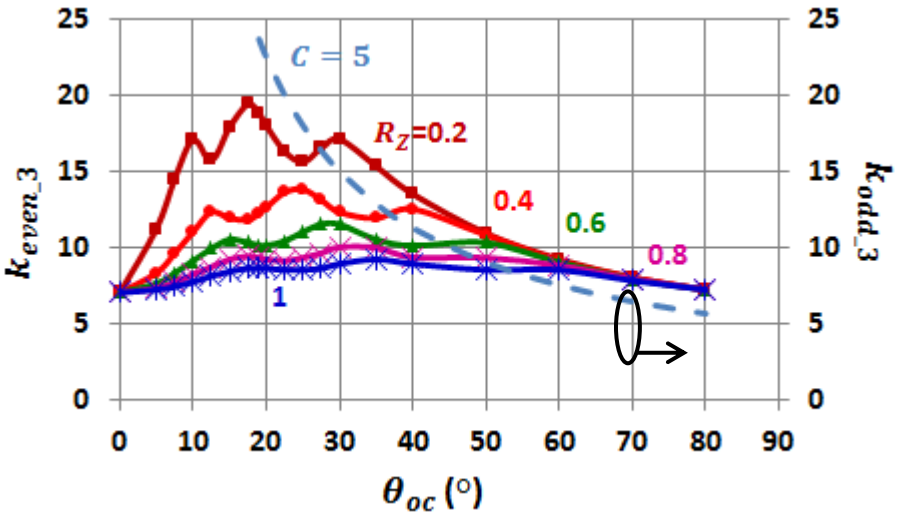

(c)

Figure III-6. Normalized spurious frequencies k_{even_i} and k_{odd_i} versus the electrical length θ_{oc} of the open-ended resonator.

The optimal θ_{oc} value for obtaining the widest out-of-band rejection is obtained for $k_{even\_1} = k_{odd\_1} = k_h$('$h$' for highest first spurious frequency due to odd or even modes). Thus the highest first spurious frequency is:

$$f_{sp1} = k_h \cdot f_0 \tag{III.8}$$

and the widest out-of-band rejection cannot extend over $k_h \cdot f_0$.

According to Figure III-6, the open-ended electrical lengths chosen in order to obtain this condition are given in Table III-1 versus $R_Z$values.

For a proof-of-concept, three third-order PC-SLR bandpass filters were designed, with passband ripple of 0.01 dB, a relative bandwidth of 2 %, and a center frequency f_0 of 1 GHz. These filters were designed and simulated considering ideal transmission lines. They were then carried out by using the resonators described in Table III-1. The first filter (Filter1) was designed with "Case 1" resonators, Filter2 with "Case 3".

Table III-1. Spurious resonant frequencies of five SLR according to Figure III-6 (Computed by using Mathematica).

	R_Z	θ_{oc} (°)	f_{sp1}	f_{sp2}	f_{sp3}	f_{sp4}
Case 1	0.2	12.3	$7.3 \cdot f_0$	$13.6 \cdot f_0$	$15.7 \cdot f_0$	$22 \cdot f_0$
Case 2	0.4	16.7	$5.4 \cdot f_0$	$9.7 \cdot f_0$	$11.74 \cdot f_0$	$16.1 \cdot f_0$
Case 3	0.6	19.8	$4.5 \cdot f_0$	$8.1 \cdot f_0$	$10.1 \cdot f_0$	$13.6 \cdot f_0$
Case 4	0.8	22.3	$4.1 \cdot f_0$	$7.1 \cdot f_0$	$9.1 \cdot f_0$	$12.2 \cdot f_0$
Case 5	1	23.9	$3.7 \cdot f_0$	$6.5 \cdot f_0$	$8.5 \cdot f_0$	$11.2 \cdot f_0$

a) Filter1: R_z = 0.2

The open-ended transmission line electrical length was set to 12.3° (Case 1 in Table III-1). This value of θ_{oc}, as previously mentioned, was chosen in order to equalize the first spurious resonant frequency off odd and even modes. The characteristic impedances of the open-ended transmission line and the short-circuited stub are 50 Ω and 250 Ω, respectively. Table III-2 gives the electrical parameters considered for Filter1.

Table III-2. Parameters of the PC-SLR Filter1.

		Parameters	Values
Electrical parameters of The PC-SLR	**Parallel-Coupled Lines for input/output resonators**	Z_{0e01}	112.8 Ω
		Z_{0o01}	32.4 Ω
		Θ_{oc}	12.3°
	Internal parallel-coupled lines	Z_{0e01}	52.9 Ω
		Z_{0o01}	47.5 Ω
		Θ_{oc}	12.3°
	Short-circuited stub	Z_{sc}	250 Ω
		Θ_{sc}	24.6°

Figure III-7 shows the simulation responses of the filter1, in a narrow band (Figure III-7 (a)) and a wide band (Figure III-7 (b)), respectively. The first four

spurious are located at $7.3 \cdot f_0$ (odd-even mode), $13.6 \cdot f_0$ (even mode), $15.7 \cdot f_0$ (even mode), and $22 \cdot f_0$ (odd-even mode), and validate the calculus given in Table III-1.

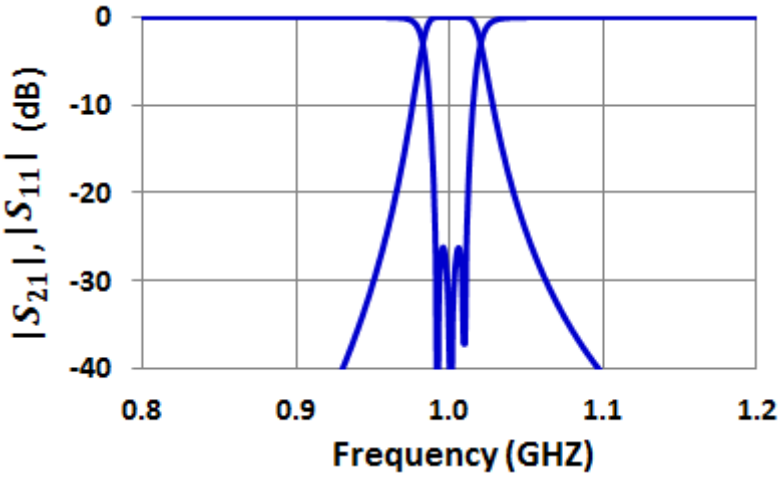

(a)

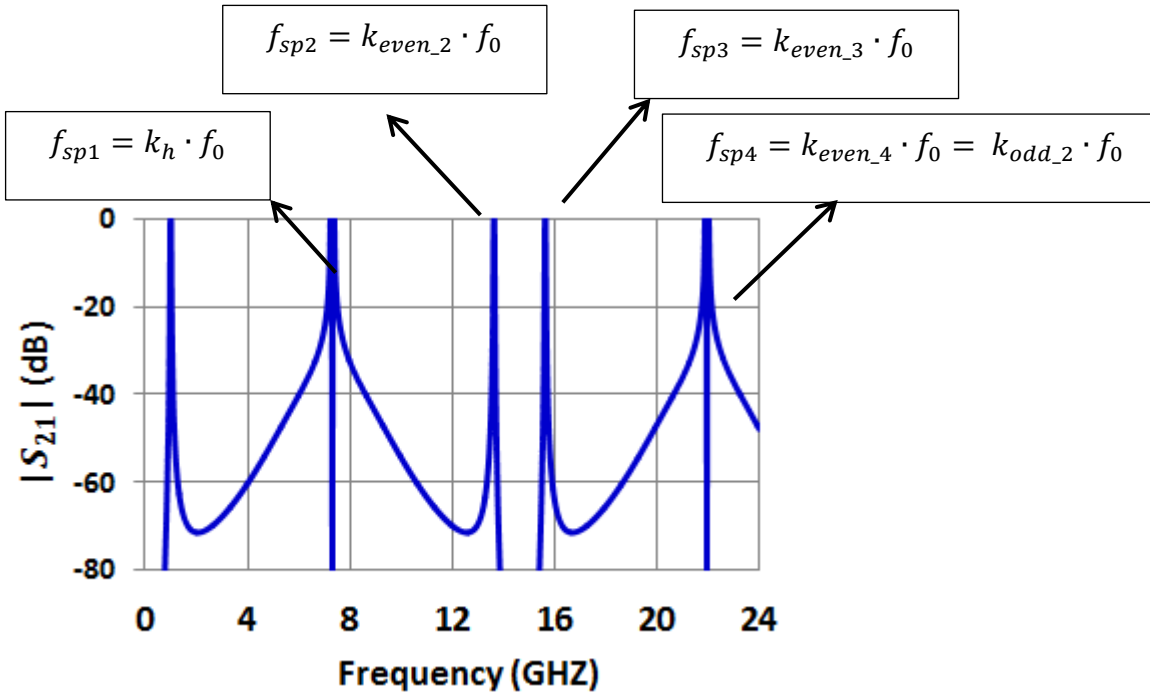

(b)

Figure III-7. S parameters of filter1: Simulation with ideal transmission lines (a) Narrow band behavior, (b) Large band behavior.

b) Filter 2: $R_z = 0.6$

Here again, the open-ended transmission-line electrical length $\theta_{oc}$was set to 19.8° (Case 3 in Table III-1) to equalize the first spurious resonant frequency off odd- and

even modes. The characteristic impedances of the open-ended transmission line and the short-circuited stub are 50 Ω and 83.3 Ω, respectively. Table III-3 gives the electrical parameters considered for Filter2.

Table III-3. Parameters of the PC-SLR Filter2.

		Parameters	Values
Electrical parameters of The PC-SLR	Parallel-coupled Lines for input/output resonators	Z_{0e01}	92.9 Ω
		Z_{0o01}	34.5 Ω
		θ_{oc}	19.8°
	Internal parallel-coupled lines	Z_{0e01}	53.2 Ω
		Z_{0o01}	47.2 Ω
		θ_{oc}	19.8°
	Short-circuited stub	Z_{sc}	83.3 Ω
		θ_{sc}	39.8°

Figure III-8 shows (a) the narrow band and (b) the wide band simulated S parameters of filter2. The first four spurious are located at $4.5 \cdot f_0$(odd-even mode), $8.1 \cdot f_0$(even mode), $10.1 \cdot f_0$ (even mode), and $13.6 \cdot f_0$(odd-even mode), and validate the calculus given Table III-1.

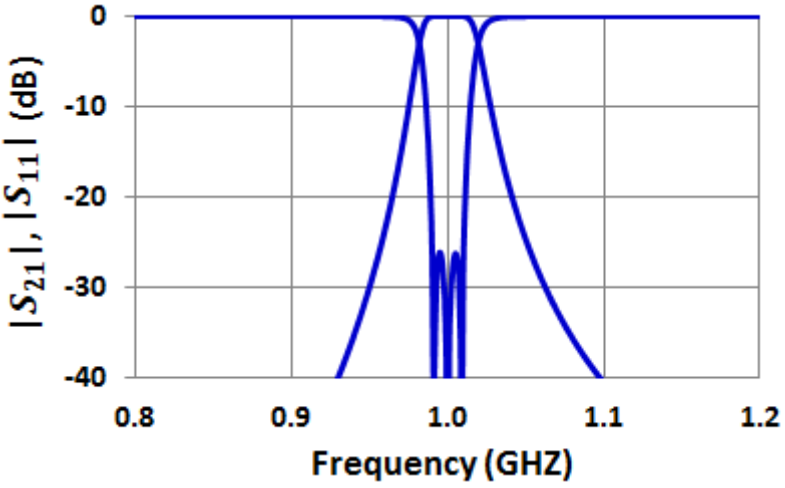

(a)

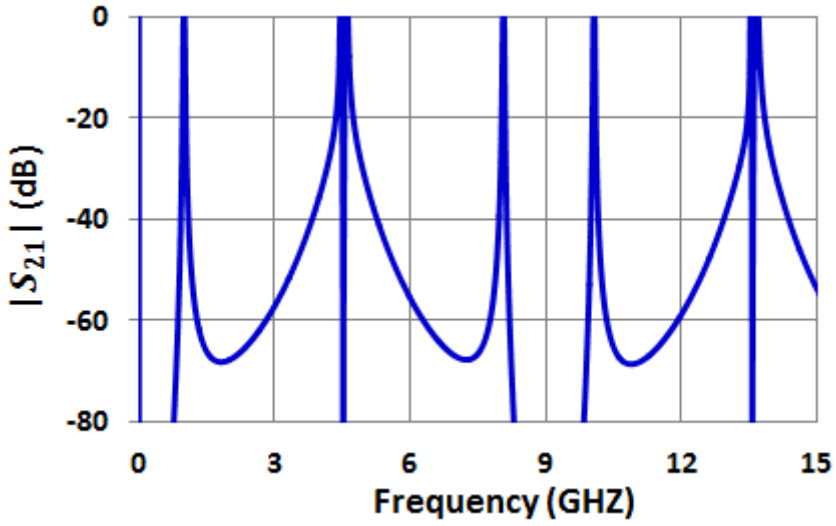

(b)

Figure III-8. S parameters of the PC-SLR bandpass filter: simulation with ideal transmission lines (a) Narrow band, (b) Large band.

III.2.4. Intermediate conclusion

Advantages in size reduction, wide out-of-band rejection were hence demonstrated for the PC-SLR bandpass filter due to the flexibility of its resonators. The first spurious frequency can be easily controlled by choosing the convenient θ_{oc} value leading to the widest out-of-band rejection. Moreover, a reduction of longitudinal filter dimension is achieved since the coupled lines are smaller than quarter wavelength.

III.2.5. Convenient choice of the substrate

Realizable microstrip-line characteristic impedance values depend on the dielectric constant and the thickness of the substrate, and the accuracy of the fabrication process. In our technology the minimum achievable signal width is around 0.25 mm.

Figure III-9 gives the maximum characteristic impedance and the R_z value, versus the substrate thickness, for two popular substrates, RT 5880 and RO 4003, respectively. It is clear that the smallest R_Z ratio ($R_{Zmin} = \frac{Z_{oc}}{Z_{scmax}}, Z_{oc} = 50\ \Omega$) leading

to the widest out-of-band rejection is obtained by considering the highest available substrate thickness.

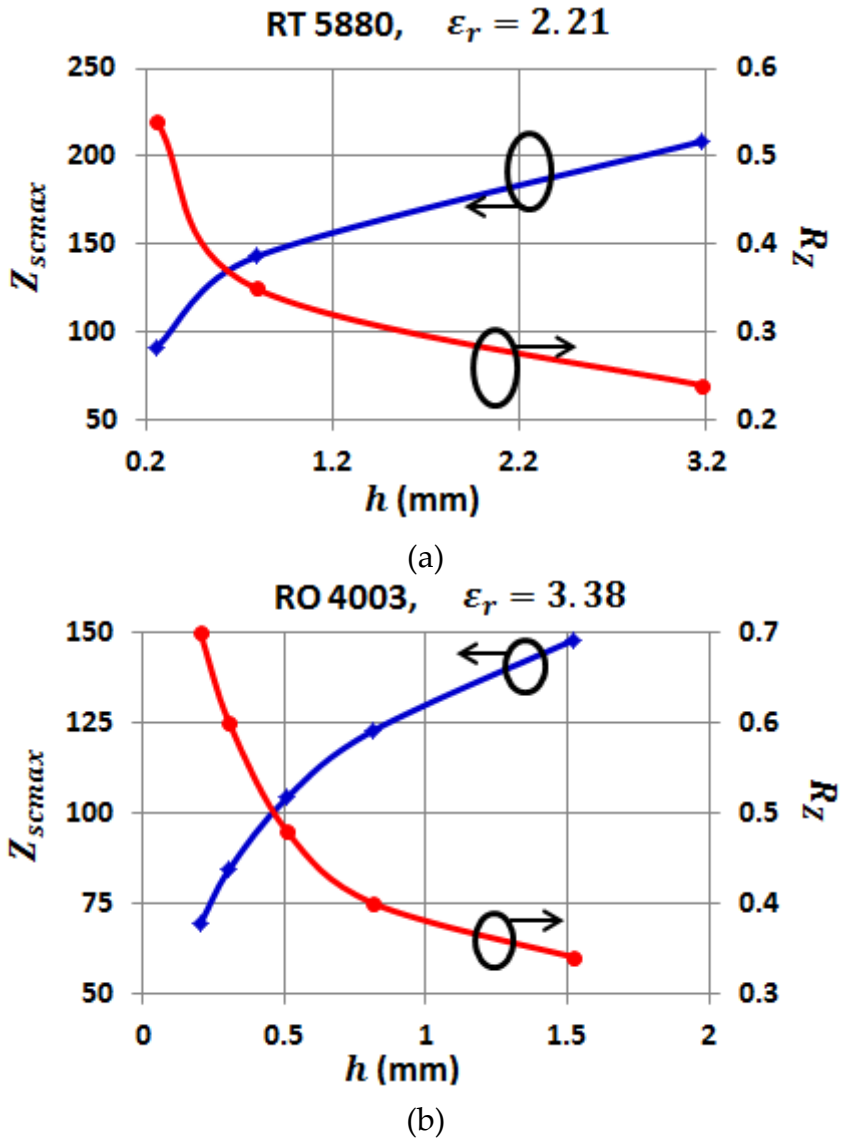

Figure III-9. Characteristic impedance and relative characteristic impedance ratio versus the substrate thickness for (a) RT 5880, and (b) RO 4003 substrates.

For issues of fabrication process and availability we used the substrates RT 5880 of thickness 0.787 mm and RO 4003 of thickness 0.813 mm, respectively, for the filters design. In that case, the highest realizable characteristic impedance reaches 143 Ω and 122.7 Ω, respectively, leading to a characteristic impedance ratio of 0.35 and 0.4, respectively.

III.2.6. Third-order proof-of-concept filter

a) Input and output gaps issue

By using the synthesis method of the PC-SLR bandpass filter introduced in the previous chapter, the small gap size of the first and the last coupling stages is a recurring problem for this topology. In these filters, critical values ($< 100\mu m$) of the gaps are required to obtain targeted coupling, especially when small open-ended electrical length θ_{oc} are used, which will make the fabrication very difficult. This also depends on the dielectric constant and thickness of the substrate. Example when substrate RT 5880 of thickness 0.787 mm with a characteristic impedance ratio of 0.35 (Table III-4) is used in the design of the PC-SLR filter the minimal θ_{oc} value for obtaining realizable gap is 30°. For RO 4003 substrate of thickness 0.813 mm with characteristic impedance ratio of 0.4 (Table III-4) the minimal θ_{oc} value for obtaining realizable gap is 25°. One possible way to overpass this problem is to use a three parallel-coupled line structure, as shown in Figure III-10 (a), which is better suited to realize strong couplings.

θ_{oc} (°)	10	15	20	25	30
S(µm)	15.2	27.7	52.2	76.4	101.5

(a)

θ_{oc} (°)	10	15	20	25	30
S(µm)	19.2	41.9	70.6	101.9	133.8

(b)

Table III-4. Gap size for input/output coupled lines for a PC-SLR bandpass filter fabricated on (a) RT5880 and (b) RO4003 substrate (for a 2 % relative bandwidth and different coupled line lengths).

b) Equivalence between the three parallel-coupled lines structure and the classical two parallel-coupled line

Figure III-10 (a) shows the three parallel-coupled lines section as a six port network and Figure III-10 (b) illustrates the proposed coupling structure composed of three parallel-coupled lines with electrical length θ_{oc}. Right ends of line I and III are open-circuited, whereas left ends are connected to each other to form a two port network, with termination condition:

$$\begin{gathered} V_i = V_1 = V_3 \\ V_o = V_5 \\ I_i = I_1 + I_3 \\ I_2 = I_4 = I_6 = 0 \\ I_o = I_5 \end{gathered} \tag{III.9}$$

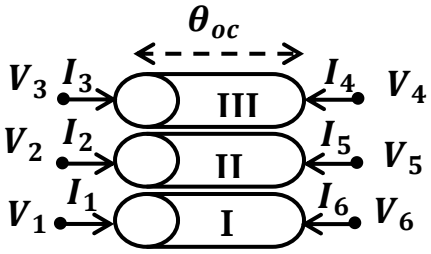

Figure III-10. (a) Three parallel-coupled lines as a six port network. (b) A symmetrical two port coupled line structure.

The proposed coupled-line structure can be treated as a two-port network from the general expression of the six-port network, as shown in Figure III-10 (b). The parameters of the *ABCD* matrix can be extracted by applying the termination

conditions in (III.9) to the impedance matrix of the three coupled lines (Figure III-10 (a)).

The voltages and currents of the six port network in Figure III-10 (a) can be expressed as:

$$[V] = [z] \cdot [I] \tag{III.10}$$

where $[V]$ and $[I]$ are six-dimensional column vectors and [z] is a 6×6 impedance matrix:

$$\begin{bmatrix} V_1 \\ V_2 \\ V_3 \\ V_4 \\ V_5 \\ V_6 \end{bmatrix} = \begin{bmatrix} z_{11} & z_{12} & z_{13} & z_{14} & z_{15} & z_{16} \\ z_{12} & z_{22} & z_{12} & z_{15} & z_{25} & z_{15} \\ z_{13} & z_{12} & z_{11} & z_{16} & z_{15} & z_{14} \\ z_{14} & z_{15} & z_{16} & z_{11} & z_{12} & z_{13} \\ z_{15} & z_{25} & z_{15} & z_{12} & z_{22} & z_{12} \\ z_{16} & z_{15} & z_{14} & z_{13} & z_{12} & z_{11} \end{bmatrix} \cdot \begin{bmatrix} I_1 \\ I_2 \\ I_3 \\ I_4 \\ I_5 \\ I_6 \end{bmatrix} \tag{III.11}$$

Since there exists three fundamental modes (two even modes, denoted as "ee" and "oo" modes), and one odd mode "oe", z parameters depends on of Z_{oe}, Z_{oo}, and Z_{ee} [15]. Note that, when the coupling structure is symmetric and excited in a symmetric way, the odd mode does not exist. The impedances of the "ee" and "oo" modes in symmetric three lines can be approximated by the even- (Z_{0e}) and odd- (Z_{0o}) modes characteristic impedances used in the case of parallel-coupled two lines [15], [16].

Applying the terminal condition in (III.9) to this six port matrix, a 3×3 impedance matrix for the proposed coupled line structure is then deduced:

$$\begin{bmatrix} V_1 \\ V_3 \\ V_o \end{bmatrix} = \begin{bmatrix} z_{11} & z_{13} & z_{15} \\ z_{13} & z_{11} & z_{15} \\ z_{15} & z_{15} & z_{22} \end{bmatrix} \cdot \begin{bmatrix} I_1 \\ I_3 \\ I_o \end{bmatrix} \tag{III.12}$$

Consequently, a two-port network can be obtained in terms of Input/Output currents and voltages, as:

$$\begin{bmatrix} V_i \\ V_o \end{bmatrix} = \begin{bmatrix} \frac{z_{11}+z_{13}}{2} & z_{15} \\ z_{15} & z_{22} \end{bmatrix} \cdot \begin{bmatrix} I_i \\ I_o \end{bmatrix} \tag{III.13}$$

Then the *ABCD* matrix can be deduced:

$$\begin{bmatrix} V_i \\ I_i \end{bmatrix} = \begin{bmatrix} A & B \\ C & D \end{bmatrix} \cdot \begin{bmatrix} V_o \\ -I_o \end{bmatrix} \quad \text{(III.14)}$$

$$A = \frac{z_{11}+z_{13}}{2 \cdot z_{15}}$$

$$\mathrm{B} = \frac{z_{22} \cdot (\mathrm{z}_{11} + \mathrm{z}_{13})}{2 \cdot \mathrm{z}_{15}} - z_{15}$$

$$C = \frac{1}{z_{15}}$$

$$D = \frac{z_{22}}{z_{15}}$$

III.3. Design of feed lines with"U Corner"

In order to improve input/output couplings of the PC-SLR filter, three-coupled microstrip lines were used to replace simple coupled-lines at near- and far-ends of the filter as previously described (Figure III-11 (b)). Then, symmetrical feeding lines (paths 1 and 2, with $\theta_a = \theta_b$) are needed to correctly feed these coupled transmission lines, as shown in Figure III-11 (a). The design of these feed lines, called "U corner", because of the U shape, can be conveniently optimized ($\theta_a \neq \theta_b$) to improve the bandwidth rejection by adding transmission zeros in the out-of-band rejection. This new technique of suppressing spurious can be generalized for other parallel-coupled bandpass filter topologies, for example the classical parallel-coupled lines topology shown in Figure III-11 (c). Without modifying the in-band filtering characteristics, the out-of-band rejection can be enlarged up to more than eight times the working frequency in the case of the PC-SLR bandpass filter, and more than three times for classical parallel-coupled bandpass filter. This out-of-band improvement is achieved without scarifying the filter surface area by only adjusting the U-corner structure. A detailed design methodology is described below.

For a proof-of-concept, five three-pole bandpass filters (PC-SLR and classical parallel-coupled bandpass filter) with non-optimized and optimized U corners were designed and fabricated, to demonstrate the efficiency of the proposed concept.

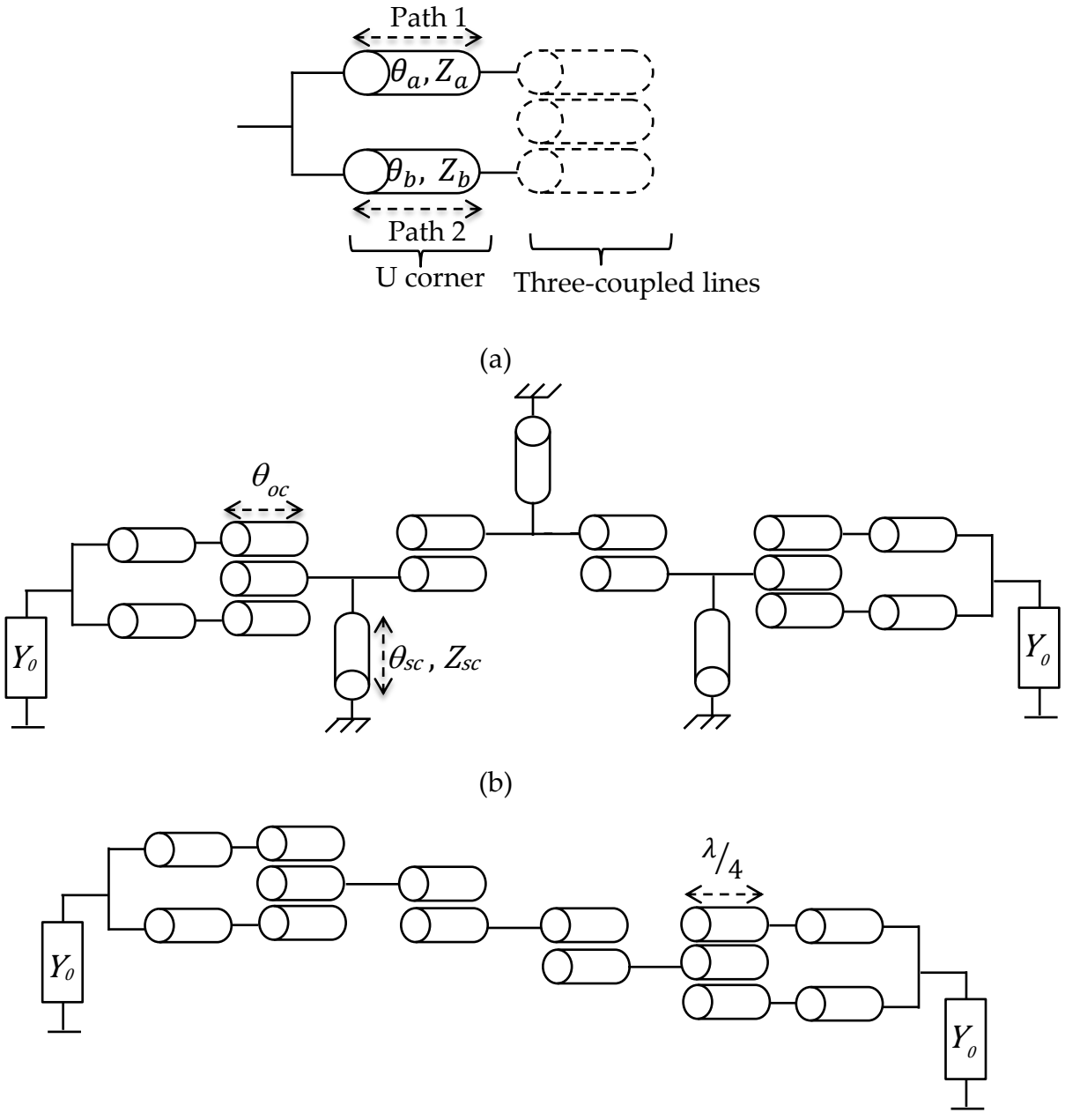

Figure III-11. (a) Schematic circuit of the feed lines, and layouts of (b) PC-SLR bandpass filter and (c) classical parallel-coupled bandpass filter.

III.3.1. Optimized U Corner for Transmission Zero Placement

Design rules were derived for transmission zero placement at the out-of-band rejection. These zeros can reject specific spurious frequencies by adjusting the length of one path of the U corner. It is proven that these zeros appear either when the output of the U corner is virtually short-circuited (when the signals from both U corner paths are in opposite phase) or when the output admittance of the U corner equals 0 (infinite output impedance) as it will be discussed below.

a) Infinite output impedance

The output admittance Y_L of the U corner (as shown in Figure III-12) can be calculated by considering *ABCD* and *Y* matrix operations. Ideal lossless transmission lines and same characteristic impedances Z_a and Z_b were considered for the calculus.

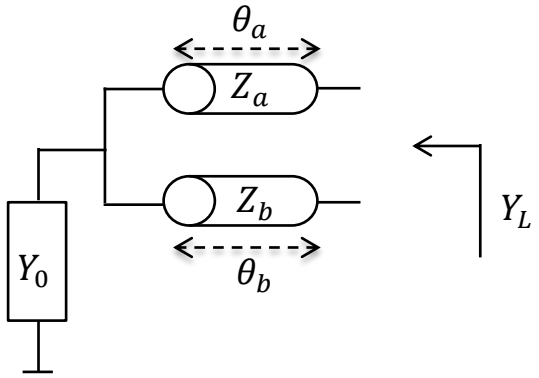

Figure III-12. U corner design with different electrical lengths of paths 1 *and* 2.

The *ABCD* matrix of each path (1 and 2) is:

$$\begin{bmatrix} A & B \\ C & D \end{bmatrix} = \begin{bmatrix} cos(\theta_{a,b}) & jZ_a\, sin(\theta_{a,b}) \\ \frac{jsin(\theta_{a,b})}{Z_a} & cos(\theta_{a,b}) \end{bmatrix} \quad \text{(III.15)}$$

By calculating the sum of the corresponding $[Y_a]$ and $[Y_b]$ matrices of path 1 and 2, one obtains the equivalent $[Y]$matrix:

$$\begin{bmatrix} Y_{11} & Y_{12} \\ Y_{21} & Y_{22} \end{bmatrix} = \begin{bmatrix} -jY_a(cot(\theta_a) + cot(\theta_b)) & \frac{j}{Z_a}(\frac{1}{sin(\theta_a)} + \frac{1}{sin(\theta_b)}) \\ \frac{j}{Z_a}(\frac{1}{sin(\theta_a)} + \frac{1}{sin(\theta_b)}) & -jY_a(cot(\theta_a) + cot(\theta_b)) \end{bmatrix} \quad \text{(III.16)}$$

Then, since transmission lines are symmetrical and reciprocal devices, the output admittance Y_L of the U corner can be calculated as:

$$Y_L = Y_{11} - \frac{{Y_{12}}^2}{Y_{11} + Y_0}$$

$$Y_L = -jY_a(cot\,\theta_a + cot\theta_b) + \frac{\frac{{Y_a}^2}{Y_0}\left(\frac{1}{sin\theta_a} + \frac{1}{sin\theta_b}\right)^2}{1 - j\frac{Y_a}{Y_0}(cot\theta_a + cot\theta_b)} \quad \text{(III.17)}$$

where Y_0 is the reference admittance.

When the admittance Y_L equals 0, no signal can be transmitted from the input of the filter to the first resonator of the filter. This condition corresponds to:

$$\theta_a + \theta_b = 2k\pi, with\ k \in N^* \quad \text{(III.18)}$$

Thus, transmission zeros appear when the total electrical length of the U corner is an even multiple of π.

b) Virtually short-circuited U corner output

When the signals from both U-corner paths are in opposite phase with the same magnitude, it can be written:

$$\theta_a - \theta_b = (2k + 1)\pi, with\ k \in N \quad \text{(III.19)}$$

For frequencies corresponding to this particular case, the output of the U corner is virtually short circuited, and prevents the transmission of the signal to the three-coupled microstrip lines. As reported in [17], [18], this concept of generating transmission zeros due to the signal interference technique was already described by using two parallel transmission lines of different electrical lengths.

III.3.2. Validation of the concept on Parallel-coupled Bandpass Filter

For a proof-of-concept, three three-pole bandpass filters based on classical parallel-coupled resonators were fabricated. The first-one (filter a) is the classical bandpass filter designed with simple coupled lines. In the second one (filter b), end stages were replaced by three coupled lines feeded with non-optimized U corners. In the third one (filter c), optimized U corners were used in order to increase the out-of-band rejection and create a transmission zero near the passband.

a) Filter a: Classical parallel-coupled bandpass filter

The classical bandpass filter was designed, with a passband ripple of 0.01 dB, a relative bandwidth of 10 %, and a center frequency of 2.9 GHz. The electrical length of each coupled stage is set to 90°.

The filter was designed with Agilent ADS™ and fabricated on a RT5880 substrate (dielectric constant $\varepsilon_r = 2.21$, dielectric loss tangent $tan\delta = 0.9.10^{-3}$, substrate thickness $h = 0.787$ mm, copper thickness $t = 17$ µm). Using the values obtained for the electrical parameters, the physical parameters were calculated (Table III-5).

Table III-5. Physical parameters of the classical parallel-coupled bandpass filter.

		PARAMETERS	VALUES
Physical parameters	Parallel-coupled lines for input/output resonators	w_{01}	1.61 mm
		S_{01}	120 µm
		L_{01}	16.14 mm
	Internal parallel-coupled lines	w_{12}	2.27 mm
		S_{12}	840 µm
		L_{12}	16.64 mm

Figure III-13 gives the photograph of the fabricated filter. Its total size is 75 mm x 10 mm (0.72 λ_0 x 0.1 λ_0), leading to a surface of 0.072 ${\lambda_0}^2$.

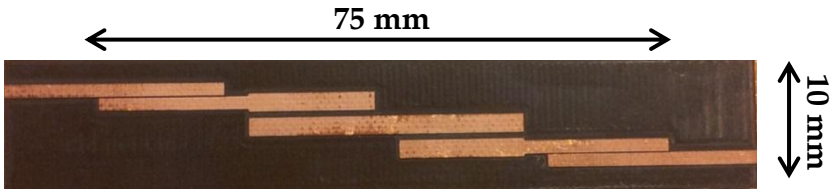

Figure III-13. Photograph of the third order classical parallel-coupled bandpass filter in microtrip technology.

Figure III-14 shows the simulation and measurement responses of the classical PC bandpass filter. Simulation and measurement results are in good agreement. Detailed data shows that the in-band insertion loss is 1 dB while return loss is better than 15 dB. The 3-dB bandwidth is 10 % as expected.

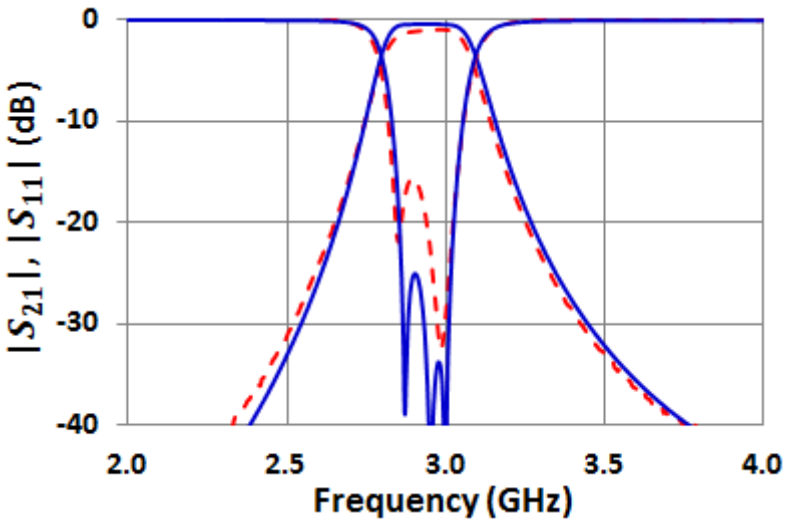

(a)

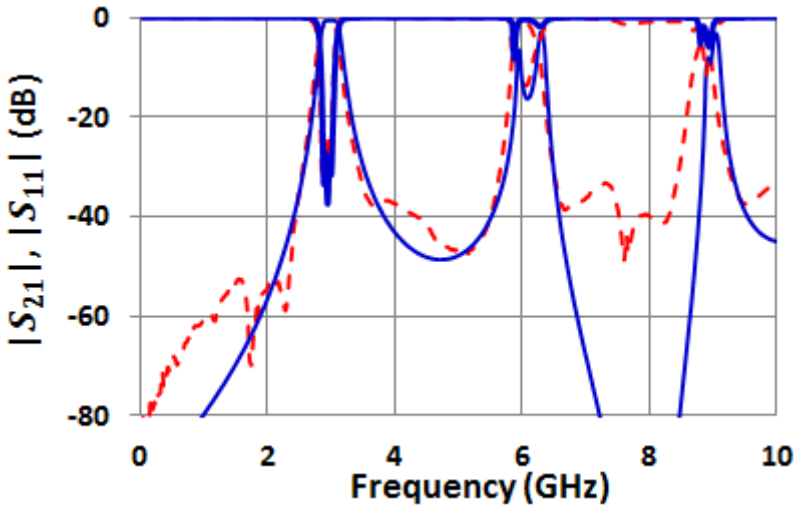

(b)

Figure III-14. S parameters of the classical coupled-line bandpass filter : measurements (red dashed line) and circuit simulations (blue solid line), (a) Narrow band, (b) large band.

We can notice the presence of the expected spurious at the harmonics of the passband center frequency f_0. Spurious peaks appearing in the upper out-of-band rejection at even harmonics ($2.f_0$, $4.f_0$…) are due to the inequality of even-and odd-mode phase velocities of coupled lines, whereas spurious peaks at $3.f_0$, $5.f_0$are due to distributive nature of resonators and coupled stages.

b) Filter b: parallel-coupled bandpass filter with non-optimized U corner structure

Three parallel-coupled lines replaced the simple coupled lines of the first and last coupled stages. The electrical length of the three coupled lines was set to 90°. A U corner structure was used to correctly feed these three parallel-coupled lines. The characteristic impedance of the two U corner paths is 100 Ω (Figure III-15).

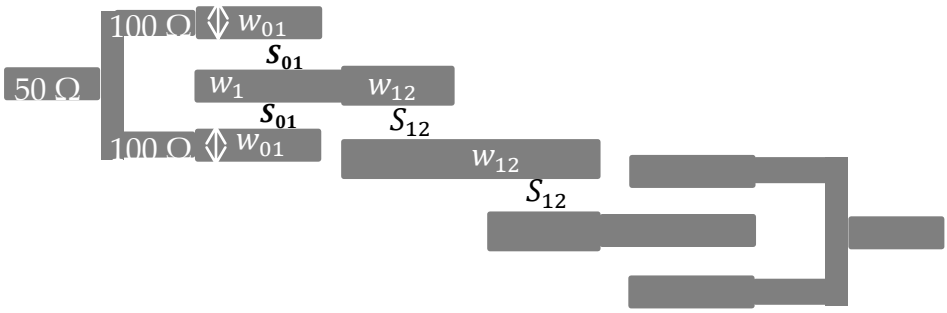

Figure III-15. Schematic view of the proposed bandpass filter layout.

Since the proposed coupling structures are symmetric, the odd mode will not appear. As previously mentioned, the characteristic impedances of the "oo" and "ee" even modes in symmetric three lines can be approximated by the even- (Z_{0e}) and odd- (Z_{0o}) modes characteristic impedance in the case of parallel-coupled two lines. Thus physical parameters of the bandpass filter feeded by the U corners can be deduced from the classical one after a slight optimization to obtain the desired passband. The obtained physical parameters are given in Table III-6.

Table III-6. Physical parameters of the classical parallel-coupled bandpass filter.

		PARAMETERS	VALUES
Physical parameters	Parallel-coupled lines for input/output resonators	w_{01}	1.51 mm
		w_1	1.61 mm
		S_{01}	120 µm
		L_{01}	16.24 mm
	Internal parallel-coupled lines	w_{12}	2.27 mm
		S_{12}	860 µm
		L_{12}	16.64 mm
	U corner structure	*w_c	0.67 mm
		* $L_a = L_b$	5.3 mm

*w_c is the line width of the U corner structure.
*L_a and L_b are the physical lengths of the paths 1 and 2 of the U corner structure.

A very good agreement between measurement and circuit simulation results is obtained for narrow band (Figure III-16 (a)) and large band (Figure III-16 (b)). As expected, the center frequency of the filter is 2.9 GHz, the insertion loss remains 1 dB as for the classical bandpass filter, while the return loss is better than 25 dB for both

simulation and measurement results. Here again, spurious frequencies appear at the harmonics of the passband center frequency. It has to be noted that the passband responses are unchanged when the new proposed couplings at the end stages are incorporated.

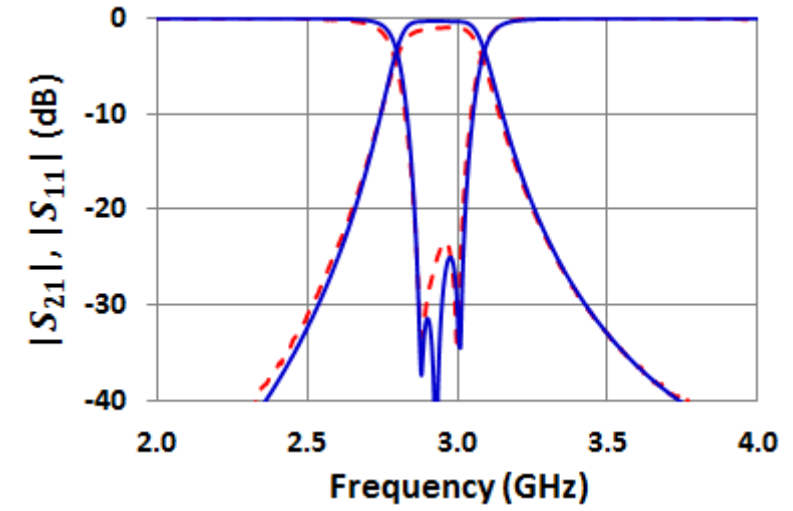

(a)

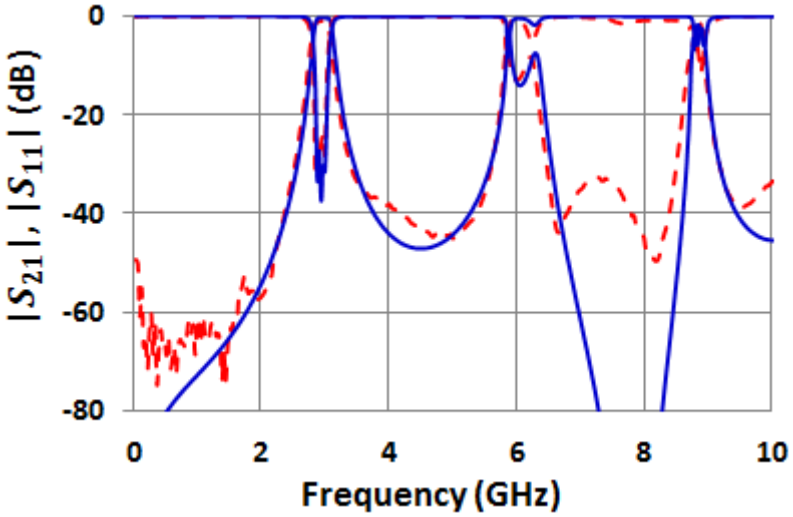

(b)

Figure III-16. S parameters of the parallel-coupled bandpass filter with non-optimized U corner: measurements (red dashed line) and circuit simulations (blue solid line), (a) Narrow band, (b) large band.

Figure III-17 gives the photograph of the realized filter. Its longitudinal size is 82 mm (0.79 λ_0).

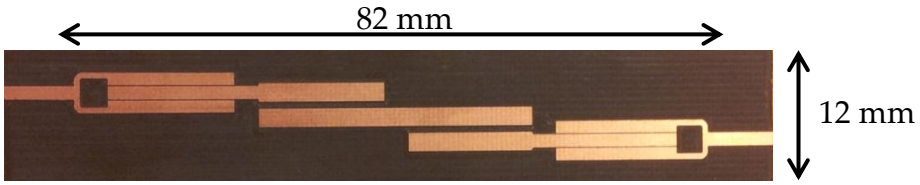

Figure III-17. Photograph of the third order parallel-coupled bandpass filter with non-optimized U corner.

This filter has been designed as an intermediate phase in the comparative study with the filter with optimized U corner structure.

c) Filter c: parallel-coupled bandpass filter with optimized U corner structure

Based on the design rules given by equations (III.17) and (III.18), the U corner was optimized to create transmission zeros at the upper out-of-band rejection. The photograph of the resulting filter is given in Figure III-18. By only modifying the length of the U corner paths while maintaining the filter dimensions, a deeper out-of-band rejection was obtained. The first and second spurious frequencies are attenuated by more than 20 dB.

Figure III-18 gives the photograph of the realized filter. Its longitudinal size is 82 mm (0.79 λ_0), i.e. 9.3 % greater as compared to the classical coupled-line filter. A folded U corner could be realized to obtain a compact transversal filter dimension.

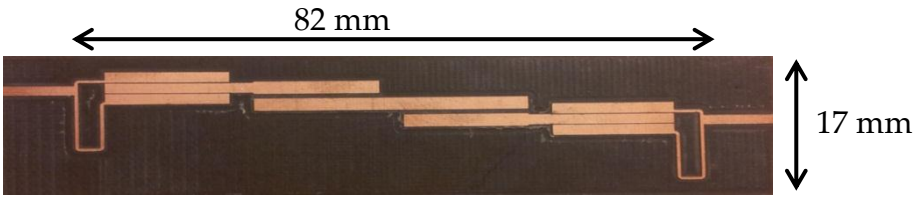

Figure III-18. Photograph of the third order parallel-coupled bandpass filter with optimized U corner.

Figure III-19 shows the simulation and measurement responses of the parallel-coupled bandpass filter with optimized U corners. Simulation and

measurement results are in good agreement. A transmission zero is located at $\sim 2.2 \cdot f_0$ where the U corner output is virtually short-circuited ($\theta_b - \theta_a = \pi$ at 6.6 GHz). The other zero is located at 8.4 GHz ($\sim 3 \cdot f_0$) where the U corner presents an infinite impedance at its output. The in-band insertion loss is still limited to 1 dB and the return loss is better than 15 dB.

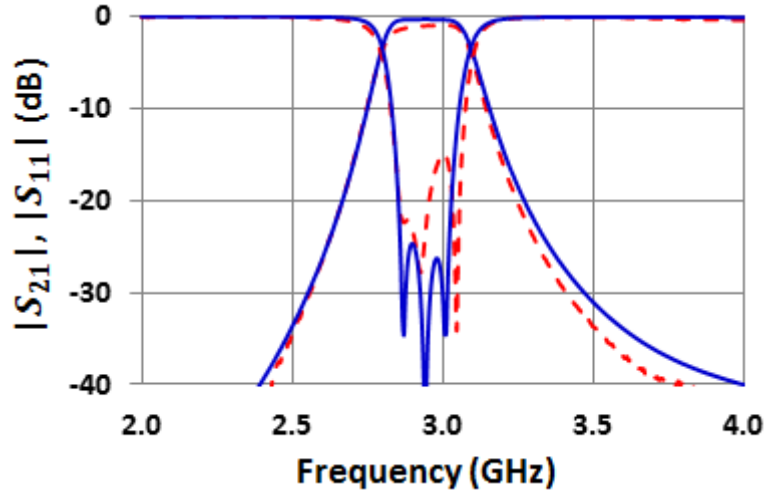

(a)

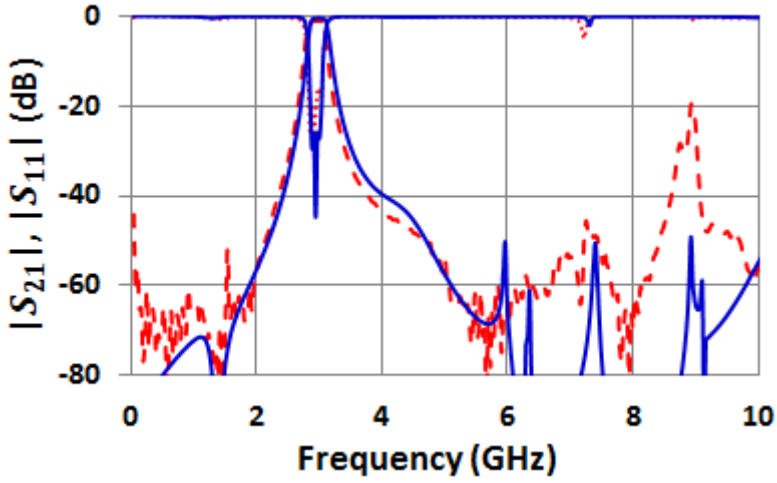

(b)

Figure III-19. S parameters of parallel-coupled bandpass filter with optimized U corner: measurements (red dashed line) and circuit simulation (blue solid line), (a) Narrow band behavior, (b) large band behavior.

Finally, Figure III-20 shows the comparison of the measurements of both classical filter (filter a) and filter with optimized U corners (filter c) on the same graph in order to emphasize the improvement of the out-of-band rejection. The filter with optimized

U corners presents a wide out-of-band rejection, without any modification in the passband, up to more than three times the working frequency is achieved. The rejection level in the out-of-band rejection is better than 20 dB from $1.13 \cdot f_0$ to more than $3.9 \cdot f_0$ and better than 40 dB from $1.3 \cdot f_0$ to more than $2.97 \cdot f_0$. These results validate the concept of the U-corner.

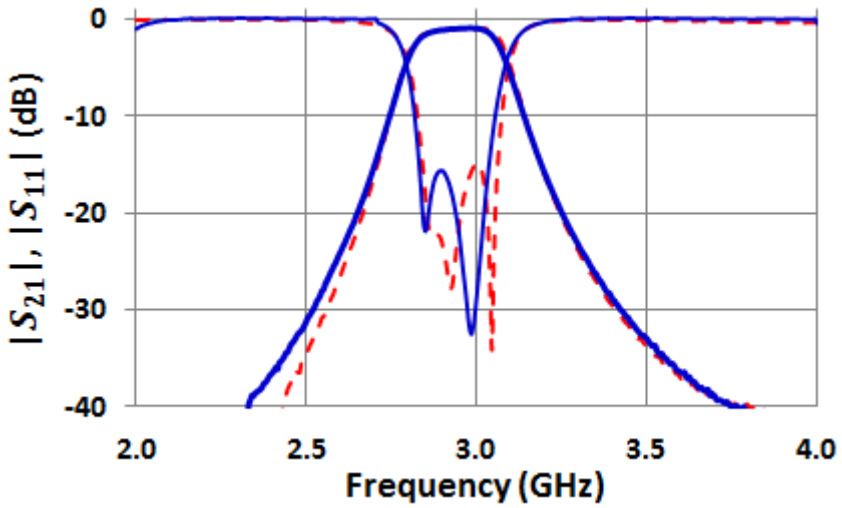

(a)

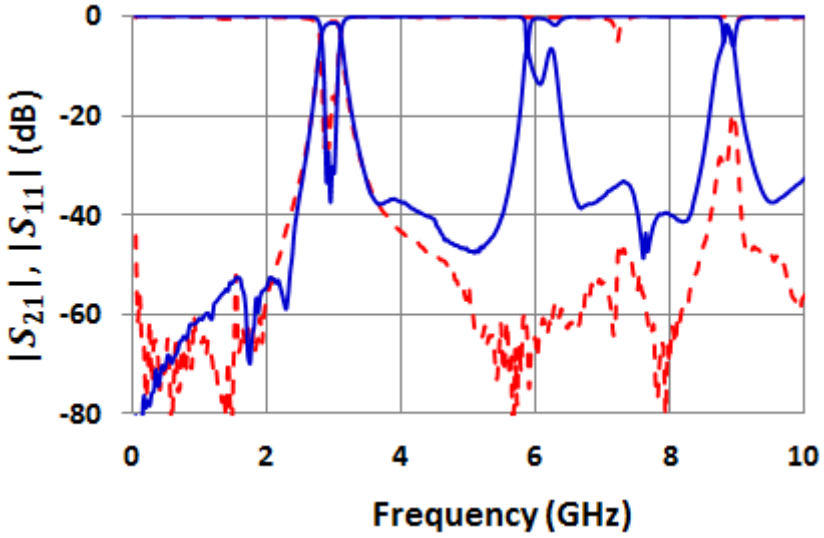

(b)

Figure III-20. Comparison of S parameters measurement of the classical bandpass filter (blue solid line) and the bandpass filter with optimized U corners (red dashed line), (a) narrow band behavior, (b) large band behavior.

III.3.3. Validation of the concept on PC-SLR bandpass filter

As for the classical coupled-line bandpass filter, two-pole bandpass filters based on stub-loaded resonators were fabricated. The first one (filter 1) is constructed with cascaded simple coupled lines and three-parallel coupled lines at its ends feeded by non-optimized U corners. In the second one (filter 2), optimized U corners were used in order to increase the bandwidth rejection.

a) Filter 1: PC-SLR with non-optimized U corners

The PC-SLR filter is designed and synthesized based on the classical *J*-inverter method. The center frequency and the fractional bandwidth were chosen as 1 GHz and 7 %, respectively. The filter were designed with Agilent ADS™ and fabricated on a RT 5880 substrate (dielectric constant $\varepsilon_r = 2.21$, dielectric loss tangent $tan\delta = 0.9.10^{-3}$, substrate thickness $h = 0.787$ mm, copper thickness $t = 17$ µm).

Based on the analysis carried out in previous sections in this chapter and chapter II, it is convenient to consider small characteristic impedance ratio ($R_Z = \frac{Z_{oc}}{Z_{sc}}$ <1, where R_Z is the characteristic impedance of the open-ended resonator Z_{oc} and is the characteristic impedance of the short circuited stub Z_{sc}) in order to achieve compact size filter and wide out-of-band rejection. For issues of fabrication process we choose $R_Z = 0.4$ ($Z_{sc} = 125\,\Omega$, $Z_{oc} = 50\,\Omega$). The electrical length θ_{oc} of the open-ended resonator is equal to 18.5°. Notice that, this value of θ_{oc} was chosen in order to approximately equalize the first spurious resonant frequencies of odd and even modes in order to obtain the widest out-of-band rejection bandwidth. These even and odd resonance frequencies are given respectively by equations (III.3) and (III.7).

Figure III-21 gives the odd and even first order resonant frequencies as previously seen in Figure III-6. Table III-1 proves that the optimal θ_{oc} value for obtaining the wide-out-of band rejection is 16.7° for a first spurious frequency at $5.4 \cdot f_0$. For issues

of fabrication process we set θ_{oc} at 18.5° for obtaining a realizable gap size. With this θ_{oc} the first spurious frequency is approximately at $5.1 \cdot f_0$.

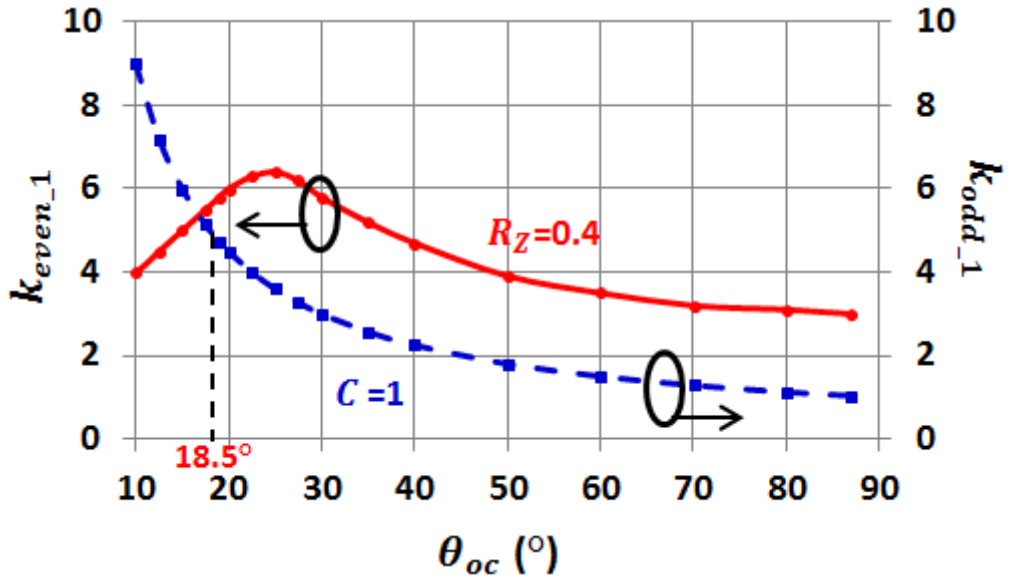

Figure III-21. Normalized first spurious frequencies k_{even_1} and k_{odd_1} versus the electrical length θ_{oc} of the open-ended resonator.

Figure III-22 gives the photograph of the realized filter. Its total size is 60 mm x 27 mm (0.2 λ_0 x 0.09 λ_0) for a surface of $0.018 \cdot \lambda_0^2$. The overall dimension of the filter is given in Table III-7.

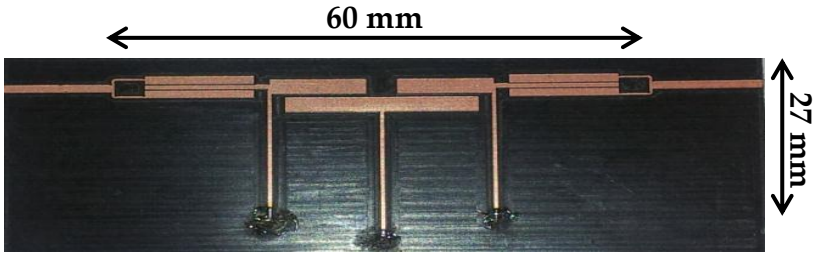

Figure III-22. Photograph of the third-order PC-SLR bandpass filters with non-optimized U corner.

Table III-7. Physical dimension of the PC-SLR filters with non-optimized U corners.

		PARAMETERS	VALUES
Physical parameters	**Parallel-Coupled Lines for input/output resonators**	w_{01}	1.27 mm
		w_1	0.73 mm
		S_{01}	111 µm
		L_{01}	12.05 mm
	Internal parallel-coupled lines	w_{12}	2.34 mm
		S_{12}	560 µm
		L_{12}	9 mm
	Short-circuited stub	w	0.44 mm
		L	19.8 mm
	U corner structure	w_c	0.3 mm
		$L_a = L_b$	7.9 mm

Figure III-23 gives the simulation and measurement responses of the PC-SLR filter with non-optimized U corner. Simulation and measurement results are in good agreement. As expected from the previous analysis, the first spurious frequency is located at approximately five times the center frequency.

Detailed data shows that the in-band minimum insertion loss is lower than 2 dB while the return loss is better than 18 dB. The 3-dB bandwidth is 7 %, as expected.

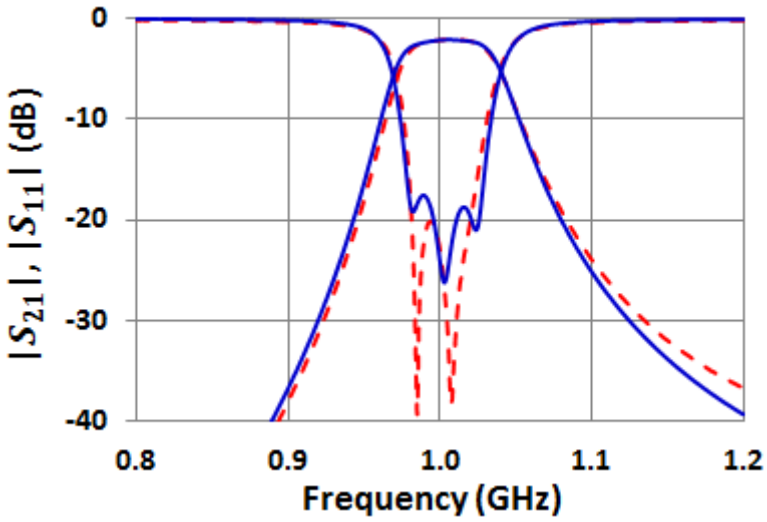

(a)

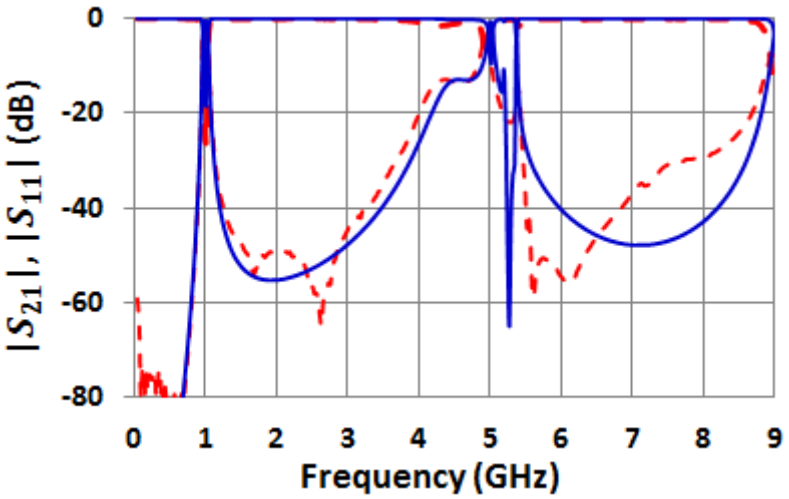

(b)

Figure III-23. S parameters of PC-SLR bandpass filter with non-optimized U corner: measurements (red dashed line) and circuit simulations (blue solid line), (a) Narrow band, (b) large band.

b) Filter 2: PC-SLR with optimized U corners

Based on the design rules given by equations (III.18) and (III.19), the U corner was optimized to create transmission zeros in the out-of-band rejection. The photograph of the resulting filter is given in Figure III-24. The overall dimension of the filter is given in Table III-8. By modifying the length of the U corner paths while maintaining the filter dimensions, a deeper out-of-band rejection was obtained.

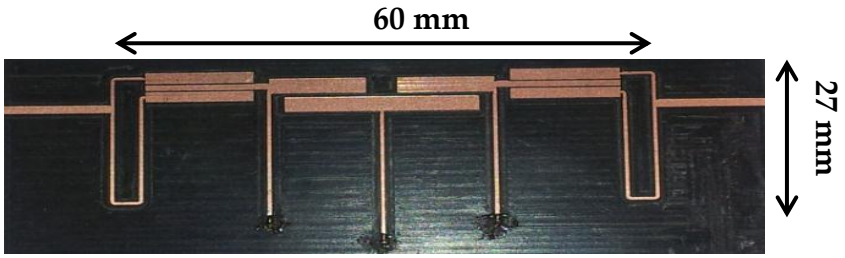

Figure III-24. Photograph of the third-order PC-SLR bandpass filters with optimized U corner.

Table III-8. Physical dimension of the PC-SLR filters with optimized U corners.

		PARAMETERS	VALUES
Physical parameters	**Parallel-coupled lines for input/output resonators**	w_{01}	1.69 mm
		w_1	0.95 mm
		S_{01}	111 µm
		L_{01}	12.05 mm
	Internal parallel-coupled lines	w_{12}	2.34 mm
		S_{12}	560 µm
		L_{12}	9 mm
	Short-circuited stub	w	0.44 mm
		L	19.8 mm
	U corner structure	w_c	0.4 mm
		L_a	7.9 mm
		L_b	33.7 mm

Figure III-25 shows the simulation and measurement responses of the PC-SLR filter with optimized U corners. Simulation and measurement results are in very good agreement. A wide out-of-band rejection is achieved, with **a first spurious frequency located at nine times the center frequency**. The rejection level in the upper out-of-band rejection is better than 25 dB from 1.1 GHz to 8.7 GHz. A transmission zero, located at 1.15 GHz, allows increasing the filter selectivity at the lower stop band side. The in-band minimum insertion loss is still lower than 2 dB while the return loss is still better than 18 dB. The 3-dB bandwidth is still 7 %, as expected.

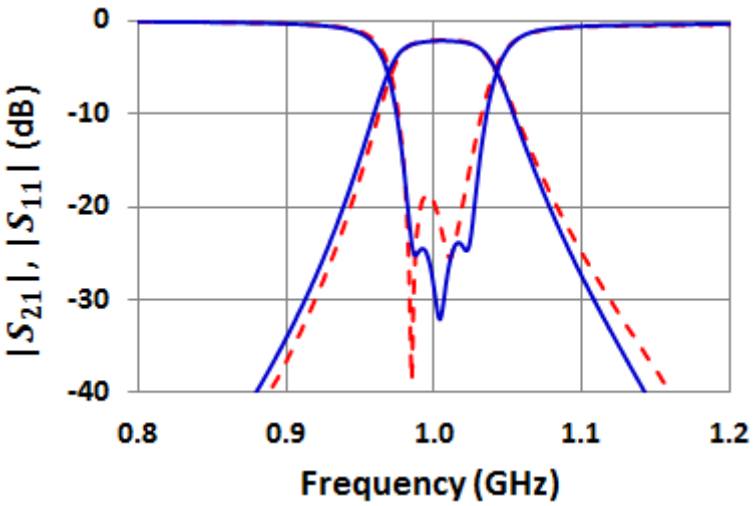

(a)

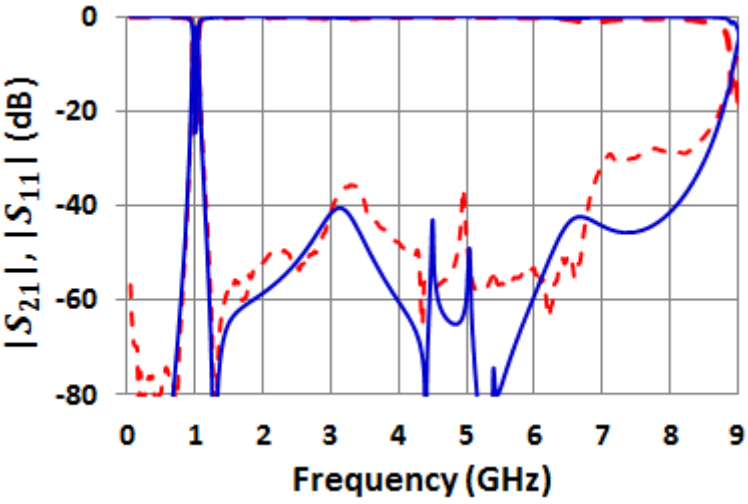

(b)

Figure III-25. S parameters of PC-SLR bandpass filter with optimized U corner: measurements (red dashed line) and circuit simulations (blue solid line), (a) Narrow band, (b) large band.

Finally, Figure III-26 shows the comparison of the measurements of both filters on the same graph in order to emphasize the improvement of the out-of-band rejection, without any modification in the passband.

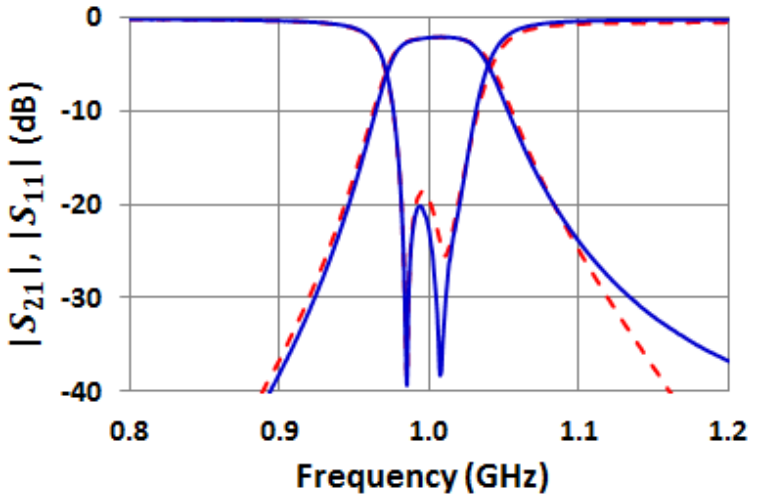

(a)

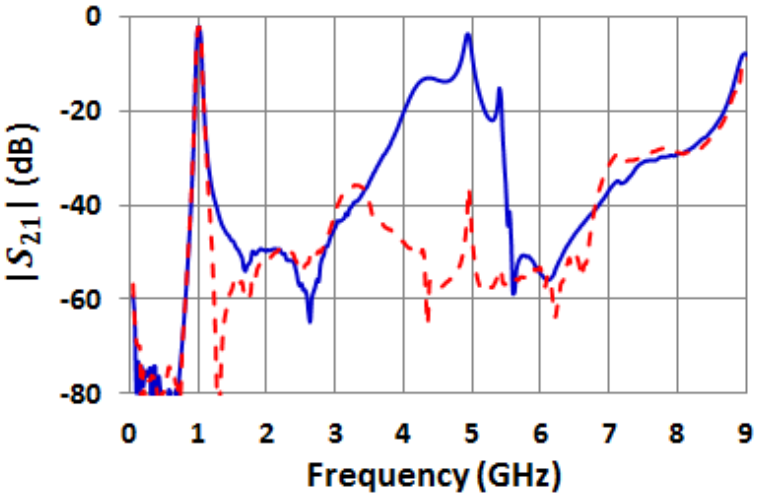

(b)

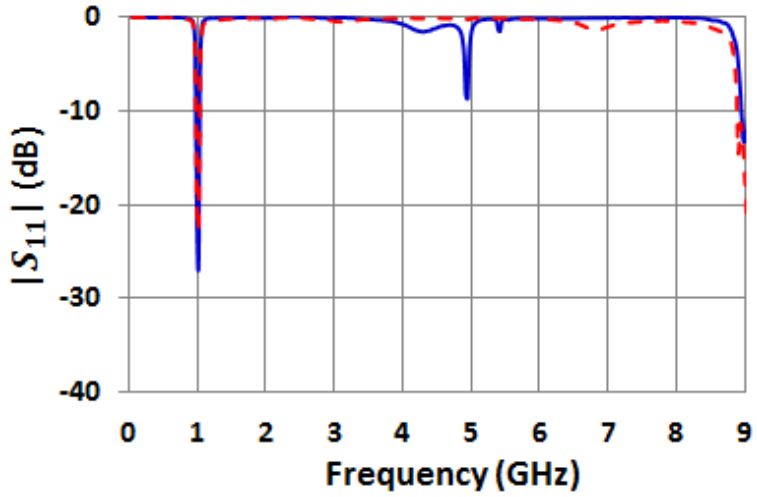

(c)

Figure III-26. Comparison of S-parameters measurement of the PC-SLR filter with non-optimized U corners (blue solid line) and with optimized U corners (red dashed line).

The total size of the PC-SLR with optimized U corners is 60 mm x 27 mm (0.2 λ_0 x 0.09 λ_0) for a surface of $0.018 \cdot \lambda_0^2$ while the classical coupled line bandpass filter (filter a) has a total size of 82 mm x 12 mm (0.79 λ_0 x 0.12 λ_0) for a surface of $0.095 \cdot \lambda_0^2$.

III.4. State-of-the-art comparison

The PC-SLR filter with optimized U corners carried out in this work was compared with several filters having a large out-of-band rejection in Table III-9. The comparison is not easy concerning the insertion loss because the fractional bandwidth and filters order are not the same. However, Table III-9 highlights that the proposed filter exhibits a very wide upper out-of-band rejection compared to the state-of-the-art. The compactness of these filters is also very interesting. The filter presented [13] is much smaller than the PC-SLR with optimized U corners but with a sacrifice in the return and insertion losses.

Table III-9. Comparison of the PC-SLR filter with optimized U corners with the state-of-the-art.

Reference	*Order n*	*f_0 (GHz)*	*FB[1] (%)*	*IL[2] (dB)*	*RL[3] (dB)*	*OR[4]*	*Surface ($x\lambda_0^2$)*
[1]	**3**	**2**	**20**	**~1.2**	**~17**	**2.7 f_0 (25 dB)**	**—**
[1]	**5**	**2**	**15**	**~2.4**	**~10**	**2.8 f_0 (25 dB)**	**—**
[2]	**5**	**2**	**8**	**1.4**	**—**	**4.6 f_0 (20 dB)**	**0.067**
[3]	**5**	**2.2**	**10**	**~2.2**	**~13**	**5.75 f_0 (20 dB)**	**0.106**
[3]	**5**	**2.5**	**15**	**~2.5**	**~11**	**6.7 f_0 (20 dB)**	**0.029**
[4]	**3**	**2.5**	**10**	**—**	**—**	**>2.4f_0 (25 dB)**	**0.032**
[5]	**3**	**2.45**	**—**	**—**	**20**	**2.8 f_0 (20 dB)**	**0.026**
[6]	**3**	**2.45**	**8**	**~1**	**18**	**5.1 f_0 (20 dB)**	**—**
[6]	**5**	**2.45**	**8**	**~1**	**14**	**7.8f_0 (20 dB)**	**—**
[7]	**3**	**2**	**10**	**2.45**	**18.8**	**4.25 f_0 (20 dB)**	**0,063**
[8]	**1**	**2.3**	**6.5**	**0.67**	**23**	**>4.3 f_0 (20 dB)**	**0.087**
[10]	**3**	**1.5**	**6**	**~3**	**—**	**4.3 f_0 (20 dB)**	**0.041**
[10]	**5**	**1.5**	**10**	**~3**	**~15**	**8.3 f_0 (20 dB)**	**0.061**
[11]	**4**	**1.97**	**6.7**	**2.68**	**~15**	**4.9 f_0 (20 dB)**	**0.029**
[12]	**3**	**2.45**	**8**	**1.5**	**15**	**~5.3 f_0 (25 dB)**	**0.03**
[12]	**5**	**2.45**	**8**	**2**	**18**	**~5.3 f_0 (25 dB)**	**0.052**
[13]	**4**	**1.5**	**10**	**2.35**	**12**	**~8.3 f_0 (25 dB)**	**0.009**
This work	**3**	**1**	**7**	**2**	**18**	**8.7 f_0 (25 dB)**	**0.018**

[1]***FB: Fractional Bandwidth rej***ection [2]***IL: Insertion Loss*** [3]***RL: Return Loss*** [4]***OR : Out-of-band***

References

[1] J.-T. Kuo, S.-P. Chen, and M. Jiang, "Parallel-Coupled microstrip filters with over-coupled end stages for suppresion of spurious responses", IEEE Microwave and Wireless Components Lett. , vol. 13, no. 10, pp. 440-442, Oct. 2003.

[2] M. Jiang, M.-H.Wu, and J.-T.Kuo, "Parallel-coupled microstrip filters with over-coupled stages for multispurious suppression", in IEEE MTT-S Int. Symp. Dig., Long Beach, CA, June 12-17, 2005.

[3] M.-A. Sanchez-Soriano, G. Torregosa-Penalva, and E. Bronchalo, "Multispurious suppression in parallel-coupled line filters by means of coupling control", IET Microwave Antennas Propag., vol. 6, no. 11, pp. 1269-1276, Aug. 2012.

[4] T. Lopetegi, M.-A. G. Laso, J. Hermandez, M. Bacaicoa, D. Benito, M.-J. Garde, M. Sorolla, and M. Guglielmi, "New Microstrip "Wiggly-Line" Filters with Spurious Passband Suppression", IEEE Trans. Microwave Theory and Tech., vol. 49, no. 9, pp. 1593-1598, Sept. 2001.

[5] S.-Sun, and L. Zhu, "Periodically Nonuniform Coupled Microstrip-Line Filters With Harmonic Suppression Using Transmission Zero Reallocation",IEEE Trans. Microwave Theory and Tech., vol. 53, no. 5, pp. 1817-1822, May 2005

[6] J.-T. Kuo, and M.-H. Wu, "Corrugated parallel-coupled line bandpassfilters with multispurious suppression", IET Microwave Antennas Propag., vol. 1, no. 1, pp. 718-722, June 2007.

[7] F. Karshenas, A. R. Mallahzadah, and J. Rashed-Mohassel, "Size reduction and harmonic suppression of parallel coupled-line bandpass filters using defected ground structure", in the 13th Antenna Technology and Applied Electromagnetics and the Canadien Radio Science Meeting, Toronto, ON, Feb. 15-18, 2009.

[8] C.-S. Kim, D.-H. Kim, I.-S. Song, K.- M.K.H. Leong, T. Itoh, and D. Ahn,"A Design of a Ring Bandpass Filters With Wide Rejection Band Using DGS and Spur-Line Coupling Structures", in IEEE MTT-S Int. Symp. Dig., Long Beach, CA, June 12-17, 2005.

[9] M. Makimoto, " Microwave Resonators and Filters for Wireless Communication", Springer, 2000.

[10] J.-T. Kuo, and E. Shih, "Microstrip Stepped Impedance Resonator Bandpass Filter With an Extended Optimal Rejection Bandwidth",IEEE Trans. Microwave Theory and Tech., vol. 51, no. 5, pp. 1554-1559, April 2003.

[11] P.-H. Deng, S.-C. Lin, Y.-S. Lin, C.-H. Wang, and C.-H. Chen, "Microstrip bandpass filters with dissimilar resonators for suppression of spurious responses", in the 35th European Microwave Conf. Dig., Paris, France, Oct. 4-6, 2005.

[12] Y.-C. Chiou, M.-H. Wu, and J.-T. Kuo, "Periodic stepped-impedance resonator bandpass filters with multispurious suppression", in IEEE MTT-S Int. Symp. Dig., San Fransisco, CA, June 11-16, 2006.

[13] T.-N. Kuo, W.-C. Li, C.-H. Wang, and C.-H. Chen, "Wide-Stopband Microstrip Bandpass Filters Using Quarter –Wavelength Stepped –Impedance Resonators and Bandstop Embedded Resonators", IEEE Trans. Microwave Theory and Tech., vol. 18, no. 6, pp. 389-391, June 2008.

[14] M. Akra, H. Issa, E. Pistono, A. Jrad, N. Carrao, and P. Ferrari, "Parallel-Coupled Stub-Loaded Resonator Filters with Wide Spurious Suppression," in the 42th European Microwave Conf. Dig., Amsterdam, Nierland, Oct. 29-Nov. 1, 2012.

[15] D. Pavlidis, and H.-L. Hartnagel, "The Design and Performance of Three-Line Microstrip Couplers", IEEE Trans. Microwave Theory and Tech., vol. 24, no. 10, pp. 631-640, Oct. 1976.

[16] C.-P. Chen, Z. Ma, Y. Takakura, H. Nihei, and T. Anada, "Novel wideband bandpass filter using open-ended stub loaded parallel coupled short-circuited three-line unit", in IEEE MTT-S Int. Symp. Dig., Boston, MA, June 7-12, 2009.

[17] R.-G. Garcia, J.-I. Alanso, "Design of sharp rejection and low loss wide bandpass filters using signal interference techniques", IEEE Microwave and Wireless Components Lett. , vol. 15, no. 8, pp. 530-532, Aug. 2005.

[18] C.-W. Tang, and M.-G. Chen, "A miscrostrip ultra-wideband bandpass filter with cascaded broadband bandpass and bandstop filters", IEEE Microwave and Wireless Components Lett. , vol. 55, no. 11, pp. 2412-2418, Nov. 2007.

Chapter IV. Tunable Compact Filters Based on Stub-Loaded Resonators

IV.1. Introduction

In recent years, to meet the requirements in mobile telephony and wireless communication services, much effort has been made to develop high performance bandpass filters having a low insertion loss, compact size, wide stopband, high selectivity, and tunability. The compactness, low insertion loss in passband and wide stopband are main standards for judging the performance of a filter. Tunable bandpass filters are in increasing demand in various applications for both electronic and communication systems to enable multiband operation. Compactness, tuning range and linearity are the main features of tunable filters. Miniaturized filters are always more practical in modern communication systems where circuit space is very costly.

The great number of recent publications demonstrating tunable microwave filters confirms their importance [1]-[17]. These reconfigurable filters include designs that can independently reconfigure their parameters to precisely cover bands of interest: center frequency ([2] and [4]-[7]), bandwidth ([1] and [10]-[13]), both center frequency and bandwidth ([3], [9] and [16]), or selectivity ([14] and [15]).

Electronically tunable filters have been realized by devices such as FET transistors, PIN diodes ([1], [11], [12], [14]), varactor diodes ([4], [10] and [16]), RF Micro-Electro-Mechanical Systems (MEMS) ([3], [5]-[9]) and dielectric varactors ([2], [13]). Varactor diodes offer a fast tuning speed over a wide tuning range, compactness, but they lead to a variation in insertion loss within tuning range, due to the variation of their quality factor, and distortion problems because of non-linearity. RF-MEMS as tuning capacitors (varactors) lead to low insertion loss, small size, high

linearity, but this technology still needs improvement in terms of speed, voltage actuation and reliability.

This chapter presents the structure of the capacitor loaded stub-loaded resonator (SLR), and then a complete resonant mode analysis is investigated. Tunability is achieved by using varactor diodes. For a proof-of-concept, filters based on these resonators are realized and characterized.

IV.2. Theoretical study of capacitor loaded SLR

In order to achieve a tunable PC-SLR filter, the idea is to capacitively load the short-circuited stub. By using varactors as variable capacitances the fundamental resonance frequency f_0 can be electronically tuned. Based on the analysis carried out in a previous work [17], it is convenient to place varactor near the tee-junction between the short-circuited stub and the open-ended transmission line, in order to maximize the tunability of the resonant frequency f_0.

Figure IV-1 shows the structure of the proposed capacitor loaded SLR. A capacitance (the loading element) is connected at the center of the SLR, the resonant condition of the resonator can be changed by varying the capacitance *C*, as explained further.

This section discusses the dependence of the capacitance *C* on the fundamental resonance frequency f_0. The expression of this resonance frequency is derived from the input admittance Y_{in}. Simplifications on the expression of $f_0$are proposed in order to propose a simple study of the loaded SLR. These simplifications are then validated theoretically by simulations. Since this structure is symmetrical, along AB plane (see Figure IV-1), it is convenient to analyze it by using the even- and odd-mode analysis technique in order to derive the resonance modes of the proposed structure.

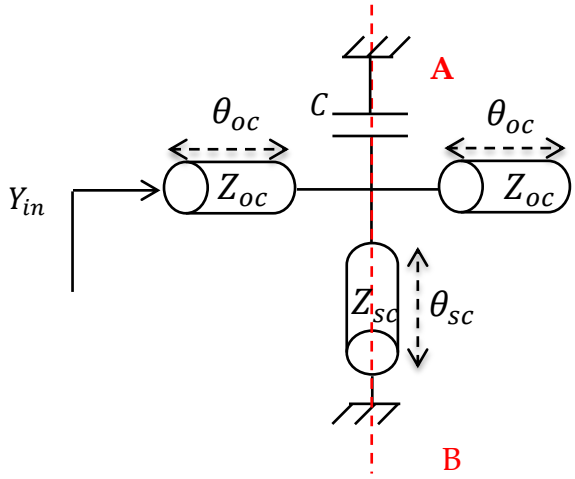

Figure IV-1. Schematic view of the proposed loaded SLR.

IV.2.1. Fundamental resonance frequency of the capacitor loaded SLR

a) Expression of the fundamental resonance frequency

The resonator structure to be considered here is shown in Figure IV-1. The input admittance Y_{in} of the loaded SLR can be calculated by considering $ABCD$ matrix operations. Ideal lossless transmission lines are considered as first approximation.

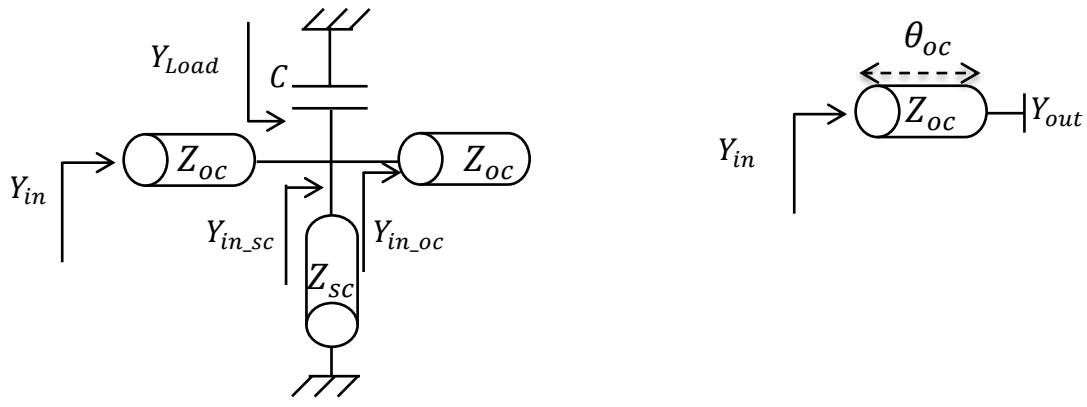

(a) (b)

Figure IV-2. (a), Capacitor loaded SLR and (b) equivalent circuit for derivation of the input admittance Y_{in}.

Based on the analysis carried out in chapter II, the input admittance Y_{in_sc} and Y_{in_oc} are given by:

$$Y_{in\_sc} = \frac{1}{j \cdot Z_{sc} \cdot tan(\theta_{sc})} \quad \text{(IV-1)}$$

$$Y_{in\_oc} = \frac{j \cdot tan(\theta_{oc})}{Z_{oc}} \quad \text{(IV-2)}$$

The load admittance of the capacitor C can be written as:

$$Y_{Load} = j \cdot C \cdot \omega \quad \text{(IV-3)}$$

The output admittance Y_{out} in Figure IV-2 can be expressed from (IV-1), (IV-2) and (IV-3) by:

$$Y_{out} = j \cdot (Y_{oc} \cdot tan(\theta_{oc}) - Y_{sc} \cdot cot(\theta_{sc}) + C \cdot \omega) \quad \text{(IV-4)}$$

Using the expression of Y_{out} and based on the equivalent circuit in Figure IV-2 (b), the input admittance is then expressed by:

$$Y_{in} = jY_{oc} \cdot \frac{2 \cdot \tan(\theta_{oc}) - R_Z \cot(\theta_{sc}) + Z_{oc} \cdot C \cdot \omega)}{1 - \tan(\theta_{oc}) \cdot (\tan(\theta_{oc}) - R_Z \cdot \cot(\theta_{sc}) + Z_{oc} \cdot C \cdot \omega)} \quad \text{(IV-5)}$$

The resonance condition of the capacitor loaded SLR can be easily obtained for $Y_{in} = 0$ and it can be approximated as:

$$f_0 = \frac{1}{2\pi} \sqrt{\frac{R_Z}{C \cdot Z_{0c} \cdot k_{sc} + 2 \cdot k_{sc} \cdot k_{oc}}} \quad \text{(IV-6)}$$

where $R_Z = \frac{Z_{oc}}{Z_{sc}}$ is the characteristic impedance ratio, and K_{sc} and K_{oc} are the phase delays of short and open-ended transmission lines, respectively.

From (IV.6), the resonant frequency f_0 is inversely proportional to the capacitance value C.

b) Validation: simulated capacitor loaded SLR resonator

In order to verify the resonance condition given by equation (IV.6), an unloaded resonator was first designed with Agilent ADS™ on a RT5880 substrate (relative permittivity ε_r= 2.21; dielectric loss tangent $tg\ \delta$ = 0.0009; dielectric thickness h = 787 µm ; copper thickness t = 17 µm).

For this resonator, the characteristic impedances Z_{sc} and Z_{oc} equal 118.6 Ω and 50.7 Ω, respectively, leading to a characteristic impedance R_Z ratio of 0.4. The microstrip widths of short and open-ended transmission lines are 0.4 mm and 2.3 mm, leading to effective relative permittivities ε_{reff_sc}= 1.7 and ε_{reff_oc} = 1.9, respectively. The physical lengths were fixed to 19.8 mm for the short-circuited transmission line and 11.22 mm for the open-ended transmission line (Figure IV-3), to obtain a resonance frequency equal to 1 GHz as shown in Figure IV-5 (blue solid line).The resonator was excited using a gap of 0.5 mm in order to not modify its resonant frequency.

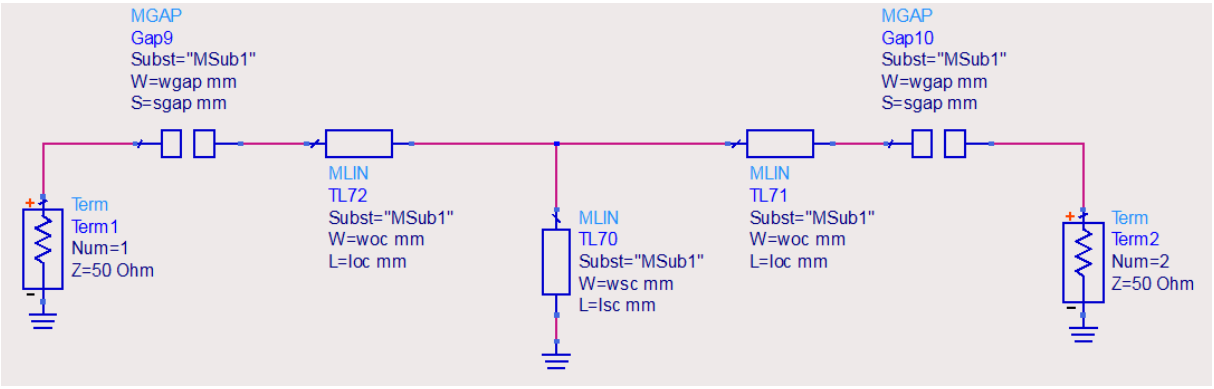

Figure IV-3. Electrical circuit of the SLR resonator.

By placing a capacitance near the tee-junction between the short-circuited stub and the open-ended transmission line as in Figure IV-4, f_0 varies versus the capacitance value.

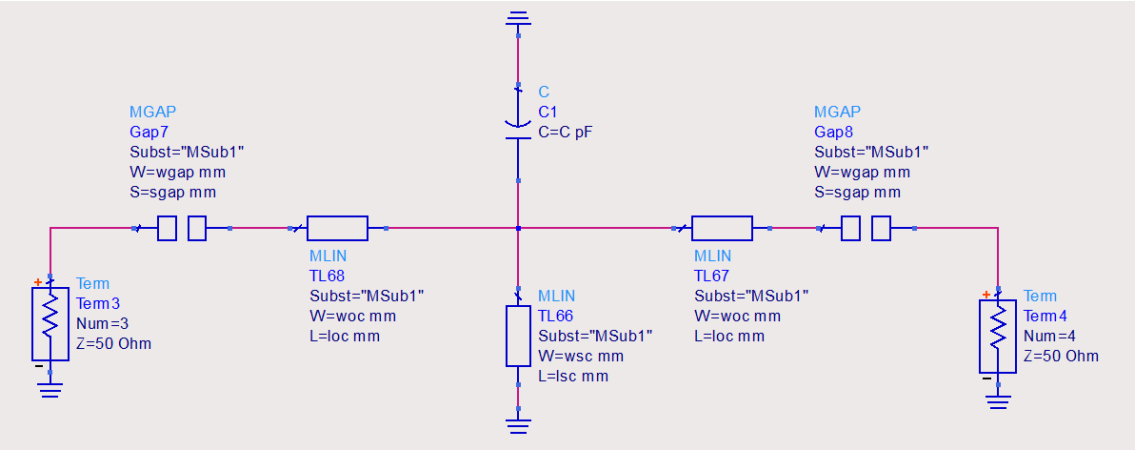

Figure IV-4. Electrical circuit of the capacitor loaded SLR.

Figure IV-5 gives the simulated results of the elementary SLR resonator and the capacitor loaded resonator for several C values. The simulated and computed (from IV.6) fundamental resonant frequency $f_0$is given in Table IV-1, for $C = 1$ pF, $C = 2$ pF, and $C = 3$ pF, respectively. As summarized in Table IV-1, simulated and computed values are in a good agreement, thus providing the validity of the approximated resonant frequency expression.

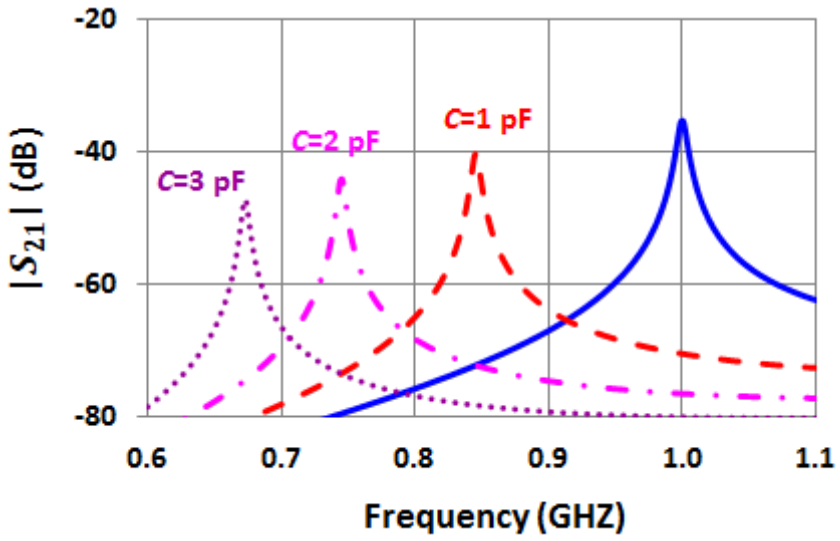

Figure IV-5. Simulated transmission parameter of: the slightly coupled SLR (blue solid line), and the capacitor loaded SLR for several C values (1 pF, 2 pF and 3 pF).

Table IV-1. Simulated and computed fundamental resonant frequency value.

C (pF)	f_0*(MHz)	f_0¯(MHz)	*uncertainty*
1	846	870.6	2.8 %
2	745.5	755.2	1.3 %
3	673.5	676.2	0.4 %

*simulated value ¯computed value

IV.2.2. Resonance modes of the capacitor loaded SLR

a) Odd-mode resonance frequencies

When odd mode excitation is applied, the midpoint is short-circuited; the stub and the loaded capacitance can be ignored. This leads to the odd-mode equivalent circuit shown in Figure IV-6.

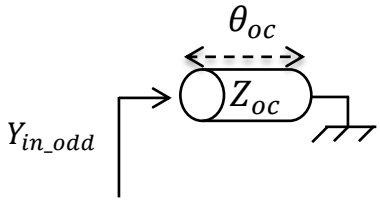

Figure IV-6. Odd-mode equivalent circuit.

Similarly to the odd-mode input admittance of the elementary SLR resonator presented in chapter III, the odd-mode input admittance of the capacitor loaded resonator is given by:

$$Y_{in\_odd} = \frac{1}{j \cdot Z_{oc} \cdot \tan(\theta_{oc})} \qquad \text{(IV-7)}$$

The resonance condition can be obtained by considering the open-ended condition, for $Y_{in\_odd} = 0$. Then the odd-mode resonant frequency can be easily obtained from (IV.7) and can be approximated as:

$$f_{odd} = i_{odd} \cdot \frac{c}{4 \cdot \sqrt{\varepsilon_{reff\_oc}} \cdot l_{oc}} \quad \text{(IV-8)}$$

where $i_{odd} = 1, 2, 3 \ldots$, c is the light velocity in vacuum, ε_{reff_oc} and l_{oc} are the effective relative permittivity and the physical length of the open-ended transmission line, respectively.

From (IV.8) it is obvious that the odd-mode resonant frequencies (f_{odd}) of the capacitor loaded SLR are determined by the electrical length of the open-ended resonator without any impact of the loading capacitance.

b) Even-mode resonance frequencies

For even-mode excitation, we can symmetrically bisect the capacitor loaded SLR to obtain the equivalent circuit given in Figure IV-7

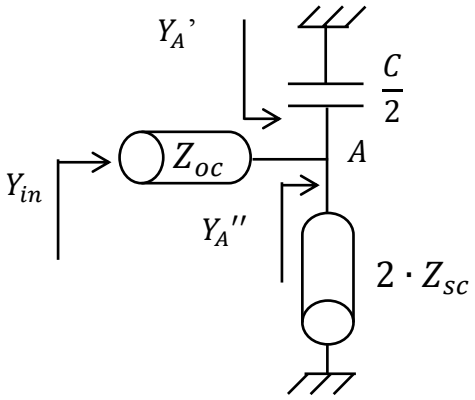

Figure IV-7. Even-mode equivalent circuit.

By considering the short-circuited condition, the input admittance Y''_A is given by:

$$Y''_A = \frac{1}{j \cdot (2 \cdot Z_{sc}) \cdot \tan(\theta_{sc})} \quad \text{(IV-9)}$$

The input admittance Y'_A can be approximated as:

$$Y'_A = j \cdot \frac{C}{2} . \omega \quad \text{(IV-10)}$$

If a varactor is used as a tunable reactive loading element, the input admittance can be rewritten as:

$$Y'_A = j \cdot \frac{C}{2} . \omega = j \cdot b(V) \quad \text{(IV-11)}$$

where V is the reverse voltage applied to the varactor diode.

Using (IV.9) and (IV.11), it can be derived:

$$Y_A = Y'_A + Y''_A$$

$$Y_A = j \cdot b(V) - j \cdot \frac{1}{(2 \cdot Z_{sc}).\tan(\theta_{sc})} = j \cdot \left[b(V) - \frac{1}{(2 \cdot Z_{sc}).\tan(\theta_{sc})} \right] = j.B(V) \quad \text{(IV-12)}$$

with $B(V) = \left[b(V) - \frac{1}{(2 \cdot Z_{sc}).\tan(\theta_{sc})} \right]$

The even-mode admittance can be expressed from (IV.11) as:

$$Y_{in\_even} = \frac{j \cdot \frac{\tan(\theta_{oc})}{Z_{oc}} + Y_A}{1 + j \cdot Z_{oc} \cdot \tan(\theta_{oc}) \cdot Y_A} = j \cdot \frac{\frac{\tan(\theta_{oc})}{Z_{oc}} + B(V)}{1 + j \cdot Z_{oc} \cdot \tan(\theta_{oc}) \cdot Y_A} \quad \text{(IV-13)}$$

The approximated resonance condition can be obtained by considering the open ended condition ($I = 0$):

$$f_{even} = \frac{k.c}{2.l_{oc} \cdot \sqrt{\varepsilon_{eff\_oc}}} + \text{atan}[-\frac{B(V)}{Y_{oc}}] . \frac{c}{2 \cdot \pi \cdot l_{oc} \cdot \sqrt{\varepsilon_{eff\_oc}}} \quad \text{(IV-14)}$$

where $k = 0, 1, 2, ...$

The fundamental resonance frequency of the PC-SLR based on capacitor loaded SLR is approximated for $k = 0$, by:

$$f_{even} = \text{atan}[-\frac{B(V)}{Y_{oc}}] . \frac{c}{2 \cdot \pi \cdot l_{oc} \cdot \sqrt{\varepsilon_{eff\_oc}}} \quad \text{(IV-15)}$$

The even-mode resonant frequencies can be electrically tuned by varying the reverse capacitor biased voltage applied to the varactor diode. **As analyzed above, when SLR is capacitively loaded it has fixed odd-mode resonance frequencies and tunable even-modes.**

c) Validation of the concept: Parallel-coupled bandpass filter with capacitor loaded SLR

For a proof-of-concept, a third-order PC-SLR bandpass filter was designed (case 3 in chapter III), with passband ripple of 0.01 dB, a relative bandwidth of 2 %, and a center frequency of 1 GHz. This filter was designed and simulated considering ideal transmission line in order to study the even- and odd-mode resonance frequencies of the PC-SLR with capacitor loaded resonators. Figure IV-8 shows the simulation responses (blue solid line) where the first four spurious resonant modes are odd-even mode located at 4.5 GHz, even-mode (8.1 GHz), even-mode (10.1 GHz) and even-odd mode (13.6 GHz), as already shown in chapter III, and the PC-SLR based on capacitor loaded SLR for several *C* values (1 pF, 2 pF, and 3 pF). Figure IV-8 (a) illustrates the expected variation of the fundamental frequency (even-mode) for the PC-SLR, with a fundamental resonance occurring at 1 GHz for the PC-SLR based on unloaded SLRs. As expected, odd-modes (studied in Chapter III) located at 4.5 GHz and 13.6 GHz (Figure IV-8 (b)) are unchanged as expected, while it is seen that changing the value of the loaded capacitance modifies the even-mode resonant frequencies.

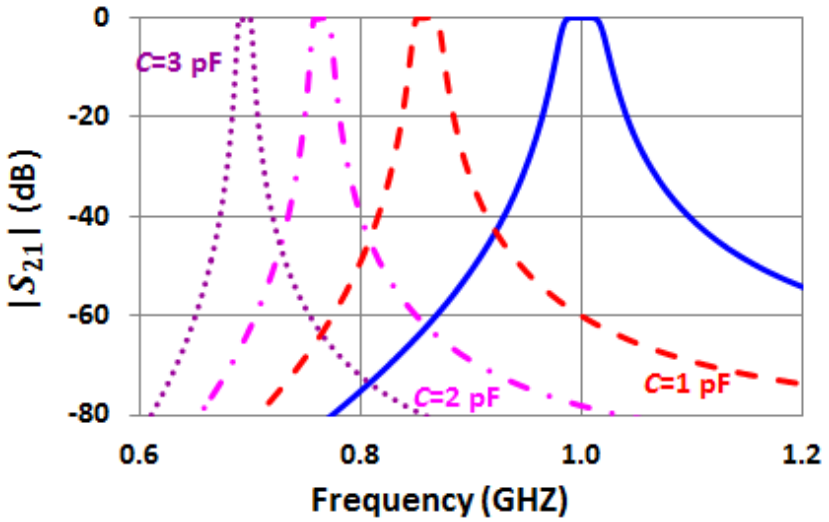

(a)

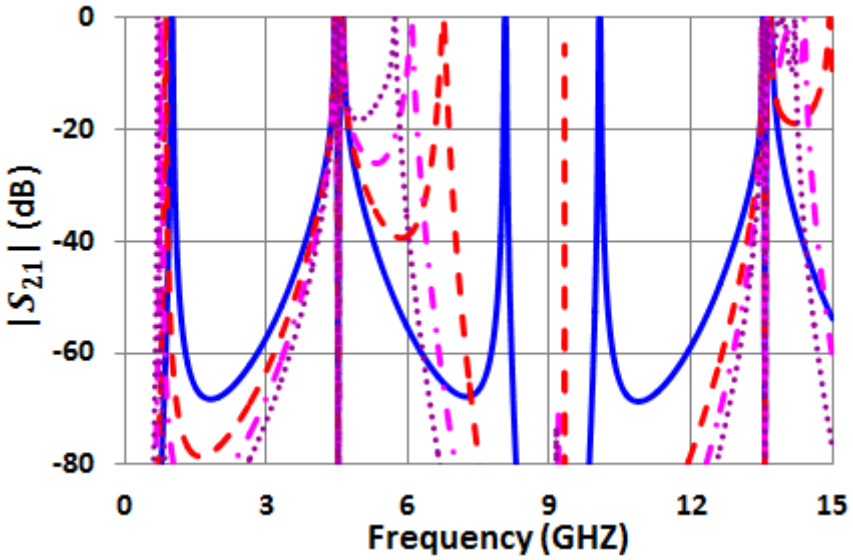

(b)

Figure IV-8. S parameters of the PC-SLR bandpass filter based on classical SLR (blue solid line) and compared with three capacitor loaded SLR bandpass filters: for capacitance values, 1 pF (red dashed line), 2 pF (pink dashed dotted line, 3 pF (dotted mallow line)) (a) narrow band (fundamental mode (even-mode)), (b) wide band .

It can be seen from Figure IV-8 (a), that the significant shift of the fundamental resonance is achieved with the sacrifice of the bandwidth. The filter bandwidth is reduced as the passband is shifted to lower frequencies. This is due to the fixed coupling sections between resonators. Indeed, these fixed couplings do not allow to obtain a constant loaded factor $Q = \frac{f_0}{f_2 - f_1} = \frac{f_0}{\Delta f_{3dB}}$, where f_1 and f_2 are the limits of the first frequency band measured where the insertion loss is 0.01 dB. Thus, in order to maintain a constant bandwidth while shifting the resonant frequency, the inter-resonators coupling should be varied. This therefore will require three more tuning capacitances [16] Simulations show that the required values of these capacitances are in the range of 0.006 pF to 0.02pF. Since available varactor diodes exhibit a minimal capacitance value of approximately 0.02 pF, it is not easy to change the inter-resonators coupling.

IV.3. The varactor diode

Varactor diode is a semiconductor diode that essentially consists of pn junction operated in reverse bias. When reversed biased voltage is applied, the capacitance across the pn junction is controlled. The property of the capacitance change is utilized to achieve a change in the frequency and/or the phase of an electrical circuit. This behavior provides a voltage controllable variable capacitance component. The reverse voltage and the junction capacitance are related by [18]:

$$C_j = \frac{C_{j0}}{(1+\frac{V}{V_j})^{\gamma}} \qquad \text{(IV-16)}$$

where $C_j$is the variable junction capacitance of the varactor diode, V is the applied reverse bias voltage, V_j is the built-in junction potential, γ is a coefficient that depends on the junction doping profile, $C_{j0}$is the junction capacitance without an external bias and it is given by:

$$C_{j0} = A \cdot \sqrt{(\frac{\varepsilon \cdot e \cdot N_d}{V_j})} \qquad \text{(IV-17)}$$

where A is the area of the diode, ε the dielectric constant of the epitaxial layer material, e the electronic charge, N_d epitaxial layer doping density.

When modeling a varactor diode, one should take the parasitic elements that are due to the package into account, in order to obtain an accurate equivalent electrical circuit model at the frequency band of interest. The classical varactor model diode is shown in Figure IV-9, where R_s is the parasitic variable series resistance of the diode, L_s and C_p represent the parasitic inductance and capacitance due to the package, respectively. In this model, R_s varies with the applied voltage.

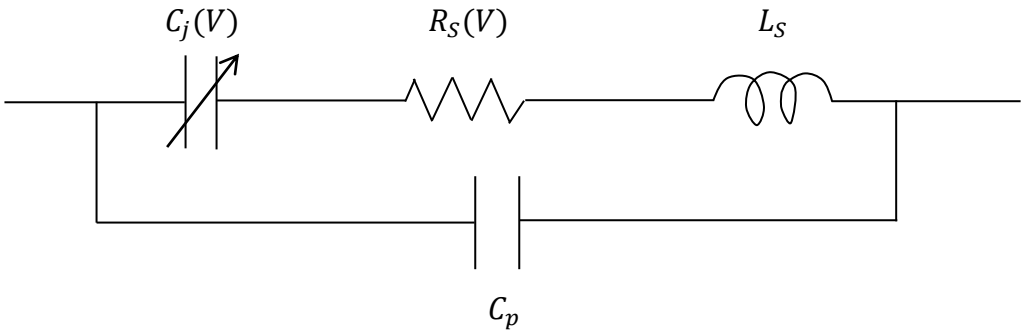

Figure IV-9. Simple model of a packaged varactor diode.

There are several types of varactor diode. However, the voltages involved have sometimes large range according to the application. It is important to emphasize that the choice of the diode must be focused on a component that has the lowest series resistance, and convenient capacitance ratio depending on the required application. One of the key parameters for a varactor diode is the capacitance ratio. This is commonly expressed in the form $\frac{C_{max}}{C_{min}}$ where C_{max} corresponds to the lowest reverse biased voltage.

For the filter developed in this work, the varactor diode used is the MA-COM MA46H071 GaAS varactor. It offers a capacitance ratio of $\frac{C_{max}}{C_{min}} = 6$, which is convenient for this work. After extracting data from the $C_j(V)$ curve, the capacitance of the MA46H071 varactor diode was modeled by the equation:

$$C_j = \frac{2.69}{(1+\frac{V}{0.92})^{0.57}} \quad [\text{pF}] \qquad (\text{IV-18})$$

Based on this equation the capacitance versus the reverse voltage is presented in Figure IV-11. Note that, the parasitic elements are not taken into account in this equation but can be extracted by comparing measured *S* parameters of the varactor diode (extracted from the datasheet) with the simulated model shown in Figure IV-9.

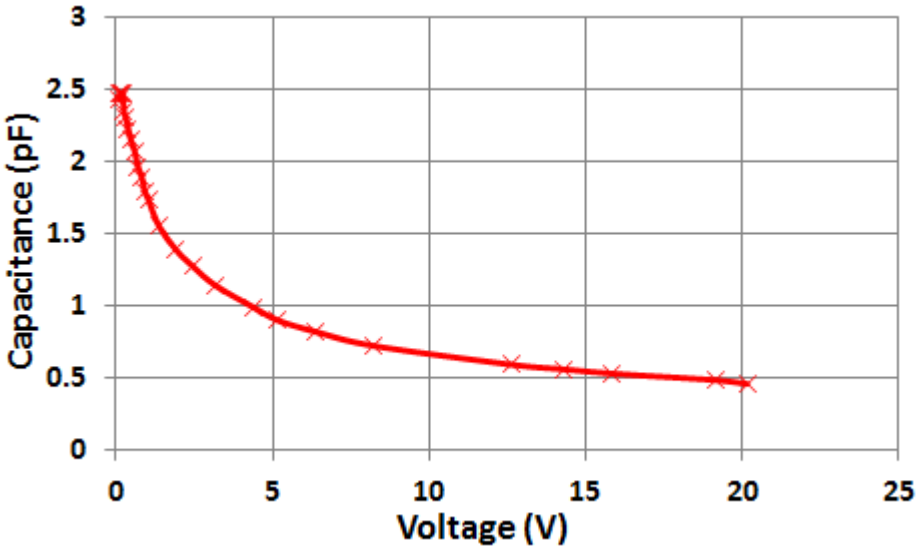

Figure IV-10. Capacitance versus reverse voltage for the varactor diode MA46H071 at 1 MHz, based on equation (IV-18).

Thus, the complete model considering parasitic effects R_s, L_s and C_p can be achieved: R_s varies from 0.1 Ω (at 20 V) to 3 Ω (at 1 V) with , $L_s = 1.1$ nH and $C_p = 0.1$ pF. Finally, taking these effects into account, the equivalent capacitance range versus the reverse voltage varied from 0.294 pF at (22 V) to 2.14 pF (0.1 V).

IV.4. Experimental results

To verify the theoretical results, an unloaded and fixed filter based on SLR was developed, and called "filter 1". Then, each of its resonators was capacitively loaded, according to the criteria outlined in the previous section. Finally, "filter 2" was optimized in order to show the performance of this kind of tunable filter.

IV.4.1. Filter 1

The PC-SLR filter was designed and synthesized based on the classical *J*-inverter method. A center frequency of 1.5 GHz with a fractional bandwidth of about 9 % was considered. The filter was designed with Agilent ADS™ and fabricated on a RT 5880 substrate (dielectric constant $\varepsilon_r = 2.21$, dielectric loss tangent $tan\delta = 0.9.10^{-3}$, substrate thickness $h = 0.787$ mm, copper thickness $t = 17$ µm).

The electrical length θ_{oc} of the open-ended resonator is equal to 32°, with a characteristic impedance ratio $R_Z = 0.4$ ($Z_{sc} = 125\,\Omega$, $Z_{oc} = 50\,\Omega$). Based on the analysis carried out in chapter III, the first spurious frequency is approximately at $2.8 \cdot f_0$ (odd mode), as seen in Figure IV-11.

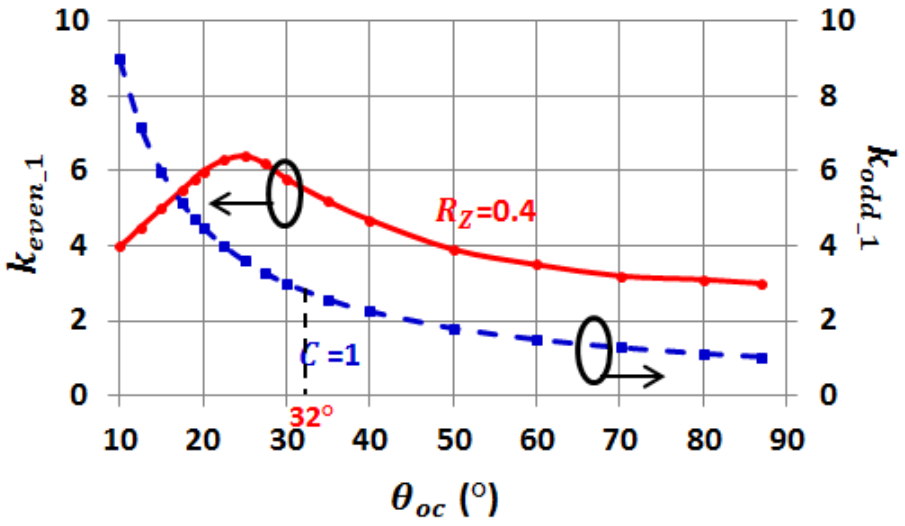

Figure IV-11. Normalized first spurious frequencies k_{even_1} and k_{odd_1} versus the electrical length θ_{oc} of the open-ended resonator.

Figure IV-12 gives the photograph of the realized filter. Its total size is 71.8 mm x 12.9 mm ($0.37\,\lambda_0 \times 0.066\,\lambda_0$) for a surface equal to $0.024 \cdot \lambda_0^2$. The overall dimensions of the filter is given in Table IV-2.

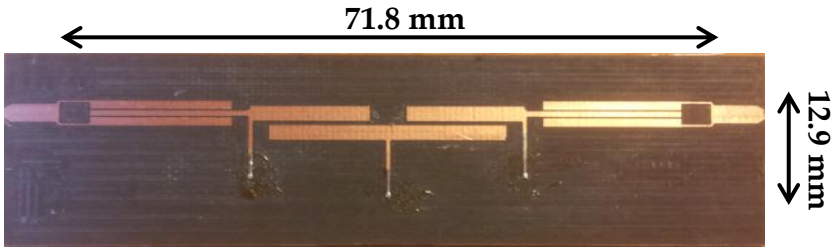

Figure IV-12. Photograph of the third-order PC-SLR bandpass filter of relative bandwidth 8.7 %.

Table IV-2. Physical dimension of the PC-SLR filter.

		PARAMETERS	VALUES
Physical parameters	**Parallel-coupled Lines for input/output resonators**	w_{01}	1.1 mm
		w_1	0.7 mm
		S_{01}	250 µm
		L_{01}	15.32 mm
	Internal parallel-coupled lines	w_{12}	2 mm
		S_{12}	540 µm
		L_{12}	11.05 mm
	Short-circuited stub	w_{sc}	0.45 mm
		L_{sc}	7.09 mm
	U corner structure	w	0.3 mm
		$L_a = L_b$	7.9 mm

Figure IV-13 gives the simulation and measurement responses of the PC-SLR filter, "filter 1". Simulation and measurement results are in good agreement. As expected from the previous analysis, the first spurious frequency is located at approximately 2.8 times the center frequency (odd mode) (Figure IV-13(b)).

Detailed data shows that the in-band minimum insertion loss is 1.5 dB while the return loss is better than 15 dB. The 3-dB bandwidth is 8.7 %, as expected.

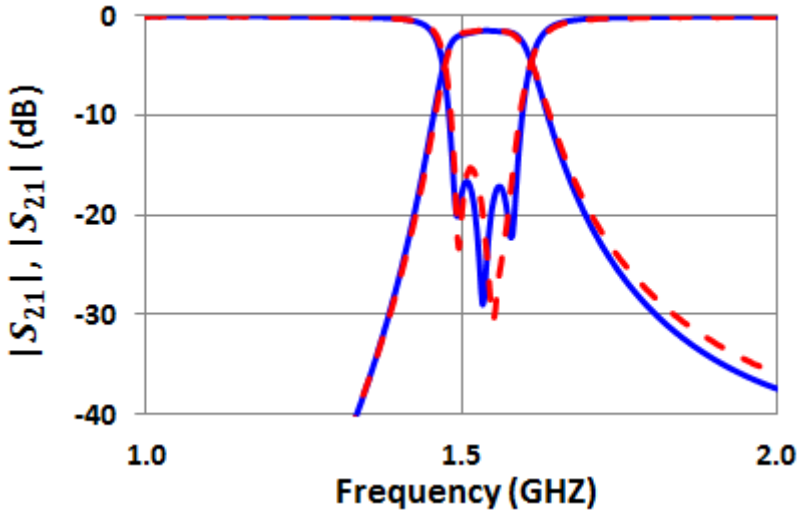

(a)

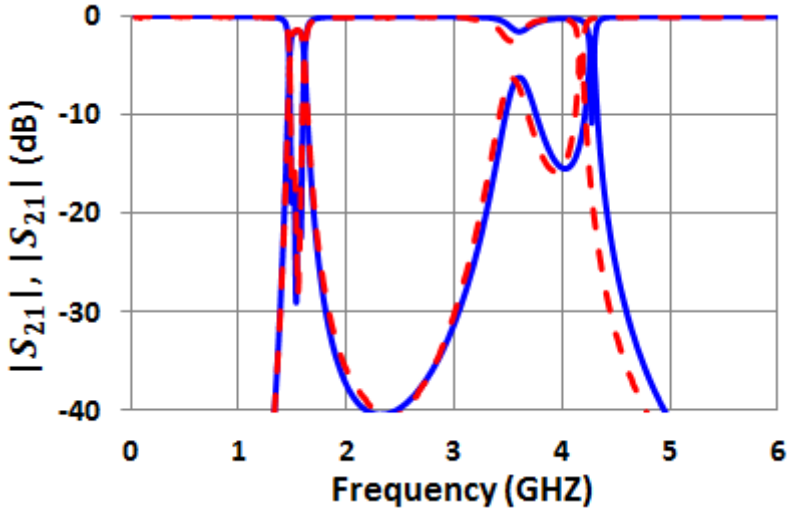

(b)

Figure IV-13. S parameters of PC-SLR bandpass filter: measurements (red dashed line) and circuit simulations (blue solid line), (a) Narrow band, (b) wide band.

IV.4.2. Stub reduction versus capacitance value

As previously demonstrated, by loading the short-circuited stub by variable capacitance (varactor diode), the working frequency of the filter can be electronically tuned. The length of the stub is also reduced, leading to even more compact filters.

As given in Table IV-2, the length of the short-circuited stub is 7.09 mm. Figure IV-14 is considered to study the length reduction of the capacitor loaded SLRs at the working frequency of the PC-SLR bandpass filter ("filter 1").

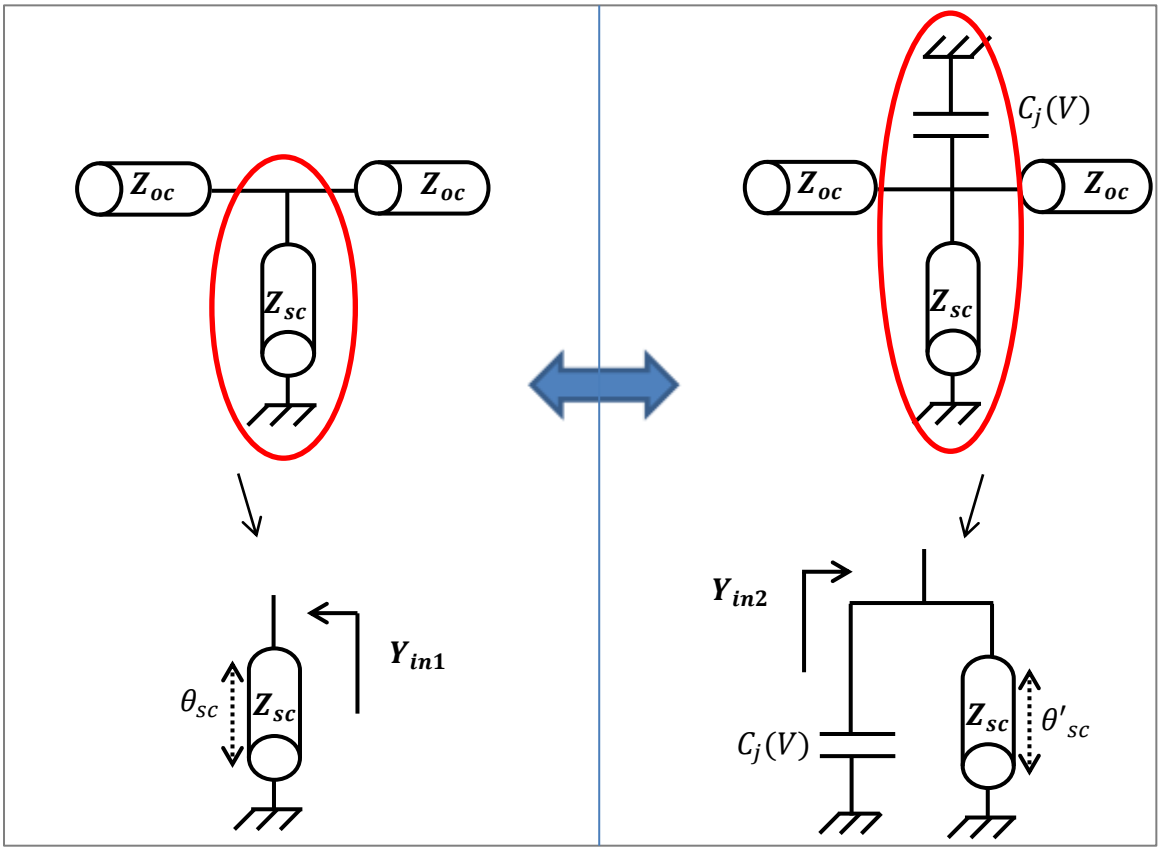

Figure IV-14. Schematic view of the SLR (of filter 1) and the capacitor loaded SLR.

Without considering neither the loss of transmission lines nor the parasitic elements of the varactor diode, the two resonators (unloaded and loaded SLRs) in Figure IV-14 resonate at the same frequency when:

$$Y_{in1} = Y_{in2} \tag{IV-19}$$

Y_{in1} and Y_{in2} can be expressed as:

$$Y_{in1} = \frac{1}{j \cdot Z_{sc} \cdot tan(\theta_{sc})} \tag{IV-20}$$

and

$$Y_{in2} = j \cdot \left[C_j \cdot \omega - \frac{1}{Z_{sc}.\tan(\theta'_{sc})} \right] \tag{IV-21}$$

By equating (IV-20) and (IV-21), the capacitance value can be written as:

$$C_j = \frac{1}{Z_{sc} \cdot \omega} \cdot \left[\frac{1-\frac{\tan(\theta'_{sc})}{\tan(\theta_{sc})}}{\tan(\theta'_{sc})}\right] \quad \text{(IV-22)}$$

Based on the resonators of "filter 1", Figure IV-15 gives the reduction of the stub length to achieve the working frequency versus the capacitance value. It is obvious that the reduction increases with the capacitance value. It reaches 51.5 % for a reduced physical length of 3.4 mm for a 3.2 pF capacitance value and 21.5 % for a reduced physical length of 5.5 mm.

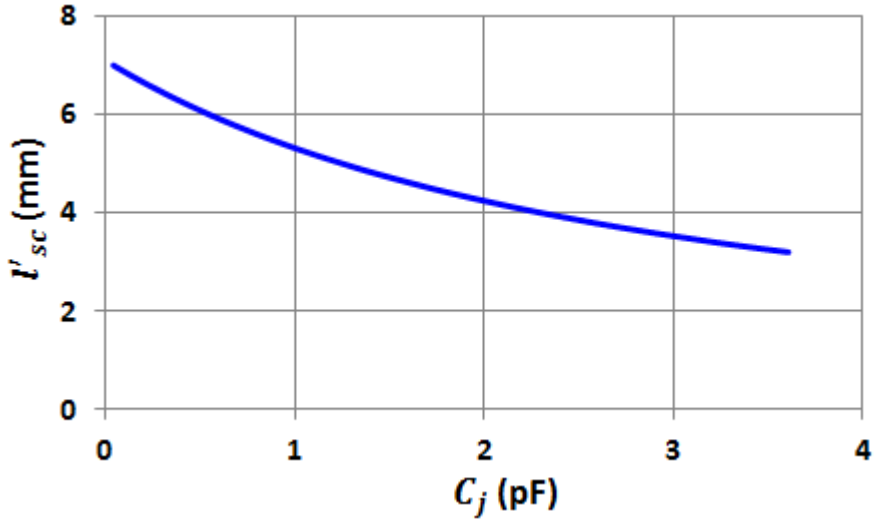

(a)

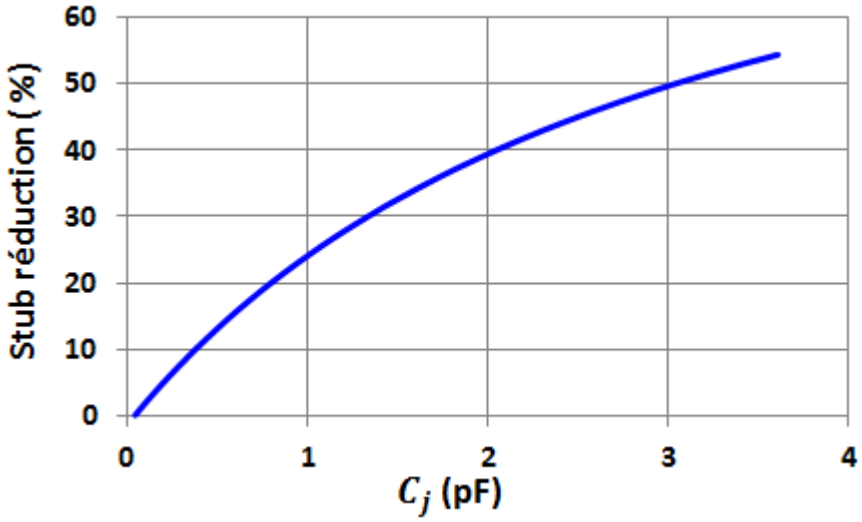

(b)

Figure IV-15. Effect of the variable capacitance on the short circuited stub at the working frequency of "filter 1": (a) physical stub length and (b) stub length reduction versus capacitance value.

For a proof-of-concept, a three-pole bandpass filters based on capacitor loaded resonators was fabricated. The physical parameters of the tunable bandpass filters can be deduced from "filter 1" with modified stub lengths. "Filter 2" was constructed with 5.5 mm stub length. The photograph of resulting filters is given in Figure IV-16.

The concept was validated using three varactor diodes (connected to the center of each resonator) as shown in Figure IV-16. These varactor diodes were biased with only two DC voltages, $V_1$to control the lateral varactors C_1 and $V_2$to control the central varactor C_2, respectively.

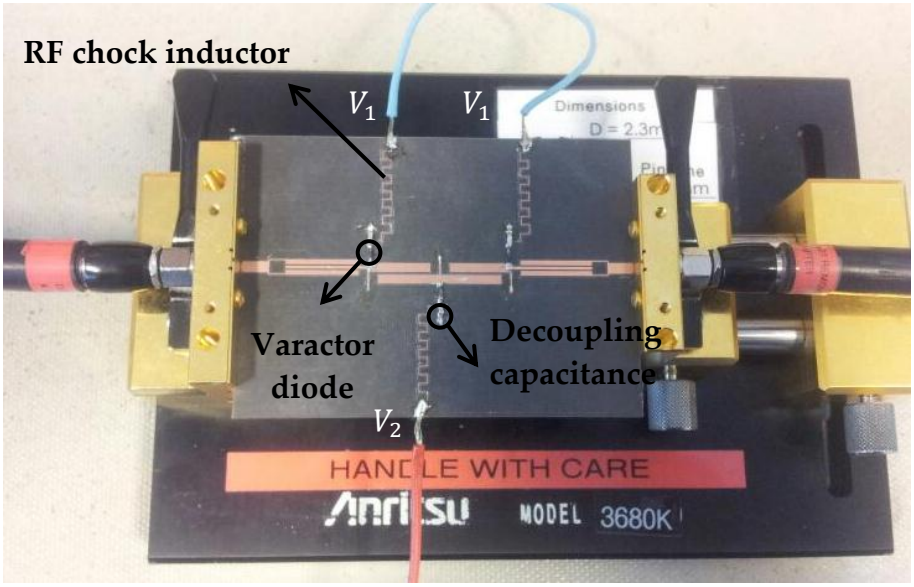

Figure IV-16. Photograph of the third order tunable parallel-coupled bandpass filter.

IV.4.3. Filter 2 simulation and measurement responses

"Filter 2" was based on the dimensions of "filter 1". Only the short-circuited stub length was modified (5.5 mm instead of 7.09 mm). For a 5.5 mm stub length the capacitance value needed to fix the same working frequency as "filter 1" (as shown in Figure IV-15) is included in the capacitance range value of the varactor diode (0.291 pF to 2.14 pF). Thus, the center frequency tuning range will be localized around 1.5 GHz.

Simulated *S*-parameters of the "filter 2" are illustrated in Figure IV-17. The insertion loss varied from around -6.8 dB to -2.1 dB. The simulated tuning range is 1.36-1.57 GHz corresponding to a relative tuning range of (+/- 7.2 %) around 1.47 GHz. The 3-dB relative bandwidth was included between about 5 % at 1.36 GHz to 8.2 % at 1.57 GHz, as shown in (a).

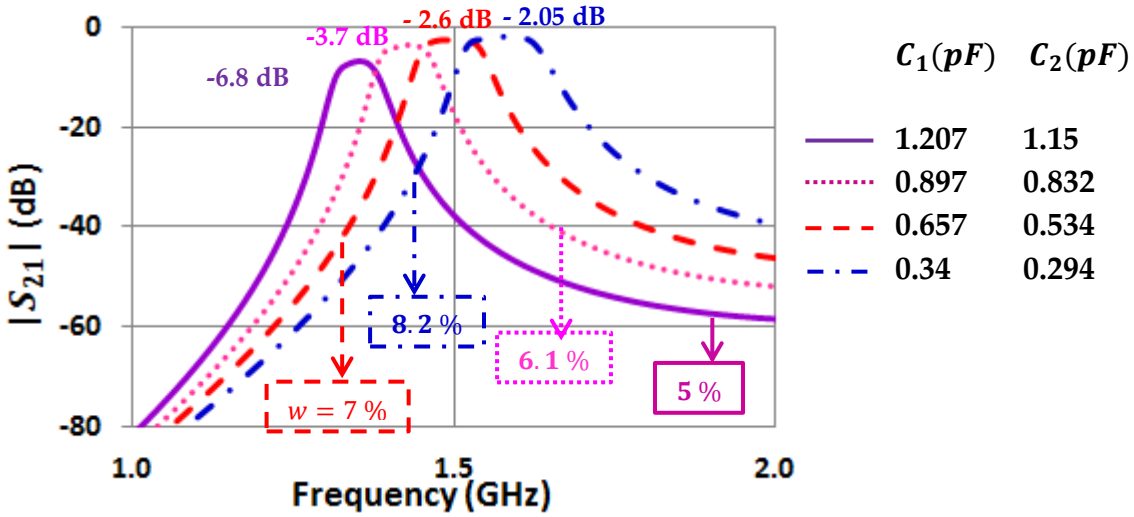

(a)

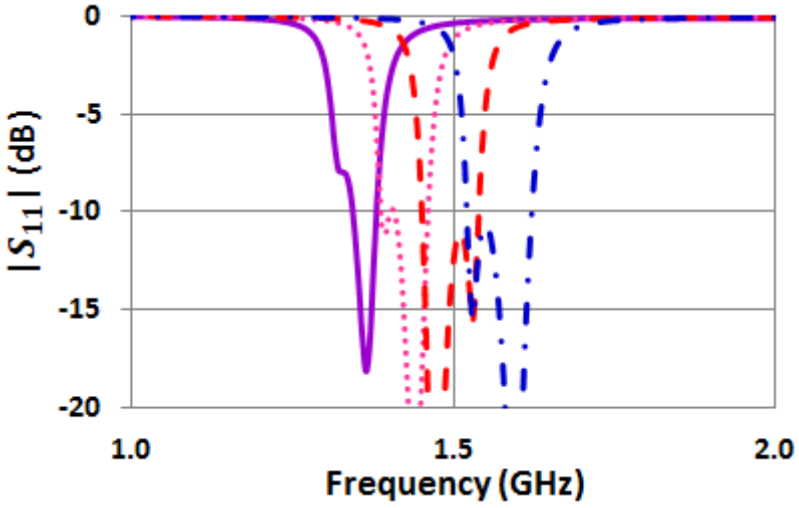

(b)

Figure IV-17. Simulated S parameters of the PC-SLR bandpass filter based on capacitor loaded SLR("Filter 2") with different values of $C_1$and C_2: (a) transmission coefficient, (b) return loss.

Measurements of the filter were carried out. Results are shown in Figure IV-18. Detailed data shows that the filter insertion loss varied from around -6.8 dB to -2.4 dB. The measured tuning range is 1.34-1.56 GHz (+/- 7.6 %) around 1.45 GHz. The 3-dB relative bandwidth was found to increase from approximately 5.5% at 1.34 GHz to 8.3 % at 1.56 GHz, as illustrated in (a) while return loss is better than

10 dB (Figure IV-18 (b)). Due to technological resolution, especially concerning the gap width, the insertion loss behavior in the passband is affected for the narrowest bandwidth.

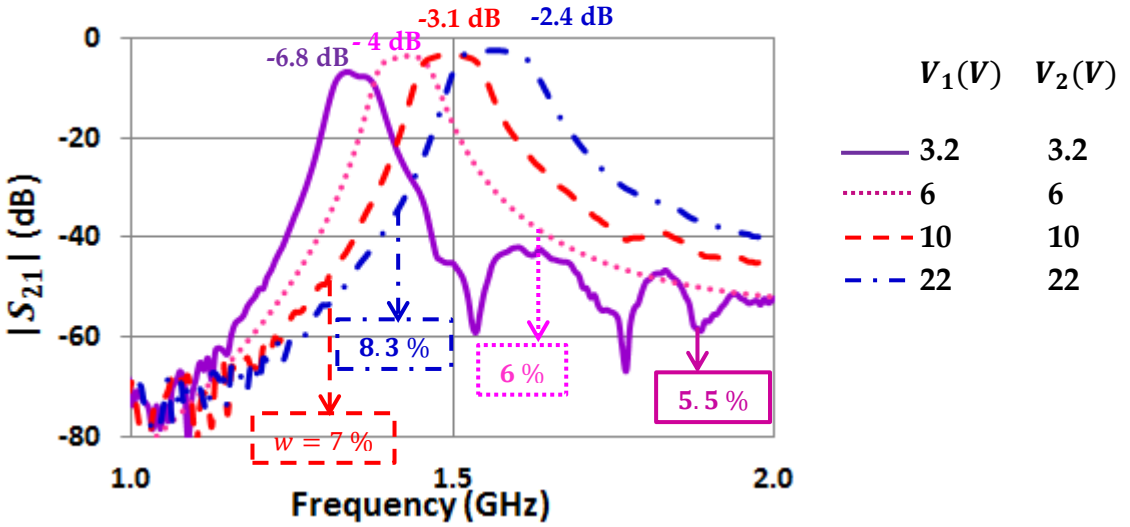

(a)

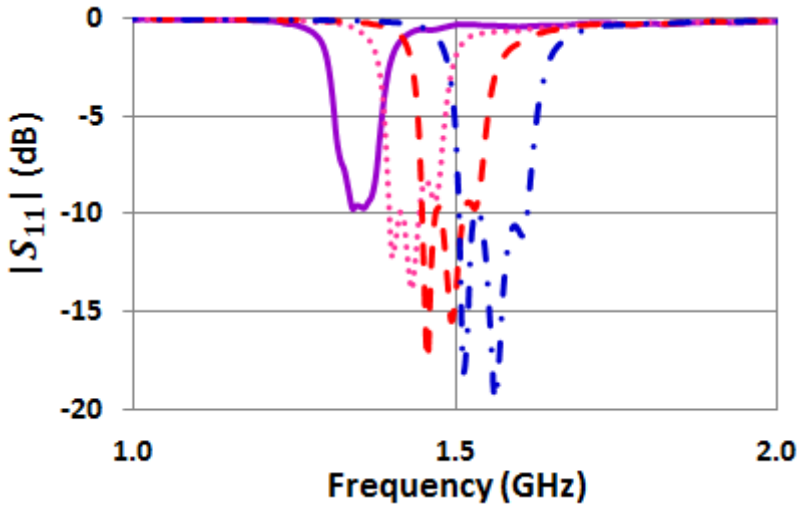

(b)

Figure IV-18. Measured S parameters response of ("Filter 2") for DC voltages $V_1$and V_2: (a)transmission coefficient S_{21}, (b) return loss S_{11}.

Finally, Figure IV-19 shows the comparison of the simulated (solid lines) and measured (dashed lines) results. Here again, simulation and measurement results are in good agreement.

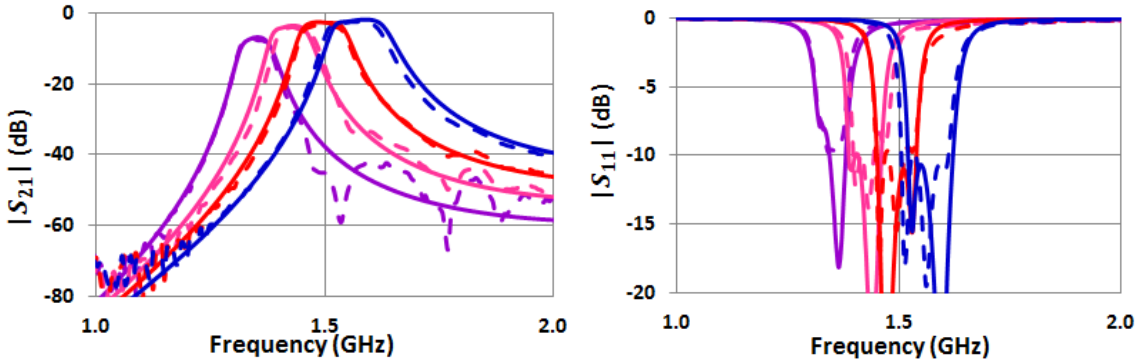

(a) (b)

Figure IV-19. Comparison of the measured and simulated S-parameters of "filter 2".

Figure IV-20, shows the simulation (blue solid line) and measurement (red dashed line) responses in a wide band for $V_1 = 16.5\,V, V_2 = 22\,V$ (corresponding to C_1=0.34 pF, and $C_2 = 0.294$pF). As expected from the previous analysis, the first spurious frequency is located at approximately 4 GHz.

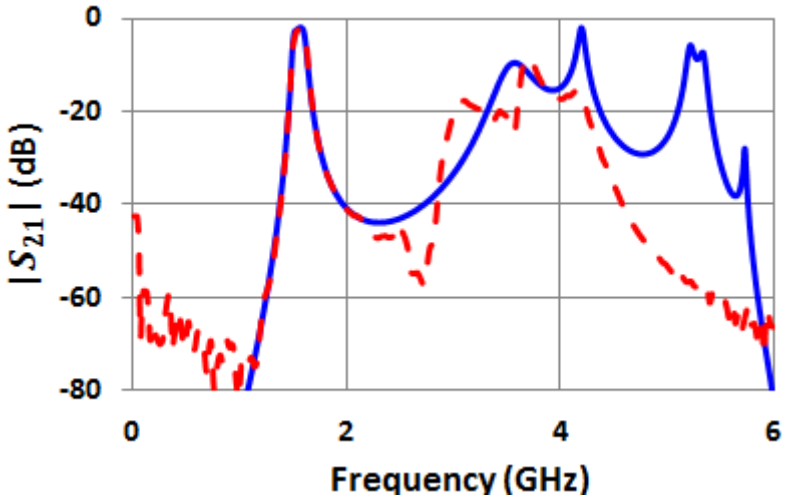

(a)

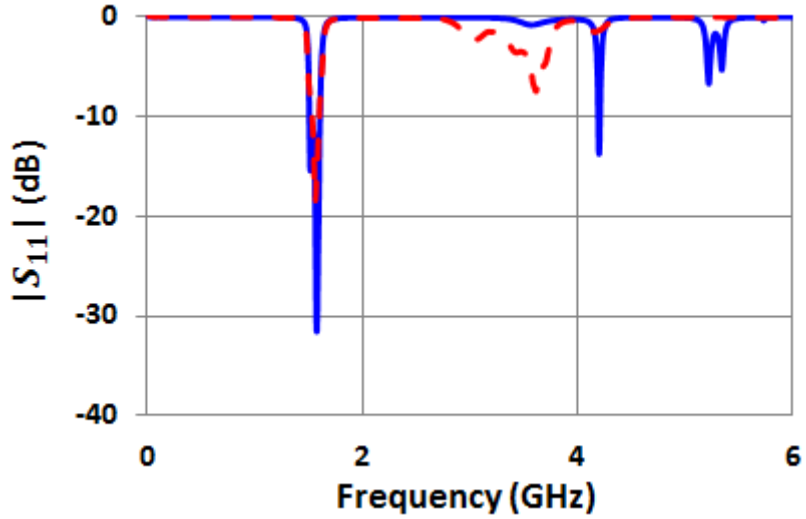

(b)

Figure IV-20. S-parameters of the "filter 2": measurements (red dashed line) (for $V_1 = 16.5\ V, V_2 = 22\ V$*), and circuit simulations (blue solid line).*

IV.4.4. Conclusion

Both theory and experiments have proven that the center frequency of the PC-SLR bandpass filter can be easily controlled by loading the short-circuited stubs and choosing accordingly their convenient length. Measurement and simulations are in a good agreement, except in the out-of-band region where some unexpected spurious appear. Insertion loss depends on the varactor diodes quality factor, and varies from about 2.2 dB to a maximum of 6 dB, with a working frequency variation of +/- 7.6 %. These first results show that the simple approach proposed in this work can lead to very fast designs of tunable filters. Further works could focus on the tuning of the bandwidth independently from the center frequency.

References

[1] C. Rauscher, “Reconfigurable bandpass filter with a three-to-one switchable passband width,” IEEE Trans. Microwove Theory Tech., vol.51, no. 2, pp. 573–577, Feb. 2003.

[2] T.-S. Yun, H.-S. Kim, T.-S. Hyun, and S.-S. Kwoun, "Tunable stepped impedance resonator bandpass filter using ferroelectric materials", in the 18th Asia-Pacific Microw. Conf. Dig., Proc. Yokahoma, Tokyo, Dec. 12-15, 2006.

[3] A. Pothier, J.-C. Orlianges, G. Zheng, C. Champeaux, A. Catherinot, D. Cros, P. Blondy, and J. Papapolymerou, “Low-loss 2-bit tunable bandpass filters using MEMS DC contact switches,” IEEE Trans. Microwave Theory Tech., vol. 53, no. 1, pp. 354–360, Jan. 2005.

[4] M.-S. Chung, I.-S. Kim, and S.-W. Yun, "Varactor-tuned hairpin bandpass filter with enhanced stopband performance" in the 18th Asia-Pacific Microw. Conf. Dig., Proc. Yokahoma, Tokyo, Dec. 12-15, 2006.

[5] F. Huang, S. Fouladi, R.-R. Mansour, "A novel MEMS based tunable dielectric resonator filter", in IEEE MTT-S Int. Symp. Dig., Baltimore, US, June 5-10, 2011.

[6] W.-W. Yan, and R.-R Mansour, "Tunable Dielectric Resonator Bandpass Filter With Embedded MEMS Tuning Elements", IEEE Trans. Microwave Theory Tech., vol. 55, no. 1, pp. 154-160, Jan. 2007.

[7] S. Fouladi, F. Huang, W.-D. Yan, R.-R. Mansour, “High- Q Narrowband Tunable Combline Bandpass Filters Using MEMS Capacitor Banks and Piezomotors”, IEEE Trans. Microw. Theory Tech., vol. 61, no. 1, pp. 393–402, Jan. 2013.

[8] A. Takacs, D. Neculoiu, D. Vasilache, A. Muller, P. Pons, L. Bary, P. Calmon, H. Aubert and R. Plana, “Tunable bandstop MEMS filter for millimetre-wave

applications", in the 38th European Microwave Conf. Dig., Amsterdam, Niederland, Oct. 27-31, 2008.

[9] A.-A. Tamijani, L. Dussopt, and G.-M. Rebeiz, "Miniature and tunable filters using MEMS capacitors", IEEE Trans. Microwave Theory Tech., vol. 51, no. 7, pp. 1878 - 1885, Jul. 2003.

[10] A. Miller, J.-S. Hong, "Wideband Bandpass Filter With Reconfigurable Bandwidth", IEEE Microwave and Wireless Components Lett., vol. 20 , no. 1, pp. 28 – 30, Jan. 2010.

[11] C. Lugo, and J. Papapolymerou,"Single switch reconfigurable bandpass filter with variable bandwidth using a dual-mode triangular patch resonator", in IEEE MTT-S Int. Symp. Dig., Long Beach, CA, June 12-17, 2005.

[12] C. Lugo, and J. Papapolymerou, "Electronic Switchable Bandpass Filter Using PIN Diodes for Wireless Low Cost System-on-a-package Applications", IEE Proceedings Microwave Antennas and Porpagation, Vol. 151, No. 6, pp. 497 – 502, Dec. 2004.

[13] Y.-H. Chun, J.-S Hong, Peng Bao, T.-J. Jackson, and M.-J. Lancaster, "BST-Varactor Tunable Dual-Mode Filter Using Variable Zc Transmission Line", IEEE Microwave and Wireless Components Lett., Vol. 18, no.3, pp. 167 – 169, Mar. 2008.

[14] Z. Brito-Brito, I. Llamas-Garro, L. Pradell, "Selectivity tuned bandpass filter", Electronics Letters, vol. 45, no. 9, pp. 984-985, Sep. 2009.

[15] C. M.-Anguiano, I. L.-Garro, Z. Brito-Brito, L. Pradell, A. C.-Chavez, "Fully adaptable band-stop filter using varactor diodes", Microwave and Optical Technology Letters, vol. 52, no. 3, pp. 554 -558, Mar. 2010.

[16] E. Pistono, M. Robert, L. Duvillant, J. Duchamp, A. Vilcot, P. Ferrari, "Compact fixed and tune-all bandpass filters based on coupled slow-wave resonators", IEEE Trans. Microw. Theory Tech., vol. 54, no. 6, pp. 2790–2799, June 2006.

[17] F. Burdin, E. Pistono, and P. Ferrari, "Parallel-coupled stub-load resonators compact size tunable filter", in 22th Asia Pacific Microwave Conference, Yokahoma, Japan, Dec. 7-10, 2010.

[18] I.-C. Hunter, "Microwave electronically tunable filters", Thesis for the degree of doctor of philiosophy, in the department of electrical and electronic at the university of Leeds, May1981, http://etheses.whiterose.ac.uk/3116/1/Hunter_IC_Electrical_Electronic_Engineering_PhD_1981_.pdf.

Conclusion

Characteristic features of the Parallel-Coupled Stub-Loaded Resonator (PC-SLR) bandpass filter were presented, such as resonance conditions for the fundamental resonance frequency and for spurious ones. Miniaturization rules were discussed to illustrate the fact that the SLR can be shortened by applying a small characteristic impedance ratio R_Z. The proposed PC-SLR bandpass filter can be 50 % smaller as compared to the classical Parallel-coupled bandpass filter. A complete synthesis method of the PC-SLR bandpass filter was developed. The synthesis is based on the classical J inverter method. The filter equivalent circuits, slope parameters and admittance inverters expressions were derived. Based on this synthesis, the odd- and even-mode impedances were computed. Using these impedances the physical parameters of the filter were calculated for a homogeneous technology (such as stripline). Simulations were presented to validate the theory for three relative bandwidths of 4, 6 and 8 %, respectively. For a proof-of-concept a third-order stripline bandpass filter was designed and fabricated with a passband ripple of 0.01 dB and a relative bandwidth of 4.5 %. Theory, simulations and measurements are in good agreement and thus validate the theory. The realized bandpass filter achieves more than 36 % surface minimization in comparison to the conventional Parallel-coupled bandpass filter with the same specifications.

Next, a careful study of the spurious frequencies was achieved. A wide out-of-band rejection was demonstrated for the PC-SLR bandpass filter. The highest first spurious frequency was controlled by the convenient choice of the open-ended stub's electrical length and the characteristic impedance ratio R_Z. Based on this analysis, it is convenient to consider a small R_Z ratio (< 1) in order to achieve compact and wide out-of-band rejection. Even by properly choosing the electrical open-ended stub's length and the characteristic impedance ratio, the large out-of-band rejection cannot extend to more than five times the working frequency. Thus, to enlarge the out-of-band rejection, an original technique was proposed by using near- and far-end

three-coupled feeding lines called “U corner” structures. The implementation of this technique is very simple since only the “U corner” has to be optimized after a classical design. The out-of-band rejection is greatly improved up to 9 times the working frequency.

Finally, by properly loading the SLR with variable capacitance (varactor diode) with the convenient miniaturization of the short-circuited stub, the center frequency of the PC-SLR filter was easily controlled. It was proven that the loaded capacitor has no impact in the odd-mode resonance frequencies. Thus, when loading the SLR, the first spurious frequency is not altered. For a proof-of-concept, third-order PC-SLR bandpass filters were designed and fabricated. By loading the three SLR of the filter with capacitors, according to the theory, a working frequency tuning of 14 % can be achieved around 1.5 GHz. Insertion loss depends on the varactor diodes quality factor, and varies from about 2.2 dB to a maximum of 6 dB.

The theoretical and simulated results carried out in this thesis indicate the importance of the characteristic impedance ratio. A small value of the characteristic impedance ratio leads to a compact PC-SLR bandpass filter and a wide rejected bandwidth. This ratio is limited by the substrate’s characteristics. In order to tackle this limitation, slots could be introduced in the ground plane below the short-circuited stub to increase their characteristic impedance and thus decrease the characteristic impedance ratio.

Moreover, by properly coupling the first and the third resonators of the three-order PC-SLR bandpass filter, additional transmission zeros could be located in the upper out-of-band rejection. These transmission zeros can be located at the harmonics of the working frequency or near the passband to improve the filter selectivity. Location of these zeros can be adjusted by controlling the coupling between these resonators. The location of these zeros can be estimated based on a specific theoretical study.

Publications

Journal publication:

[1] **M. Akra**, E. Pistono, A. Jrad and P. Ferrari, "Full Study of the Parallel-Coupled Stub-Loaded-Resonator: Synthesis Method in a Narrow and Large Band with an Extended Optimal Rejection Bandwidth", submitted to IEEE Transactions on Microwave Theory and Techniques.

International conferences:

[1] **M. Akra**, H. Issa, E. Pistono, A. Jrad, N. Corrao, and P. Ferrari, " Parallel-Coupled Stub-Loaded Resonator Filters With Wide Spurious Suppression", in the 42th EuMC Proc., Amsterdam, Netherlands, Oct. 28-Nov. 2, 2012.

[2] **M. Akra**, E. Pistono, A. Jrad and P. Ferrari, "A Novel Accurate Method for Synthesinzing Parallel Coupled Line Bandpass Filter", in the 13th Microwave Mediteraneen Symposium, Beyrouth, Lebanon, Sept.2-5, 2013.

[3] **M. Akra**, E. Pistono, A. Jrad, H. Issa and P. Ferrari, "Synthesis method for the Parallel-Coupled Stub-Loaded Resonator Filters", Accepted to oral presentation in IEEE MTT-S Int. Symp. Dig., Florida, USA, June 1-6, 2014.

[4] **M. Akra**, E. Pistono, A. Jrad and P. Ferrari, "Tunable bandpass filter with high out-of-band rejection", Accepted to oral presentation in the 44th EuMC Proc., Rome, Italy, Oct. 5-14, 2014.

National conferences:

[1] **M. Akra**, E. Pistono, A. Jrad and P. Ferrari, "Nouvelle technique de suppression des remontées parasites hors bande pour les filtres passe bande à rubans couplés", 18èmes Journées Nationales Microondes, Paris, France, 2013.

[2] **M. Akra**, E. Pistono, A. Jrad and P. Ferrari, " Filtres à base de résonateurs chargés par des stubs en court-circuit: Formulation et synthèse dans un milieu homogène", 18èmes Journées Nationales Microondes, Paris, France, 2013.